Modelling and Optimization of Air Flow Sensor Within CPAP System

By

Johnny Huang

A Thesis Submitted in Partial Fulfilment of the Degree of
Master of Engineering

AUT University
Auckland, New Zealand

April 2007

STATEMENT OF ORIGINALITY

'I hereby declare that this submission is my own work and that, to the best of my knowledge and belief, it contains no material previously published or written by another person nor material which to a substantial extent has been accepted for the qualification of any other degree or diploma of a university or other institution of higher learning, except where due acknowledgment is made in the acknowledgments.'

…….. (Signature)

…….. (Date)

ACKNOWLEDGEMENTS

Many people contributed to this thesis and I wish to formally thank to all of them. Firstly, I would like to express my appreciations and gratitude to my supervisor, Professor Ahmed Al-Jumaily. He is such knowledgeable, patient and helpful. In the two years master study, he indicted the study direction and selected this project for me. His high expectation and encouragement was the driving force for me to proceed as best as I could in the research.

I would also like to thank my industrial supervisors in Fisher & Paykel Healthcare, Mr. Doug Makinson who mentored me on the commercial product development, Mr. Paul Bao who supported me in both aspects of theoretical analysis and prototype make up, Mr. Nordyn Alami who taught me a lot in the embedded programming. I wish to thank Dr. Alex Du, Mr. David White, Dr Khee Hiang Lim, Dr. David Parker and Dr. Robert Paxton for correcting this thesis. They gave me lots of help and valuable suggestions about writing. I would like to thank all the staff in the Master of Engineering programme.

To my colleagues and friends at the BioMEC, they made everyone to feel like in a family here and help each other. To Joe, Prasika, Ashis Mookerjee, Bhupendra Gohil, Vivien Lin, Lily, Mazhar, and Gijs, thank you for your help and advice.

Thanks to my dear wife Vivien Zhou, she always encourages me and share housework to let me concentrate to my study.

Finally, I'd like thank to God, my honest mentor, who helped me and guided me to achieve this important milestone in my life.

ABSTRACT

The Continues Positive Airway Pressure (CPAP) therapy is the most popular non-invasive therapy used to treat Obstructive Sleep Apnoea symptoms (OSA). Recent sleep clinic research requires more CPAP functions during patient's sleep periods. It would be an advantage to operate the CPAP system at a lower pressure whilst monitoring the patient's air flow, and raise the pressure as the OSA is detected, rather than maintaining a fixed higher minimum pressure in order to reduce OSA symptoms. In order to detect OSA, an air flow sensor is considered ideally suited to assemble within the CPAP system and the characteristics of this type of sensors are investigated by creating and validating a mathematical model.

Before determining the most suitable type of air flow sensor, several common methods of air flow measurement were investigated. Ultrasonic and hot wire air flow sensors were considered to be the most suitable sensors to be implemented. After setting up the simulation model and conducting experiments, some limitations of ultrasonic air flow sensor were found, so the hot wire sensor was selected for further investigation.

Comparing the performances of three types of hot wire sensor, Constant Voltage (CV), Constant Current (CC) and Constant Temperature (CT), the CT hot wire sensor was found to be the most suitable type for CPAP systems. In order to achieve a precise measurement, different locations for the air flow sensor within CPAP system were investigated and the blower inlet was found to be the best location for air flow sensor.

The simulation CT model hot wire sensor was developed. The experimental results were compared to the simulation model results. Comparison of the two results showed less than 1.5 % error when the air flow velocity exceeded 1.0 m/s (Average air speed is 5.0 m/s from the CPAP Blower).

Environmental conditions of temperature, humidity and wire property effects were analysed by processing the simulation model under different conditions. The following conclusions were drawn out:

The output current to the hot wire air flow sensor rise significantly as the hot wire diameter increases, however, the sensor response time increases significantly. It was found that platinum wire of a diameter 0.02 mm can meet the response time requirement for diagnosis of sleep disorders.

Various wire lengths produce no significant effect on both aspects of output wire current and response time. Therefore wire length can be designed to fit the inlet channel of the CPAP blower.

Higher wire temperature causes higher wire current flow at the same air flow velocity, however, lower wire temperatures achieve a faster response speed. The temperature range of 50 to 100^{o}C over ambient was found to be an optional setting.

To achieve the desired level of accuracy a temperature compensation circuit was required for the hot wire air flow sensor. Otherwise it was necessary to keep the sensor in a stable room temperature environment to gain the same result. The percentage error of ambient temperature was about 0.65% per ^{o}C.

TABLE OF CONTENTS

LIST OF FIGURES

LIST OF TABLES

NOMENCLATURE

A	Cross area of wire	m^2
A_w	Wire surface area	m^2
a	Constant in Nusselt number expression	
a_t	Coefficient depended on air temperature	
a_1 to a_6	Coefficients of water vapour pressure	
b	Coefficient of Nusselt number expression	
C	Sound velocity in static air	m/s
C_w	Wire specific heat capacity	J/kg/K
C_0	Specific heat capacity of dry air in atm pressure	J/kg/K
C_1	Specific heat capacity of moist air in atm pressure	J/kg/K
C_p	Specific heat capacity of moist air	J/kg/K
D	Wire diameter	m
dt	Time differentiation	
E	Young's modulus of platinum,	N/m^2
e	Vapour pressure of water	HPa
e_{T_a}	Vapour pressure of water in air temperature	HPa
e_{T_d}	Vapour pressure of water in dew point temperature	HPa
e_0	Potential (voltage) of hot wire	V
F_x	Force along x axis (the direction of air flow)	N
g	Gravity number	9.8 m/s^2
h	Forced convective coefficient	
h_0	Initial mean value of convection coefficient	
h_1	High of point 1	m
h_2	High of point 2	m
$\bar{h}$	Coefficient of natural convection	
I	Platinum moment of inertia	kg-m^2
i_w	Hot wire current	mA
K	Gain of first order system	

Kr_t	Wire resistivity	Ω-m^2/m
Kr_0	Wire resistivity at 0 °C	Ω-m^2/m
K_{tr}	Absolute Temperature Coefficient of wire resistance (ATC)	
K_v	Coefficient of air flow velocity	
k	Thermal conductivity of moist air	W/m/K
k_{c1}	Thermal conductivity of platinum	W/m/K
k_{c2}	Thermal conductivity of tin	W/m/K
k_e	Adiabatic exponent of air	
k_p	Temperature coefficient of platinum wire resistance	
k_t	Resistivity of platinum in ambient temperature	Ω-m^2/m
k_0	Thermal conductivity of dry air in atm pressure	W/m/K
k_1	Thermal conductivity of moisture air in atm pressure	W/m/K
L	Wire length	m
L_c	Characteristic length of the geometry	m
L_s	Distance between transmitter and receiver	m
M	Wire mass	kg
m_{dry}	Mass of dry air	kg
m_w	Actual mass of water vapour present in moist air	kg
N_u	Nusselt number	
$\overline{Nu}_L$	Mean value of Nusselt number	
P	Ambient air pressure	Pa
P_a	Pressure of moist air	Pa
P_{atm}	Standard atmosphere pressure (atm)	0.101 MPa
P_r	Prandtl number	
P_w	Partial pressure of water vapour in the moist air	Pa
P_1	Static pressure in the free air stream	Pa
P_2	Static pressure on wire surface	Pa
$Q_{conduct}$	Conductive heat loss power from hot wire	W
$Q_{convert}$	Forced convective heat loss power	W

$Q_{generate}$	Generated heat power	W
Q_{NC}	Natural convective heat loss power	W
$Q_{radiate}$	Heat loss power of radiation	W
Q_{side}	Transferred heat power in half wire side	W
q_o	Output signal	
q_i	Input signal	
$q_{radiate}$	Unit power of radiant heat loss from wire	W/m
R_a	Individual specific gas constant	286.9 J/kg-K
Ra_L	Reynolds number of characteristic length	
R_e	Reynolds number	
R_{eCr}	Critical Reynolds number	
R_i	Resistance of each wire lump in working temperature	Ω
R_{lump}	Resistance of wire lump in ambient temperature	Ω
$R_{thermal1}$	First kind of conductive thermal resistance	W/^{o}C
$R_{thermal2}$	Second kind of contact thermal resistance	W/^{o}C
R_w	Hot wire resistance	Ω
R_{water}	Individual water vapour gas constant	461.5 J/kg-K
R_{wo}	Initial wire resistance	Ω
R_0	Wire resistance at 0 °C	Ω
RH	Relative humidity of air	%
ΔR	Various wire resistance	Ω
r	Wire radius	m
r_w	Various part of wire resistance	Ω
T	Air temperature in Celsius degree	^{o}C
T_a	Ambient air temperature	K
T_{pin}	Brass pin temperature	K
$\bar{T}_s$	Mean value of wire surface temperature	K
T_w	Wire working temperature	K
T_{w1} to T_{w4}	Absolute temperatures of series lumped hot wire	K

ΔT	Temperature different of neighbour lumps	K
T_0	Initial wire temperature	K
T_1 to T_8	Temperatures of series lumps	K
T_∞	Reference fluid (air) temperature	K
Δt	Time different between inverse directions sound propagating	s
V	Effective air velocity	m/s
V_{air}	Air velocity	m/s
V_{o_HW}	Output voltage in prototype sensor	V
V_{p1}	Reference voltage in prototype sensor	V
V_0	Initial mean value of effective air velocity	m/s
V_1	Air velocity of point 1 in the stream	m/s
V_2	Stagnation air velocity of point 2 on the wire	m/s
W	Circumference of wire crosses	m
X	Specific humidity or humidity ratio	
α_d	Air thermal diffusivity	m^2/s
α	Temperature Coefficient of Resistance (TCR)	
β	Coefficient of thermal expansion for idea gases	
δ_x	Deflection along x axis	m
δ_y	Deflection along y axis	m
ε_{res}	Emissive of the hot wire	
ε_y	Strain along the wire axis	m
θ	Angle between wire axis (or sound wave) and air flow direction	o
μ	Air viscosity	kg/m/s
ν_a	Specific volume of moist air per mass unit	m^3
ν_0	Kinematic viscosity of dry air in atm pressure	m^2/s
ν_1	Kinematic viscosity of moist air in atm pressure	m^2/s
ν	Kinematic viscosity of moist air	m^2/s
ρ_p	Platinum density	kg/m^3
ρ	Air density	kg/m^3
ρ_{dry}	Density of dry air	kg/m^3

σ	*Stefan-Boltzmann* constant	5.67×10^{-8} W/m^2-K^4
σ_y	Wire stress	N/m^2
τ	Time constant	s
ω	Angle frequency of input signal	rad/s

Chapter 1 Introduction

1.1 Obstructive Sleep Apnoea

Sleeping occupies one third of person's life time thus it is a very important to maintain quality of life. Sleeping disorders can have many effects that depreciate living quality including our ability to interact with others as well as increasing health problems [1]. The most common kind of sleeping disorder is Obstructive Sleep Apnoea (OSA) [2-4]. The word "Apnoea" comes from the Greek word "want of breath" [1, 2], the clinical definition of apnoea is: the respiratory movement is reduced more than 95% in a ten second period [2]. OSA is characterized by the repetitive intermission of breathing caused by the obstructive block of the upper airway. When OSA occurs, the brain has to be awaked from its sleeping stage to give instructions to the breath muscles to work harder. This apnoea event interrupts the patient sleeping and this interruption is associated with irregular heartbeat, high blood pressure, heart attach and stroke [2]. Obese people have a high rate of OSA due to excess throat tissue or relaxed tongue muscle leading to obstructive blocking of the airway opening in multiple sites during sleep, see Figure 1.1. Obstructive blocking will cause the patient to suffer laboured breathing or choking [2], and usually a brief wake up period is unavoidable. This situation is like clipping or blocking the inlet opening of an air pump while the machine is running. This action directly strains the air pump operation and in a similar case, the patient's muscles strain when OSA occurs.

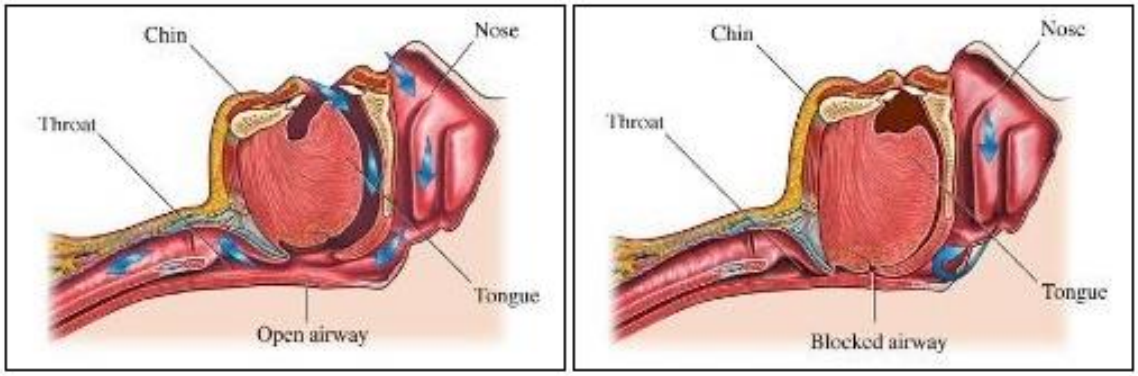

Figure 1.1 Open airway and blocked airway

1.2 Methods of OSA treatment

Though the essential principle of OSA treatment is to eliminate the airway obstruction, there are various treatments available depending upon a range of physiological factors. The few effective treatments of OSA can be sorted into three kinds: surgery, oral appliances and breathing assistance devices. Not every treatment can be applied to each patient. The most appropriate treatment depends on the type and site of the airway obstruction and the health condition of the patient. Each patient possibly has more than one effective treatment, but the cost and comfort are other important factors for OSA treatment determination. The three most common kinds of OSA treatment are briefly discussed below:

1.2.1 Surgery

Surgery is the most direct and permanent treatment for OSA. It is usually undertaken at the sites where the obstruction occurred, however, it has no effect on other sites after surgery. Surgery has a higher cost when compared to other OSA treatments. There are four types of surgery for OSA:

Uvulopalatopharyngoplasty (UPPP) surgery where parts of the uvula are removed to relax soft palate tissue and tighten the upper throat [5, 6] is considered to be the logical therapy for obstruction which includes soft palate and palatine tonsil obstructions. On the other hand this surgery involves the risks of airway swelling and post-operative medication.

Laser-Assisted Uvulaplasty (LAUP) [5, 6] where the uvula and soft palate are modified by a new laser surgery procedure is undertaken in several outpatient procedure steps. Usually it can significantly eliminate snoring, however in spite of this there is insufficient evidences to support the point that this surgery efficiently.

Nasal Surgery where the nasal passages are opened to adjust the septum improve the patient breath ability [7], however, this method can't physically eliminate the obstruction factors in the airway.

Jaw Surgery [8] where the lower and upper jaw are enlarged to expand the space for the airway, as in Nasal Surgery, does not directly remove the obstruction issue.

1.2.2 Oral Appliances

This kind of appliances used is categorized into two types:

Mandibular Repositioning Device (MRD) [9] is shown in Figure 1.2. One end of the MRD appliance tightly fits the patient's upper teeth and the other end pulls the lower Jaw forward by holding the lower teeth to the closest position to the upper teeth. The soft tissue is moved away from the airway opening by the extended lower jaw. This treatment is complicated by side effects including teeth loosing, join pain, muscle aches and tissue sores [10].

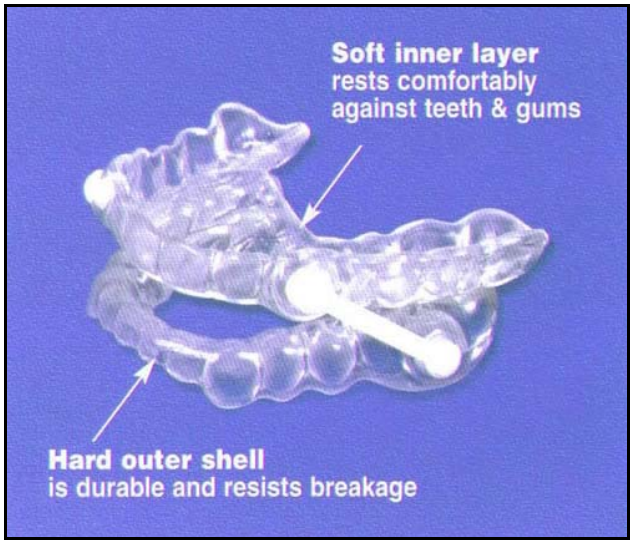

Figure 1.2 Mandibular repositioning device

Tongue Retaining Device (TRD) [10], is shown in Figure 1.3. Patients having conditions such as large tongues, no teeth or chronic joint pain are more suitable to wear TDR rather than MRD. A soft polyvinyl bubble is compressed between the tongue and teeth, a cavity is made beyond the lip to permit the patient's tongue to be placed in the projected position thereby reducing any obstruction.

Figure 1.3 Tongue retaining device

1.2.3 Breathing-Assistance Devices

This kind of OSA treatment is the most popular form of OSA therapy because it is more economical than surgery and more comfortable than using an oral appliance. Breathing assistance device is classified into four types:

Continuous Positive Airway Pressure (CPAP) [11] device is shown in Figure 1.4. Since nasal CPAP was introduced in 1980s [12], it is becoming the most common treatment for OSA patients due to its reliable and effectiveness. CPAP breathing assistance device consists of 4 main parts: Air Delivery Unit (ADU), Humidifier, air transmit tube and nasal mask, see Figure 1.4 and Figure 1.5.

Figure 1.4 600 CPAP Series

The ADU generates a positive pressure air stream that passes through the humidifier to increase the air humidity level so as to avoid patient airway dryness [13]. The humidified air stream is then transmitted to the nasal mask via a flexible tube. The nasal mask is attached on the patient face with straps [14], see Figure 1.5. The continuous, elevated pressure air stream from nasal mask to the patient's throat keeps the airway open, by inflating the airway, hopefully eliminating any obstructions. Most of OSA patients adapt to this treatment easily, however, long term compliance to treatment is relating poor.

Figure 1.5 FlexiFit 405 Nasal Mask

Bi-level Positive Airway Pressure (Bi-PAP) is one variation of CPAP therapy [12]. As the air flow sensor or pressure sensor is added into ordinary CPAP device, the patient inspiration and expiration cycle can be sensed and accordingly switch the ADU to generate a high or low pressure level air stream [15]. Bi-PAP therapy avoids some patient discomfort that can occur with ordinary CPAP devices and maintains the air pressure in the nasal mask at a constant level. An air flow sensor is necessary to identify the inspiration and expiration stage during the patient breathing cycle.

Automatic Positive Airway Pressure (APAP). This is new smart generation of breathing assistance devices, which utilize an air flow or pressure sensor on the nasal mask and a micro processor system to sample the patient breathing signal [16]. Through the use of a microprocessor which can eliminate background noise, analysis of the data by detection algorithm can justify if a obstruction occurs [17]. When the obstruction even occurs, an automatic regulation system raises the mask air pressure to overcome obstruction. After the obstruction even is over, the air pressure is gradually reduced to a lower maintain level [16]. APAP therapy improves the comfort of treatment by operating a lower pressure level but incorporating a fast response to solve emerging OSA symptoms. This smart function is due to the application of an air flow

senor and Micro processor system. The air flow sensor plays a significant role in the APAP system, and directly affects the response of the automatic regulation system.

CPAP, Bi-PAP & APAP breathing therapy systems require different roles from their respective air flow sensors. The focus of this research is therefore to investigate & optimize air flow sensor that can be implemented within a new generation CPAP device.

1.3 Literature survey

Air flow sensors are used to measure either air flow velocity or flow rate. The amount of air flow affects human comfort as well as many manufacturing processes in industries. The presence of air flow also influences various physical, chemical, and biological processes. Air velocity measurement in industries is very critical because it may affect not only the business cost of the product but also health and safety with the work environment. Therefore air flow sensing becomes very important, especially in the control systems of human comfort and industrial processes. In contrast to other sensors employed for measuring other parameters like temperature and pressure, an air flow sensor has to be in direct contact with the process environment and hence it is more difficult to implement within a closed system.

In some industrial processes, the output power depends on controlling the amount of air flow, such as in combustion control and other oxidation processes. Human health, comfort of skin and comfort of breath are adversely affected by bad air flow conditions within building heat & ventilation air condition (HVAC) system.

Many processes ranging from medical treatment to manufacturing industries require air flow measurement such as lung checking and engine operation. As the accuracy of air flow measurement becomes more important, manufactories have developed for more reliable and cost-effective air flow sensors.

1.3.1 Review of Air Flow Measurement Devices

This section deals with the basic concepts in air flow measurement and the various approaches and developments carried out in this field and also it discusses various approaches carried out to date. Some types of air flow sensors and their working principles are shown in Table 1.1.

Table 1.1 Several methods of air flow measurement

Principle	Operating Mechanism
Pressure	The pressure of flowing air varies with the velocity of air
Pneumatics	Propeller can obtain power from flowing air to rotate, the rotate speed is proportional to the air velocity
Lever	This hair sensor has cantilevers and strain gauges fabricated at the bottom of sensory hairs. The output voltage was proportional to the velocity of air flow [18].
Heat lost	The rate of heat lost from probe corresponds to the air velocity
Sound velocity	The different between measured sound velocity and known sound velocity in steady air is proportional to the air flow velocity.
Corona ion deflection	Process of corona ion deflection in a gas flow together with proper electrode geometry.
Electromagnetic	The inducted voltage of the coil in the electromagnetic varies with the speed of conductive fluid passing the coil.

There are many methods which can indicate change of the air flow velocity. The following section discusses some of the most common methods and the related development.

1.3.1.1 Digital propeller anemometer

When a propeller is fixed to face the direction of air flow in a pipe, the speed of propeller rotation is proportional to the velocity of air flow. Assuming there is no friction and the rotational speed is linear relative to the velocity of air flow, the propeller rotation speed indicates the air flow velocity [19].

Practical Mechanism

The propeller is located in the air flow stream, where the axial direction is coordinated (parallel) with the velocity direction of air flow, see Figure 1.6.

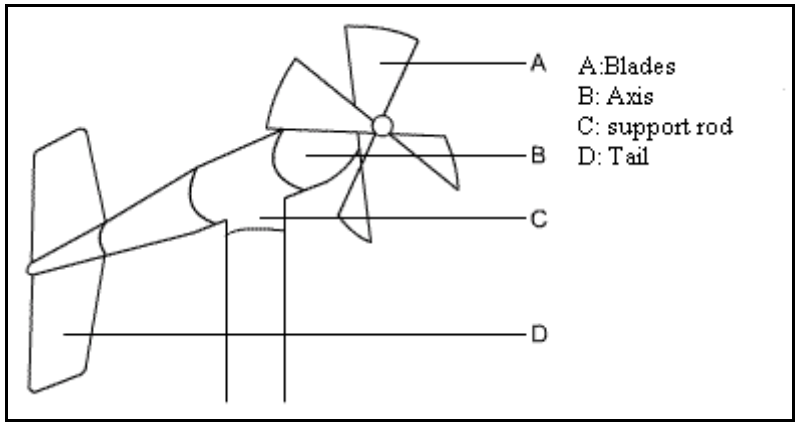

Figure 1.6 Digital propeller anemometer

Each blade of a propeller rotates pass a fix point [19], where electromagnetic induction or optical couple enables the rate of propeller rotation to be measured. Each running blade creates an electrical pulse when it passes the fixed point. The air velocity can be obtained indirectly through computing the amount of pulse in a set time period. The mathematic linear relationship between propeller speed and air velocity is depend on constant parameter K which is related to air velocity. During low speed air flow, K constant is affected by air viscosity which is influenced by ambient temperature. Due to the effect of friction, the propeller heats the air, so there is not a compensable curve relationship. In the situation of high speed air flow, parameter K does not vary in a limited range, nevertheless, the range of high speed air flow usually can't be used because it will cause high pressure loss (pressure loss is proportional to the square of air flow velocity).

Accuracy and Measurement Range

Commercial available measurement range is from 0.01 to 5,000 m/min. The time constant is 2 to 10 ms [19]. The higher the air velocity, the lower the time constant and this device can be modelled as a first order measuring system with a response time of 2-10ms. The nonlinear error can be controlled between 0.05% of the design range (usually the rate of maximum and minimum value is 10:1). Usually the output of

magnetic induction voltage is 10mv to 100mv. The output signal is of a square wave from digital pulses, which are displayed on a scope or interfaced to a microprocessor or computer. The accuracy of propeller is lower than that found in a hot wire anemometer. A thermal hot wire anemometer is commonly used in variable anemometers to detect the value of constant K.

1.3.1.2 Electromagnetic Flow meter

This measurement device uses the principle of induction. When a conductor moves with a transverse velocity across a magnetic field, the positive charged particles of the conductor will be forced to move toward one end of the conductor and the negative charges to the other. Thus a potential gradient is set up along the conductor, and there is a voltage difference between its two ends [20, 21].

Practical Mechanism

A practical flow meter is contained within a stationary pipe which must be nonmagnetic to allow the field to penetrate the fluid and is usually nonconductive, so that it does not provide a short-circuit path between the positive and negative induced potential at the fluid surface.

Features

There is no any flow obstruction in the pipe.
It can measure reverses flows.
It is insensitivity to fluid viscosity and density.
There is wide linear range of flow measurement.
Capable of measuring rapid response to flow changes.
Electromagnetic flow meters are limited by using a conductive fluid or including conductive particles in the fluid. Air is a non conductive fluid, so this device is not suitable for air flow measurement.

1.3.1.3 Laser Doppler Anemometry (LDA)

The displacement of some special near-neutrally-buoyant particles can be measured by recording their moving trace within two known time periods. The velocity can be computed depending on the known displacement and time interval.

Practical Mechanism

Using cylindrical lenses, a periodically pulsed laser beam is expanded into a two-dimensional "light sheet" defining a plane in the flow where velocity will be measured [22]. The light sheet is controlled by a spherical lens to about 1mm thickness. Using a multiple-exposure method (like that utilised in a digital camera), the locations of the particles at two instants separated by a known time interval are used to compute the magnitude and direction of the particle's velocity, that is the air velocity.

Features

LDA has a very high accuracy, but it is difficult to utilise for real time applications and it is limited by needing near-neutrally-buoyant particles in the air. Complex instrument and high cost are other limitations.

1.3.1.4 Pitot - Static Tube

The Pitot tube is a differential pressure probe and is used to measure local flow rate in a duct or pipe [23].

Practical Mechanism

There are two perpendicular holes on the probe. One of them is used to sample the total pressure of flowing air, whilst the other one is used to sample the static air pressure. Both holes are connected to inclined differential manometers. The mathematic algorithm of pressures and air velocity is as following:

$$V = \sqrt{\frac{2(p_{stag} - p_{stat})}{\rho}} \qquad (1.1)$$

where V is the air flow velocity, ρ is the fluid mass density, p_{stag} is the stagnation pressure, p_{stat} is the static pressure.

Features

As we can see from Equation (1.1), fluid mass density affects the measured result of flow velocity. The accuracy of a Pitot-static tube depends on the compressibility of the fluid. Air is a compressible fluid, its' density varies with flow acceleration.
Others factors affect the accuracy such as misalignment of the pitot tube, viscosity, density, turbulent and poor accuracy at low air speed.
One of the disadvantages is that the reading of the Pitot tube tends to become higher in turbulence flow [23].
When the velocity is low, the difference in pressure is very small, causing the error in the device to be greater than the measurement.
The slow response speed makes this device not suitable to measure dynamic air flow.

1.3.1.5 Hot wire/film Anemometer

Hot wire anemometers measure the air velocity by detecting the impact of velocity on heat transfer from a heated resistance wire located tangent to the air flow path [23].

Practical Mechanism

Three type electrical circuits are utilised with this device, constant voltage, and constant current and constant temperature.

Constant voltage or current hot wire/film sensor: Constant voltage or current is applied on the probe resistor, if it is assumed that the value of resistor does not vary with temperature and the generated heat is constant. Because of the effect of air flow, the heat lost is related to air velocities. Hence it will cause a resistor temperature change that proportional to the air flow velocity.

Constant temperature hot wire/film sensor: In order to keep the probe resistor at a constant temperature, the generated heat should be equal to the heat loss caused by the

air flow. A driver circuit is used to control the power delivered to the heated resistor to keep the temperature at a constant value.

Constant voltage or current modes are rarely used. This is because if the fluid velocity dropped rapidly, the heat loss will be much less than the generated heat, and it will cause the hot wire to quickl burn out. whilst in constant temperature mode, an anemometer uses the feedback circuit to self-balance the wire temperature

According to the different types of resistor marterial used, the thermal anemometers can be divided into hot wire and hot film. A hot film anemomter operates on the same principle as a hot wire anemometer. The metal wire resistor is replaced by a film resistor which is supported on thin silicon beams [24]. The film resistor has higher and more reliable mechanical strength. This high mechanical strength prevents disturtion of the film, thus preventing a drop of the accuracy of measurement.

Features

One main limitation of Thermal anemometers is that it can not identify the reversal air of flow because of its working principle so it is not suitable to be applied into turbulence air streams measurment. Thermal anemometers have a limited lower range of measurment due to the convective heat loss from the wire [25]. Heat generation and heat lost will cause time delay in real time meaurement. This effect is significant in high frequency dynamic measurement, such as those encounted in the automotive industry. In this application the air flow sensor itself has a response delay resulting in the measured amount of air becoming inconsistent with the amount of air flowing into the cylinders due to the time delay [26].

One solution is to design a segmented type of thermistor to have a large surface value and very small thickness, which is suitable for high speed response to rapid air flow variations. They could be placed in the air guide parallel or perpendicular to the air flow [25].

Because of the variation of ambient temperature and air temperature, the temperature compensation of a thermal anemometer will directly affect the accuracy of measurement. This problem can be solved by fabricating two symmetical probe

resistors in the circuit. One of the probes is heated via its resistor by means of a control circuit whiles the other probe is unheated and serves as an ambient temperature reference for temperature compensation. The average temperature of each probe is reflected in the temperature-dependent resistance of its nickel film [26].

The thermal anemometer circuit obtains an output through detecting the relative temperature difference between the heated probe and reference probe. When the ambient air temperature rises, not only does the temperature of the heated probe elevate but also that of reference probe. This leads to no net diffence in probe temperature and the measurement of air velocity is not affected by the fluctuation of ambient temperature.

The temperature compensation circuit maintains a constant ratio between the resistance of the heated probe and the sum of the temperature reference and temperature compensation resistances. This ratio is typically selected to maintain the heated element at about 180 ^{o}C above ambient, in order to burn off any oil and water deposits that might otherwise comdense on the the hot film and affect its heat transfer characteristics [26].

In order to get the temperature value of probes, the instantance temperature of each probe is determined by the temperature-dependent resistance of its nickel film [26]. The most suitable planar NTC thermistor geometry for an air sensor is a segmented type with an optimized surface value of 75 x 12 x 0.5mm. It is used to cover part of an open air gauge and conduct heat from flowing air. The resistivity difference obtained on the thermistors is compared with the volume velocity of air laminar flow at room ambient temperature and humidity [25].

Accuracy and Measurement Range

Previous experiment have proven that air flow can be measured within 0.5% deviation [27]. A micromachined, monolithic silicon mass-air-flow sensor has been developed for measuring engine intake air flow in the range of 1 to 60 m/s. It has a response time of under 1 millisecond (600 microseconds) and can be temperature compensated to a deviation of ±3.5% error or less in indicated flow over a temperature range of −30 ^{o}C to +40 C. The device can withstand bombardment by particles up to 50 μm in size in the air stream, or larger ones if elements with reduced accuracy are used [24].

Recent Improvements

Based on I-U (electrical current – voltage) characteristic for the PTC sensor, the relationship between the model parameters (including air velocity, electrical current, temperature, resistance...) can be discovered by mathematical analysis, and that the re-calibration of the sensor only requires one estimation of several parameters ,which is easily realised [28].

One method of calibration is based on the Takagi-Sugeno fuzzy system model, the diagnostic system is formulated by the input-output relationships between symptoms and faults [29]. The diagnostic system consists of two parts: one is to judge the fault of the sensor and the other is to identify the bias degree of the sensor [29].

Another method proposed is a self validating algorithm for constant differential temperature air flow sensor [30]. A self-validating flow sensor is developed to detect and accommodate a flow sensor fault in real time. Several faults are listed as follows [30]:

Dirt accumulation on the surface of the sensor probe causing increased time constant.

The deviation of the thermistor parameters causing imprecise ambient temperature.

Contamination, oxidization, mechanical shocks or evaporation causing heat coil burn out.

Soiling process by impurities and particles in the air stream causing increased sensor probe diameter.

Applications

Heated air flow sensors are widely implemented in many industry fields utilising automatic control systems. The measurement of air flow is becoming one of the significant elements which affect the accuracy and reliablility of a control system. A common example is the control of air/fuel system within an automobile. Recently, constant improvements are required in fuel economy which plays an increasing demand on engine fuel management systems.

A method of accurately detecting the mass of fresh air that inducted by the cylinder, to control the air-fuel ratio precisely during the throttle control, is adopted by using an

intake manifold sensor and mass air flow sensor with compensation according to the change of the mass of reverse flow gas from the cylinder [31].

Another effective system previously utilised to adjust air flow and air prediction scheme is by using a first order lead equation, which make it possible to estimate the amount of air flowing into the cylinder [26]. This method is suitable for within the CPAP system.

1.3.1.6 Ultrasonic Anemometer

The ultrasonic Anemometer measures the average velocity of flow over the path that the sound wave propagates [32]. The measurement principle is based on the linear relationship between the inverse Transit Time Difference (that is the time difference between the sound wave travelling along one direction in a constant distance and that along the inverse direction) and air velocity [23].

Practical Mechanism

Another type conversional type is Transit Time Difference (TTD) where one transmitter and one receiver, both placed along the air flow path. Another type is Inverse Tansit Time Difference (ITTD), utilising a pair of transmitters and opposing a pair of receivers, placed along the air flow path respectively.

The sound wave from the transmitter delivered to the flow stream is sent to the receiver downstream and vice versa. The time difference of sound wave propagation is proportional to the average air velocity over the path between the transmitter and the receiver [32].

There are two types of ultrasonic wave generated from the transmitter: the first is called pulsed type ultrasonic anemometer, which determines the velocity by measuring the inverse transit time difference (ITTD) of two pulses along a known path, the second is called continuous wave ultrasonic anemometer, which is based on the same principle as the pulsed type, but instead it utilises a continues wave [23].

Features

Ultrasonic anemometers avoid the need of temperature compensation over a wide temperature range [33].
The transit time different (TTD) ultrasonic anemometer has a high dynamic range, good linearly, and very low dead band [33].
Ultrasonic anemometers have faster response speed than other anemometers such as propeller, and lack any moving parts [23].
Experimental investigations on the behaviour of ultrasonic anemometers compared to a fast response propeller anemometer under foggy and rainy conditions found no correlation between the difference of wind speed and the liquid water content (LWC) during the experiment [34].
Ultrasonic anemometers need a microprocessor to generate ultrasonic waves and also to compute propagated time.

Accuracy and Measurement Range

The ultrasonic instrument is able to measure wind velocity in the horizontal plane in a range from 0 to about 100 km/h with a dead band of 2 cm/s and an accuracy better than 3 % in a temperature range from −25 to +75 ^{o}C [33]. Previous experimentation has show that when an air velocity of 0.4 m/s is measured by the ultrasonic anemometer, a simulation gives a theoretical value of 0.3951 m/s, or error 0.0049 m/s (1.2%). Engineers have simulated velocities from 0 to 2.0 m/s , which have produced a linear relationship between air velocity and ultrasonic path time [23].

In addition, during field trials of the instrument [35], engineers conducted environment trials to test the operation of the ultrasonic anemometer in extremes of temperatures (−35 to +79 ^{o}C) , humidity (5 to 100 %) and vibration. Results showed the ultrasonic anemometer to meet Marine Deck Mounted Standards.

Depending upon the sample time interval of the microprocessor, a single measurement period is less than 3 ms [33]. With the development of the microchip, ultrasonic anemometer will process and respond faster than before.

Recent improvements

There is one technique that uses hearing waves to replace the ultrasonic waves in the air flow velocity detection. Two sound propagation paths were configured by the loudspeaker (transmitter) [36], a microphone (receiver). The number of loudspeakers was reduced to one by using a reflected sound from the acoustic reflector. The propagation path of the reflected sound was tilted at an angle of 45^{o} from the propagation path of the direct sound. The reflected path was received at the microphone after reflection at the acoustic reflector.

Applications

Ultrasonic anemometers are used to precisely estimate the three dimensional direction of air flow [35] and can be implemented to detect gas leaks [37]. Farmers applied the instrument to measure an air velocity in the animal occupied zone (AOZ) to improve the ambient condition [38].

1.3.2 Sensor Selection

Summary analysis of the several methods of air flow measurement, technique required, giving their advantages and limitations for CPAP system are listed in Table 1.2. Several aspects are considered to determine the suitability of the air flow sensor to the CPAP system with respect to measurable range, sensitivity, response time, suitable dimension to locate the probe with the CPAP machine and reasonable cost. Recent developments of technology have enabled the ultrasonic transceiver to become much smaller and cheaper than before and this makes it possible for application in the CPAP system. However, some limitations of the ultrasonic air flow measure method were discovered when implemented within a CPAP system:

The ultrasonic sensor only can be located in the inlet channel of CPAP machine, it can't be located in other positions, such as outlet of blower, humidifier, tube and mask because it needs the transducers to be positioned a specific distance apart along the air flow path.

Table 1.2 Summary comparison of air flow sensors

Methods	*Advantages*	*Limitations for CPAP*
Propeller	Large range (0.01 to 15000 ft^3/min) High accuracy Fast response: 2-10 ms	Large dimension Low sensitivity Mechanical corruption
Electromagnetic	No flow obstruction Wide linear range Acceptable accuracy Rapid response time Insensitivity to viscosity and density	Require conductive fluid or including conductive particles in the fluid High cost
Laser Doppler Anemometry	Very large rang, Very high accuracy Suitable for record flow traces	Not good at real time application Need near-neutrally-buoyant particles Complex instruments Very high cost
Pitot-Static Tube	Small error: 0.46% Large range: 0-260 m/h Low cost	Limited respond speed Big dimension Accuracy is affected by many factors
Thermal hot wire/film	Properly range: 1-60 m/s Low deviation Small dimension probe Low cost	Respond time depend on probe size Accuracy is affected by ambient temperature
Ultrasonic	Large range High accuracy (< 3 %) Adapt in extremes of temperature and humidity. Fast response (< 3 ms)	Complicate set up High cost

Within the air inlet channel, the two transceivers are not suitable to be fixed at the corners as the air turbulence at this location is very complex. If the transceivers are located near the middle of air flow track, it will increase the air flow resistance slightly but will lead to better accuracy of results.

The purchase cost of the ultrasonic prototype: the acoustic transceivers and microprocessor will be approximately NZ$5.00 per set compared to the hot wire element (platinum wire) which only cost NZ$0.01 per piece.

At the same time, more reliable and smaller hot wire sensors have been produced by new technology, which makes it also practical to implement this method within a CPAP device. The hot wire sensor is not only economic but also can be mounted at different positions within the CPAP system and has less air flow resistance than the ultrasonic transceivers with a trade off in reduction in the response speed. If it can be shown that the commercial hot wire element (platinum wire) has sufficient response speed to satisfy the CPAP requirement, the hot wire sensor should also be investigated as an alternative air flow sensor to be applied within CPAP system. The simulation model of constant temperature hot wire sensor is created and validated by experimentation in the following chapters.

1.4 Objectives

Fisher & Paykel Healthcare wishes to develop an air flow sensor that will not only be used to determine whether the patient is actually using the device, a feature of existing Fisher & Paykel CPAP devices, but also be applied to measure dynamic signals of the patient's breath cycle for the diagnosis of breath disorders. Due to the absence of a robust mathematical model to predict the air flow sensor performance characteristics and accuracy, the overall objectives of this project include:

- Improve the understanding of air flow measurement within a CPAP device, in order to determine the most suitable air flow senor.
- Investigate the characteristics of a selected air flow sensor
- Develop a simulation model of air flow sensor to predict its suitability for measuring dynamic signals such as the patient's breath cycle.

In order to reach these goals, this research is divided into the following phases:

Phase one will involve the investigation of different methods of air flow caculation and comparison of various air flow sensors according to the operational requirements of the CPAP system. The physical parameters which probably influence measurement include:

dimensions, internal and external air temperature, internal and external humidity, and internal and external air pressure.

Phase two will consist of setting up good mathematical models for a range of flow sensors. Models will be implemented using Simulink^{TM} within the Matlab^{TM} environment. Simulation models can predict the sensor output signal and be used for improvement and modification.

Phase three consists of experimental verification of the simulation models and to study the effect of the environment conditions in air flow measurement process. The optimum objective is to determine a appropriate type of air flow sensor prototype and its ideal location site to be applied with in a CPAP therapy device and to evaluate the effects of changing input parameters on both static and dynamic results.

Chapter 2 Hot Wire Sensor Model

2.1 Introduction

The initial purpose of the model is to predict the output behaviour of a hot wire air flow sensor within CPAP system. The sensor is considered to be an ideal first order device as the device output is affected by a simple time delay. A mathematic model of time constant is built to determine the optimum wire dimension, according the relevant requirements of an air flow sensor within CPAP system, in Section 2.2.

As a very thin wire is intended to be used in the prototype hot wire sensor, the strength of the thin wire was verified in Section 2.3. The basic principle of the hot wire air flow sensor is the relationship between the forced convective heat loss and the air mass flow rate which is directly proportional to air velocity. The temperature distribution along the wire length is not equal, however in practice, but in order to simplify the analysis, the temperature along the wire length is assumed to be linear between the highest value at the midpoint of the wire and the lowest value at each end,. To initiate this model the wire is divided into 16 lumps in total to get more accurate result, however because of symmetric, we only need to analyse 8 lumps of half wire length. See following Figure 2.1.

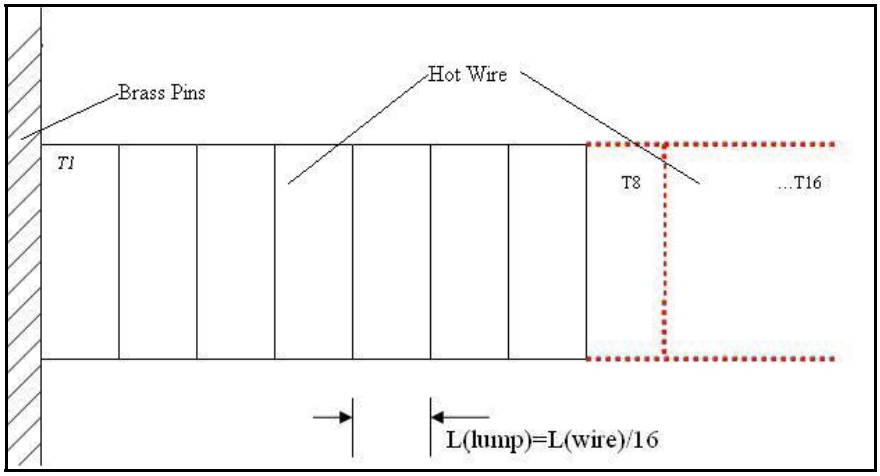

Figure 2.1 Lumped temperature distribution to midpoint of hot wire

The convection influence is analyzed and computed in Section 2.4. The heat power loss from hot wire is not only due to the forced convective heat loss of the wire but also include the conductive heat loss from the wire to the support pins, as well as the radiation heat loss. During condition of low air velocity the natural convective heat loss of the wire is also considered. In order to understand the physical process and the dynamic response within the hot wire sensor, mathematic models representing three kinds of energy conversion are developed in Section 2.5, 2.6 and 2.7, respectively.

By applying heat energy balance, the generated heat power is equal to total heat power lost. A mathematical model of this energy balance is given in Section 3.8.

2.2 Time Constant of Hot Wire Element

The first order model for a Hot Wire Element can be written as:

$$\left|\frac{q_o}{q_i}(i\omega)\right| = \frac{1}{\sqrt{\omega^2\tau^2+1}} \tag{2.1}$$

where ω is the frequency of input signal and τ is the time constant of system.

Fisher & Paykel expects to use the air flow sensor to measure the patient's breath cycle to diagnose relevant diseases (disordered breathing) during CPAP therapy. Numerous breathing waveforms, including normal breathing and disordered breathing have been collected and compared during experiments at Fisher & Paykel. Results showing the difference between a disordered waveform (a breathing pattern indicating disordered breathing) and normal waveforms enable detecting by looking at the first 14 harmonics of the inspiration waveform. Considering breathing rate of 14 breaths per minute, the harmonic occurs at a frequency of 3.27 Hz ($14\times14/60$). Assuming the sensor to be a first order system, at 3.27 Hz and the 3dB point [22] , the amplitude ratio of output signal q_o and input signal q_i results into:

$$20\log\left|\frac{q_o}{q_i}(i\omega)\right| \geq 3 \Rightarrow \left|\frac{q_o}{q_i}(i\omega)\right| \geq 0.708 \tag{2.2}$$

Substituting Equation (2.1) into Equation (2.2) yields:

$$\frac{1}{\sqrt{\omega^2\tau^2+1}} = \frac{1}{\sqrt{(2\pi\times 3.27)^2\tau^2+1}} \geq 0.708 \tag{2.3}$$

The maximum value of the time constant τ is the duration required to differentiate a disordered breath and a normal breath wave form. From Equation (2.3) the required response time is not allowed to be larger than 49 ms.

In order to calculate and verify that the time constant of the hot wire sensor is less than the maximum required response time given above, the transfer process of the hot wire air flow measurement system is analyzed by the following steps.

Step 1:
The effective air velocity V is computed.

$$V = V_{air} \cdot \sin\theta \tag{2.4}$$

where V_{air} is the velocity of air, and θ is the angle between wire axis and the flow direction. The Reynolds number R_e is computed by

$$R_e = \frac{V\times d}{\nu} \tag{2.5}$$

Where d is the diameter of wire, and ν is the kinematics viscosity of air in room temperature, given as 1.55×10^{-5} m^2/s.

Step 2:
The Reynolds number R_e should be compared with critical Reynolds number ($R_{eCr}=2\times10^5$ [45] for external flow over cylindrical surface) to determine if the air flow over the hot wire is laminar or turbulent.

Assuming the wire diameter, d , to be 0.02 mm based on the minimum available commercial size of platinum wire, the range of air velocity V_{air} is less than 10 m/s. Calculating value of R_e from Equation (2.5) gives 6.4516, much smaller than the

critical Reynolds number R_{eCr}, hence the forced heat convection on the wire is of laminar flow.

Step 3:

For cylinder in cross flow [45], the Equations of the Nusselt number N_u and Prandtl number P_r is obtained to determine the magnitude of the forced convective coefficient h. The Nusselt number N_u and Prandtl number P_r can be expressed in the following Equations (2.6) and (2.7) [45].

$$N_u = \frac{hd}{k} = 0.3 + \frac{0.62R_e^{1/2} \cdot P_r^{1/3}}{[1+(0.40/P_r)^{2/3}]^{1/4}}[1+(\frac{R_e}{282{,}000})^{5/8}]^{4/5} \tag{2.6}$$

where h is the forced convective coefficient and k is the thermal conductivity of air.

$$P_r = \frac{\nu}{\alpha} = \frac{\mu C_p}{k} \tag{2.7}$$

where α is the thermal diffusivity, μ is the air viscosity and C_p is the specific heat capacity of air at constant pressure. Combining Equation (2.5), (2.6) and (2.7) gives the equation of forced convective coefficient h [44, 45]:

$$h = \frac{k \times 0.989 \times (\frac{V_{air} \times \sin\theta \times d}{\nu})^{0.330} \times (\frac{\mu C_p}{k})^{1/3}}{d} \tag{2.8}$$

Step 4:

Apply conservation of energy to the hot wire to determine the time constant. This is achieved by initially considering the energy of forced convective heat loss E_{co} given by:

$$E_{co} = A_w \cdot h \cdot (T_w - T_a)dt \tag{2.9}$$

where A_w is the surface area of wire, T_w is the temperature of wire, T_a is the temperature of ambient air and dt is time differential. T_w relates to the wire resistance, R_w, is expressed by:

$$T_w = K_{tr} \cdot R_w \tag{2.10}$$

where K_{tr} is the Absolute Temperature Coefficient (ATC)of wire resistance which is different to the Temperature Coefficient of Resistance (TCR). TCR is a physical and electrical property of the material [46]. The resistivity of material varies depending upon the temperature of the material with accuracy exhibited over a wide range of temperature − 200 to + 650 ºC [47]. The most common use of TCR is to distinguish the purity of platinum, which is available with TCR range from 0.00375 to 0.003927. The highest TCR indicates the highest purity platinum, and is mandated by ITS-90 for standard platinum thermometers [48-50]. 0.00385 platinum is the most popular worldwide standard and is available in both wire-wound and thin-film elements [51].
The wire resistance, R_w , can be deduced from the Equation of TCR:

$$R_w = R_{w0}[1 + \alpha(T_w - T_0)] \tag{2.11}$$

where α is TCR, T_0 is the initial temperature of wire, R_{wo} is the initial resistance of wire. Comparing Equation (2.10) and Equation (2.11) shows that α is not the same as K_{tr}, but K_{tr} can be obtained from α. It is possible to calculate resistivity of platinum wire in steps of 5 °C from 20 °C to 227 °C by using the following Equation [51]:

$$R_w = R_0 (1 + a \times (T_w - 273) + b \times (T_w - 273)^2) \tag{2.12}$$

where R_0 is the resistance of wire at 0 °C, value of coefficient a is 3.9083×10^{-3} , and the value of coefficient b is -5.665×10^{-7}. The relationship of wire resistance R_w and wire resistivity Kr_t can be expressed as:

$$R_w = Kr_t \times L / A \tag{2.13}$$

Resistivity, Kr_t, is calculated in terms of absolute temperature, the formula form of Kr_t can be expressed as:

$$Kr_t = x \times T_w \tag{2.14}$$

Where x is the coefficient of temperature. Combine Equation (2.12) and (2.13) to get:

$$Kr_t = \frac{R_0(1 + a \times (T_w - 273) + b \times (T_w - 273)^2) \times A}{L} \tag{2.15}$$

By substituting in coefficients and retaining the factor variable T_w, ignore the constant factor, we get:

$$Kr_t = 0.0365 \times 10^{-8} \times T_w \tag{2.16}$$

Substituting Equation (2.16) into (2.13) and applying the wire dimension to get the wire resistance in terms of wire connectional area:

$$R_w = 0.0365 \times 10^{-8} \times T_w \times L / (\pi \cdot r^2) \tag{2.17}$$

where L is the length of wire and r is the radius of wire. Substituting Equation (2.17) into Equation (2.10) gives:

$$K_{tr} = \frac{T_w}{R_w} = \frac{(\pi \cdot r^2)}{3.65 \times 10^{-10} \times L} \tag{2.18}$$

Equation (2.18) is applied to the simulation model. As the forced convective coefficient h can be treated as being approximately linear for small changes in flow velocity, h can be expressed as:

$$h = h_0 + K_v(V - V_0) \tag{2.19}$$

where h_0 is the initial mean value of convection coefficient, K_v is the coefficient of flow velocity and V_0 is the initial mean value of effective air velocity. Differentiating Equation (2.8) with respect to flow velocity we get:

$$K_v = 413.33 \times V^{-0.6697} \tag{2.20}$$

Changes an air velocity causes a new energy balance to occur across the hot wire. The generated electrical energy deducted from the energy lost by forced convection is equal to the energy stored in the wire, shown in Equation (2.21).

$$i_w^{\,2}(R_{wo} + r_w)dt - A_w(T_w - T_a)hdt = MC_w dT_w \tag{2.21}$$

where:

i_w is the current flow through wire,

R_{w0} is the initial resistance of hot wire,

r_w is the various part of wire resistance,

A_w is the surface area of wire,

M is the wire mass,

C_w is the specific heat capacity of wire.

Substituting Equation (2.10) and (2.19) into Equation (2.21) gives:

$$i_w^{\,2}(R_{wo} + r_w)dt - A_w(K_{tr}(R_{w0} + r_w) - T_a)(h_0 + K_v(V - V_0)dt = MC_w d(K_{tr}(R_{w0} + r_w)) \tag{2.22}$$

The initial heat balance condition, where generated heat is equal to the forced convective heat loss, can be expressed as:

$$i_w^{\,2}R_{wo} - A_w(K_{tr}R_{w0} - T_a)h_0 = 0 \tag{2.23}$$

Substituting Equation (2.23) into Equation (2.22) gives:

$$-A_w K_{tr} r_w h_0 + i_w^{\,2} r_w - (A_w K_{tr} R_{w0} - A_w T_a)K_v V - A_w K_{tr} r_w K_v (V - V_0) = K_{tr} MC_w dr_w / dt \tag{2.24}$$

The last term of left hand side in Equation (2.24) includes the product of two small quantities $r_w(V - V_0)$. This product is considered to be relatively small so is neglected to add simplification. Assuming the initial air flow condition is static air, then the initial air velocity, V_0 , will be zero, Equation (2.24) can be further simplified:

$$\frac{r_w}{V} = \frac{(K_{tr}R_{w0} - T_a)A_w K_v V}{i_w{}^2 - A_w K_{tr} h - MC_w K_{tr} D} \tag{2.25}$$

According to Ohms Law, the voltage e across wire can be expressed as:

$$e = i_w r_w \tag{2.26}$$

Substituting Equation (2.26) into Equation (2.25) gives:

$$\frac{e}{V} = \frac{i_w r_w}{V} = \frac{K}{\tau D + 1} \tag{2.27}$$

where the gain K is expressed as:

$$K = \frac{A_w K_v (K_{tr}R_{w0} - T_a)}{i_w{}^2 - A_w K_{tr} h} \tag{2.28}$$

And the time constant τ is obtained as:

$$\tau = \frac{MC_w K_{tr}}{A_w K_{tr} h - i_w{}^2} \tag{2.29}$$

Equation (2.29) shows the response time of hot wire can be minimized by reducing wire mass M . The minimum diameter of platinum wire commercially available is 0.02mm. Considering the wire geometry within the CPAP system (20mm diameter), and assuming a very slow air flow rate of 0.0314 l/s, gives an air velocity of about 1 m/s. Substituting this value into Equation (2.29) yields a time constant of 22 ms. This theoretical time constant value is much smaller than the maximum value of 49 ms that are required to diagnose breathing disorders, making the 0.02mm diameter platinum wire suitable to be used as air flow sensor within the CPAP system. As the diameter of

wire is very small, the wire strength needs to be checked to ensure it is suitable for use within the CPAP device and this is done in section 2.8.

2.3 Forced Convective Heat Loss

Heat generated by the electric current passing through the platinum wire dissipates to the surrounding air. The wire is connected with brass support pins by soldering, shown as Figure 2.2,

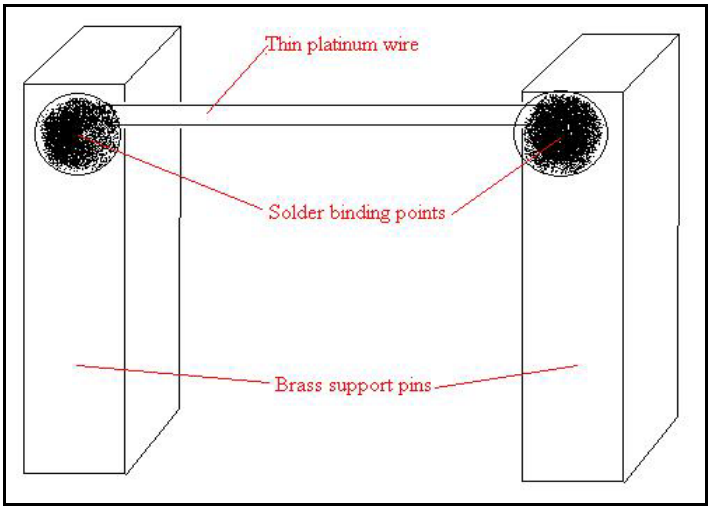

Figure 2.2 Construction of platinum probe

The only way to continuously generate heat in the wire is by electrical current, however there are four ways to dissipate heat power: Heat loss can be by forced convection from the hot wire, conduction from wire to the pins, radiation from the hot wire and natural convection from the hot wire, shown as Figure 2.3:

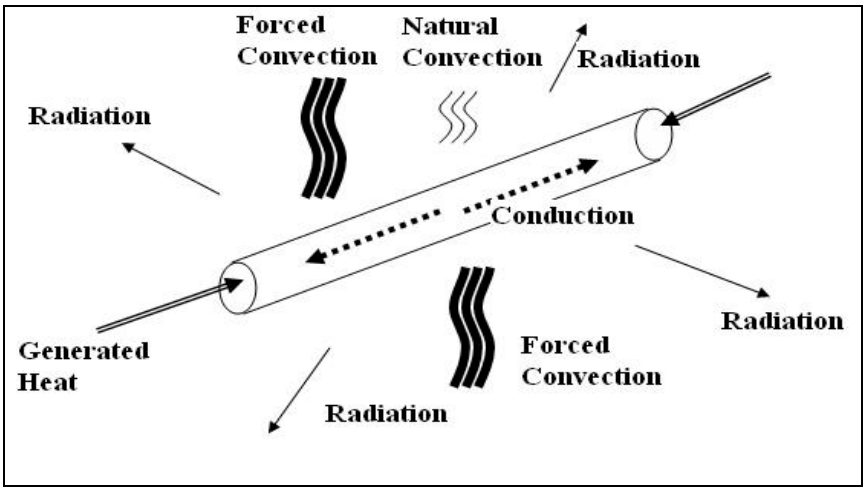

Figure 2.3 Various sorts of heat performance of hot wire

The majority of heat lost from the hot wire is by forced convection, which is the fundamental operating principle of air flow measurement. The forced convective coefficient can be obtained from Equation (2.8). The power of forced convective heat loss $Q_{convect}$ is expressed as:

$$Q_{convect} = hA_w(T_w - T_a) \tag{2.30}$$

where h is the forced convective coefficient. Apply the assumption of 8 lumps in each half side of the wire to get:

$$\begin{aligned} Q_{convect} &= h\frac{A_w}{8}\times\frac{(T_{Max}-T_a)}{8} + h\frac{A_w}{8}\times\frac{(T_{Max}-T_a)\times 2}{8} + \\ &\ldots + h\frac{A_w}{8}\times\frac{(T_{Max}-T_a)\times 8}{8} = \frac{9}{16}hA_w(T_{Max}-T_a) \end{aligned} \tag{2.31}$$

Where T_{Max} is the maximum temperature of hot wire. There are several parameters of air properties in Equation (2.8) that cause variation in h. These are thermal conductivity k, kinematic viscosity ν, viscosity μ, specific heat capacity C_p and air density ρ. The relationship between ν and μ is depending on air density ρ:

$$\nu = \frac{\mu}{\rho} \tag{2.32}$$

Almost all ρ values can be found from reference literature are for the density of dry air, however as the air condition varies, the density of air is affected by temperature, humidity and pressure. The density expression of moist air needs to be determined.

2.3.1 Computation of Moist Air Density

Density of air varies with the temperature and moisture content within the air. Higher temperature causes higher molecular motion, and the air expansion causes density to decrease. The amount of water vapour in the air also affects the density. Water vapour is a light gas compared to diatomic oxygen and nitrogen, and the unit amount of oxygen and nitrogen decreases according the increasing of water vapour content,

leading to the air density decreasing since the mass is decreasing. Based on specific volume of moist air [56], the air density can be expressed as:

$$\rho = \frac{1}{v_a} = (P_a / R_a T_a)(1 + X)/(1 + xR_{water} / R_a) \tag{2.33}$$

where:

v_a is the specific volume of moist air per mass unit of dry air and water vapour,

P_a is the pressure of moist air,

R_a is the individual gas constant, which value is 286.9 J/kg.K,

R_{water} is the individual gas constant water vapour, which value is 461.5 J/kg.K,

X is the specific humidity or humidity ratio.

As the density of dry air ρ_{dry} is dependent not only on the air temperature T_a, but also depend on pressure P [57], so ρ_{dry} is expressed as:

$$\rho_{dry} = \frac{P}{R_a T_a} \tag{2.34}$$

where R_a is the specific gas constant [57]. Combining Equation (2.33) and (2.34) gives:

$$\rho = \rho_{dry}(1 + X)/(1 + XR_{water} / R_a) \tag{2.35}$$

The gas constant ratio is obtained from water vapour characteristic gas constant (R_{water}) [56] and the value of air vapour R_a [57]. Applying the ratio into Equation (2.35) yields:

$$\rho = \frac{\rho_{dry}(1 + X)}{1 + 1.608X} \tag{2.36}$$

Specific humidity, X, from Equation (2.36), is the ratio between the actual mass of water vapour present in moist air m_w to the mass of dry air m_{dry}. Humidity is normally expressed in kilogram water vapour per kilogram dry air (SI-units) [58].

$$X = m_w / m_{dry} \tag{2.37}$$

The value X can also be expressed as the partial pressure of water vapour and air [58]:

$$X = \frac{0.622 P_w}{P - P_w} \tag{2.38}$$

where P_w is the partial pressure of water vapour in the moist air. Relative humidity, RH, may be defined as the ratio of the water vapour density (mass per unit volume) to the saturation water vapour density. RH is the ratio between the actual and the saturation vapour pressure [59, 60]:

$$RH = \frac{e_{T_d}}{e_{T_a}} \cdot 100 = \frac{P_w}{e_{T_a}} \cdot 100 \tag{2.39}$$

where e_{T_d} is the vapour pressure of water in dew point temperature, e_{T_a} is the vapour pressure of water in air temperature. Equation (2.39) is converted to:

$$P_w = e_{T_a} \cdot RH \cdot 100 \tag{2.40}$$

The relationship between vapour pressure e of water and air temperature T is shown as follow [60, 61]:

$$e_{T_a} = f(T) = a_0 + T\{a_1 + T\{a_2 + T\{a_3 + T[a_4 + T(a_5 + T \cdot a_6)]\}\}\} \tag{2.41}$$

The values of coefficients a_1 to a_6 in Equation (2.41) are obtained from Table 2.1.

Table 2.1 Coefficients of water vapour pressure [61]

	Water
a_0	6.107799961
a_1	$4.436518521 \times 10^{-1}$
a_2	$1.428945805 \times 10^{-2}$
a_3	$2.650648471 \times 10^{-4}$
a_4	$3.031240396 \times 10^{-6}$
a_5	$2.034080948 \times 10^{-8}$
a_6	$6.136820929 \times 10^{-11}$

The thermo physical properties of air are calculated from polynomial curve fits to a data set for 100 K to 1600 K. The Equation of curve was found from literature [62, 63]:

$$\rho_{dry} = 360.77819 T^{-1.00336} \tag{2.42}$$

Combining Equations (2.36), (2.38), (2.40), (2.41) and (2.42) yield:

$$\rho = \frac{360.77819 T^{-1.00336} \left(1 + \frac{0.622 \times (100 \cdot RH \cdot f(T))}{P - (100 \cdot RH \cdot f(T))}\right)}{1 + 1.608 \times \frac{0.622 \times (100 \cdot RH \cdot f(T))}{P - (100 \cdot RH \cdot f(T))}} = f(T, P, RH) \tag{2.43}$$

From Equation (2.43), it can be seen that density of moist air is a function of air temperature, pressure and humidity.

Equation (2.43) was used to test the density of dry air in the range 0 ^oC and 25 ^oC , the comparison of the values in reference [57] is shown in follow Table 2.2:

Table 2.2 Comparison of air density values

	Equation value	Reference Value
0 ^oC at 101.325 kPa	1.292638 kg/m^3	1.292 kg/m^3
25 ^oC at 100 kPa	1.168215 kg/m^3	1.168 kg/m^3

Other relevant air properties are collected by predictive software which simulates experimental result [64]. Using a curve fitting technique again results in the following

relationship between the specific air property and the air temperature, the relative pressure, air humidity.

2.3.2 Computation of Specific Heat Capacity of Air

The expression of the specific heat capacity value of dry air in the standard atmosphere pressure C_0 can be found as below [65]:

$$C_0 = 1.9327\times10^{-10}T^4 - 7.9999\times10^{-7}T^3 + 1.1407\times10^{-3}T^2 - 4.489\times10^{-1}T + 1.0575\times10^{3} \quad (2.44)$$

In order to find out the relation between the specific heat and the humidity, various input values of the relative humidity were made during conditions of constant temperature 20 °C and standard atmosphere pressure in the air properties calculator software. The trend line technique is applied in Figure 2.4 to get the Equation of specific heat capacity value of moist air, C_1, in the standard atmosphere pressure, is determined from the gradient of the trend line shown in Figure 2.4:

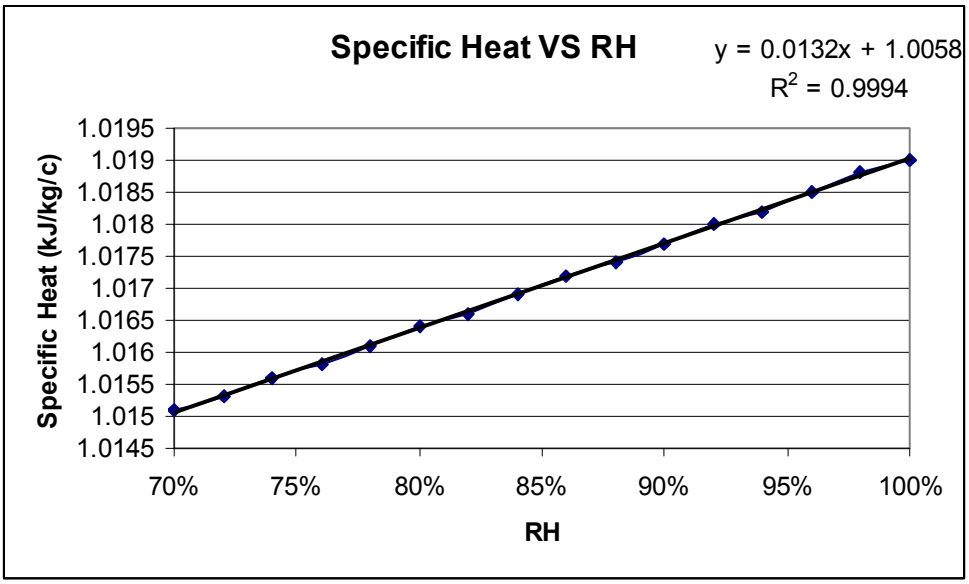

Figure 2.4 Specific heat VS relative humidity

$$C_1 = C_0 + 0.0132\times RH \quad (2.45)$$

The trend line matches the real line very well as the indicator R^2 of 0.9994 is very close to 1. In order to find out the relationship between the specific heat and the air

pressure, the input value of air pressure is varied whilst maintaining constant temperature 20 °C and relative humidity 70%. The trend line technique is now applied in Figure 2.5 to get the Equation of the specific heat capacity value of moist air C_p.

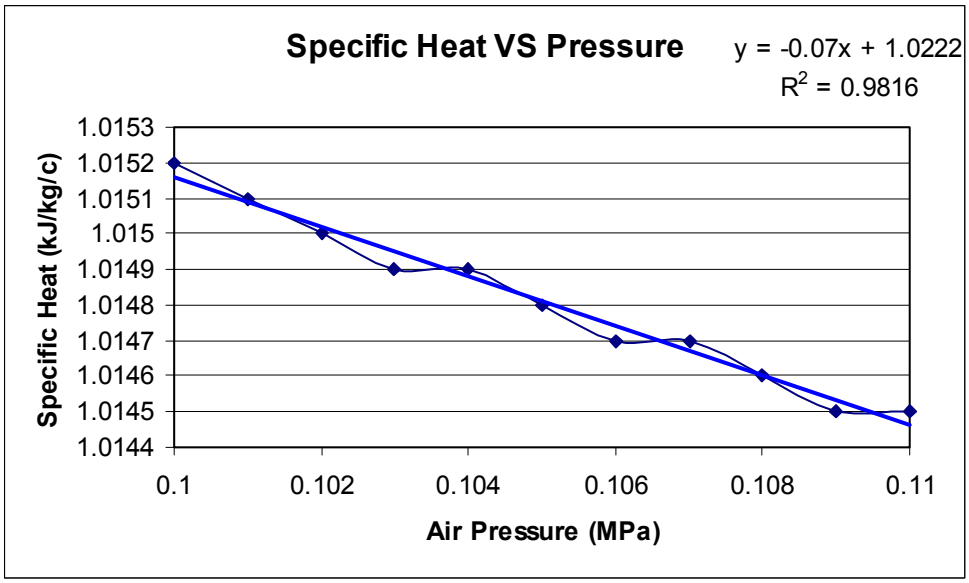

Figure 2.5 Specific heat VS Air pressure

$$C_p = C_1 - 0.07 \times (P - P_{atm}) \tag{2.46}$$

where P is the air pressure and P_{atm} is the standard atmosphere pressure of 101 kPa.

Combining Equations (2.55), (2.56) and (2.57) yields:

$$\begin{aligned} C_p = &((1.9327 \times 10^{-10} T^4 - 7.9999 \times 10^{-7} T^3 + 1.1407 \times 10^{-3} T^2 \\ &- 4.489 \times 10^{-1} T + 1.0575 \times 10^3) + 0.0132 \times RH) - 0.07 \times (P - P_{atm}) \end{aligned} \tag{2.47}$$

From Equation (2.47), it can be seen that the specific heat of moist air is a function of air temperature, pressure and humidity.

2.3.3 Computation of Air Viscosity

Dry air viscosity in the standard atmosphere μ_0 can be expressed as [66]:

$$\mu_0 = \frac{\nu_0}{\rho} = \frac{-1.1555\times10^{-14}T^3 + 9.5728\times10^{-11}T^2 + 3.7604\times10^{-8}T - 3.4484\times10^{-6}}{\rho} \tag{2.48}$$

where ν_0 is dry air kinematic viscosity in standard atmosphere. In order to find the relation between kinematic viscosity and humidity, the input value of relative humidity is varied while maintaining a constant temperature of 20 °C, and standard atmosphere pressure. The trend line technique is applied in Figure 2.6 to get the moist air kinematic viscosity in standard atmosphere, ν_1.

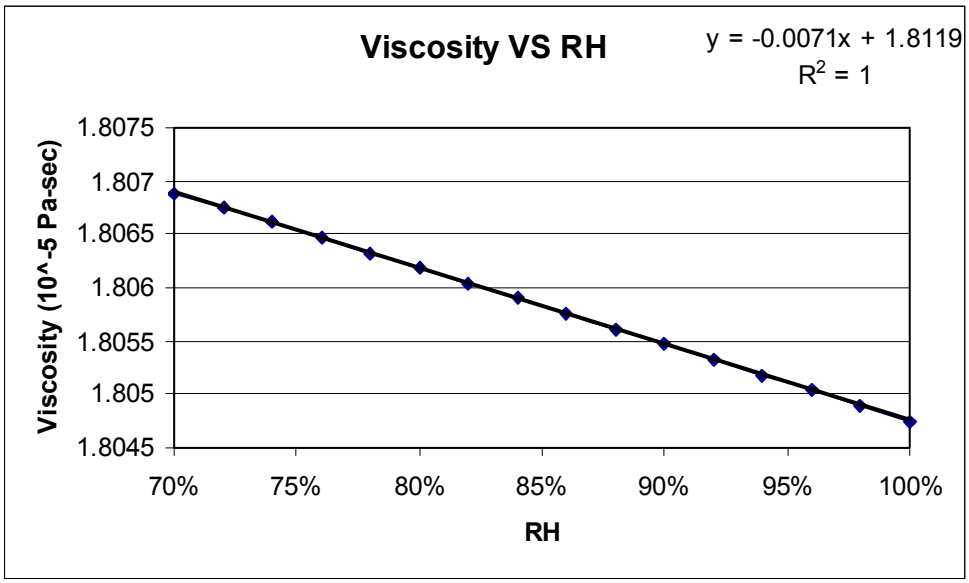

Figure 2.6 Kinematic viscosity VS relative humidity

$$\nu_1 = \nu_0 - 0.0071RH \tag{2.49}$$

The trend line matches the real line perfectly as R^2 is 1. In order to find out the relationship between kinematic viscosity and air pressure, the input value of air pressure is varied during conditions of constant temperature 20 °C and relative

humidity 70%, and the trend line technique is again applied in Figure 2.7 to get moist air viscosity ν.

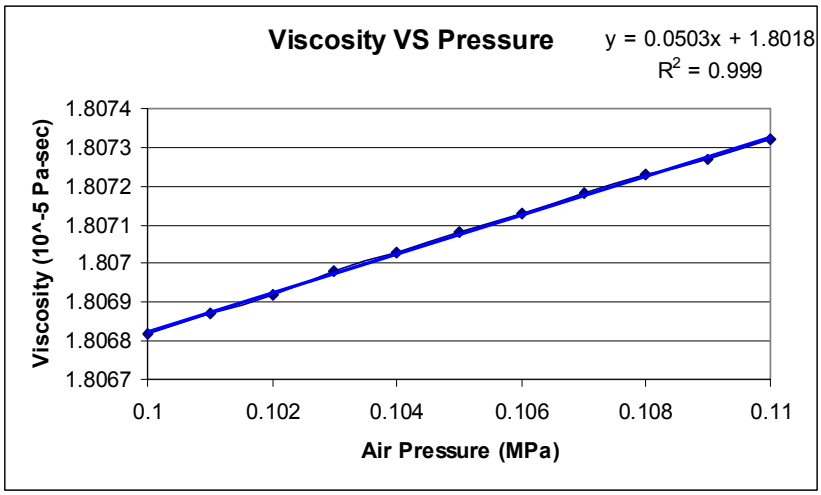

Figure 2.7 Viscosity VS air pressure

$$\nu = \nu_1 + 0.050.\times(P - P_{atm})\times 10^{-5} \tag{2.50}$$

The trend line matches the real line well as indicator R^2 is 0.999. Relative kinematic viscosity can be expressed as.

$$\mu = \frac{\nu}{\rho} \tag{2.51}$$

Combining Equations (2.48), (2.49), (2.50) and (2.51) yield:

$$\begin{aligned}\mu = &(-1.1555\times 10^{-14}T^3 + 9.5728\times 10^{-11}T^2 + 3.7604\times 10^{-8}T - 3.4484\times 10^{-6} \\ &- 0.0071RH + 0.050.\times(P - P_{atm})\times 10^{-5})/\rho\end{aligned} \tag{2.52}$$

From Equation (2.52), it can be seen that the viscosity of moist air is a function of air temperature, pressure and humidity.

2.3.4 Computation of Air Thermal Conductivity

The thermal conductivity of dry air in standard atmosphere pressure k_0 can be expressed as [67]:

$$k_0 = 1.5207\times10^{-11}T^3 - 4.8574\times10^{-8}T^2 + 1.0184\times10^{-4}T - 3.9333\times10^{-4} \quad (2.53)$$

In order to find the relationship between thermal conductivity and humidity, the input value of relative humidity is varied during conditions of constant temperature 20 °C and standard atmosphere pressure. The trend line technique is applied in Figure 2.8 to get the moisture air thermal conductivity in the standard atmosphere k_1.

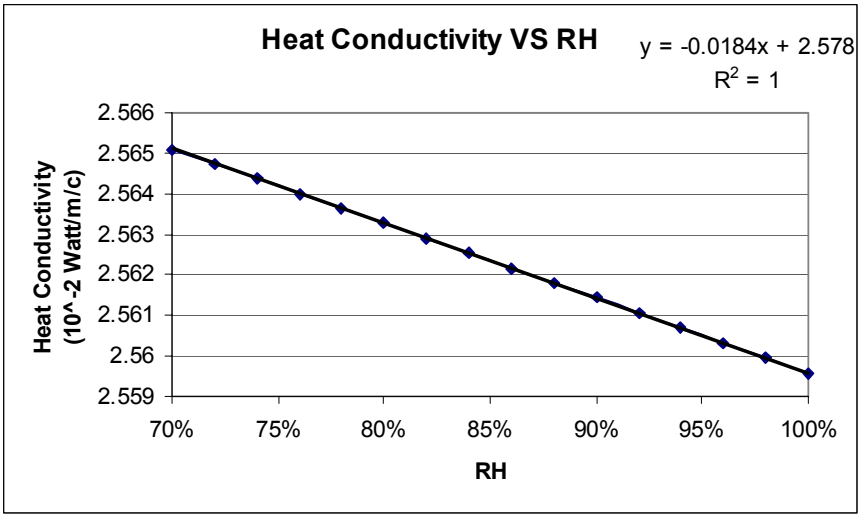

Figure 2.8 Heat conductivity VS relative humidity

$$k_1 = k_0 - 0.0187\times RH \quad (2.54)$$

In order to determine the relationship between the thermal conductivity and air pressure, the input value of air pressure is varied during conditions of constant temperature 20 °C and relative humidity 70%. The trend line technique is applied in Figure 2.9 to get moist air thermal conductivity k.

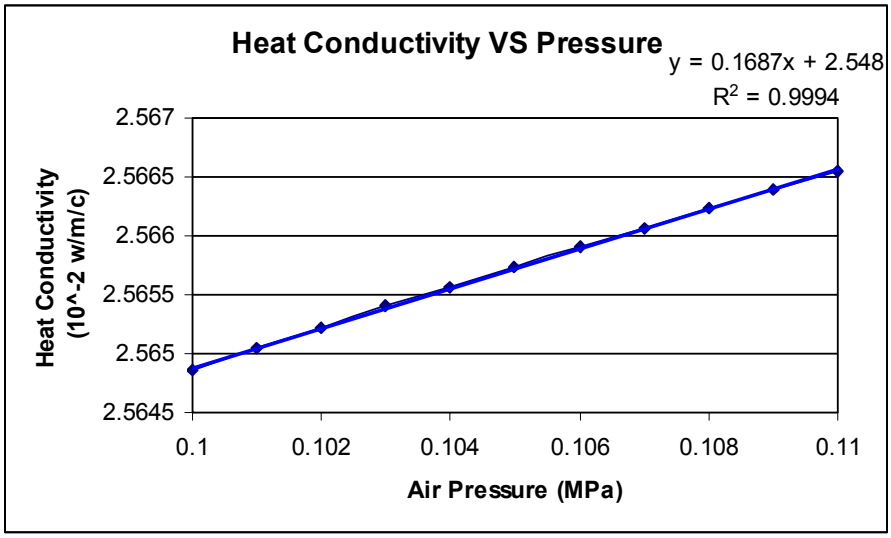

Figure 2.9 Heat conductivity VS air pressure

$$k = k_1 + 0.1687 \times P \times 10^{-2} \tag{2.55}$$

Combining Equations (2.53), (2.54) and (2.55) to yield:

$$k = 1.5207 \times 10^{-11} T^3 - 4.8574 \times 10^{-8} T^2 + 1.0184 \times 10^{-4} T - 3.9333 \times 10^{-4} - 0.0187 \times RH + 0.1687 \times P \times 10^{-2} \tag{2.56}$$

From Equation (2.56), it can be seen that thermal conductivity of moist air is a function of air temperature, pressure and humidity. Substituting Equation (2.58), (2.47), (2.52) and (2.56) into Equation (2.8) and (2.30), yields the forced convective coefficient h and the function of forced convective heat lost, $Q_{convert}$.

$$h = f(T, RH, P, d) \tag{2.57}$$

$$Q_{convect} = f(T_w, T_a, h, A_w) \tag{2.58}$$

The forced convection coefficient is a function of air temperature, relative humidity, air pressure and diameter of wire. Heat loss power can be computed by convection coefficient, surface area of wire, ambient air temperature and hot wire temperature. All relevant equations are applied to the simulation model which is detailed in Chapter 3. Forced convective heat loss effect from the hot wire is significant, but it does not mean other kinds of heat loss can be neglected. The other three types of heat loss, conduction, radiation and natural convection are investigated in the following Sections.

2.4 Conductive Heat Loss

Conductive heat loss is another significant source of heat loss from the hot wire sensor, as both the hot wire and support pin are made from metals, both have high thermal conductivities. Although the conductivities of wire and pins can be found from literature, the conductive power is depended on temperature.

As the maximum temperature value of wire is one of the input parameters, the conductive heat loss from the hot wire can be calculated from this condition. This heat conductive system can be treated as two types of thermal resistance. The first type is the normal metal internal thermal conduction from the middle point of the wire to the end point on the pin surface [45]. The wire is divided into 16 equal length lumps. The serial 8 thermal resistances from left end to midpoint (R1 to R8) are represented in Figure 2.10.

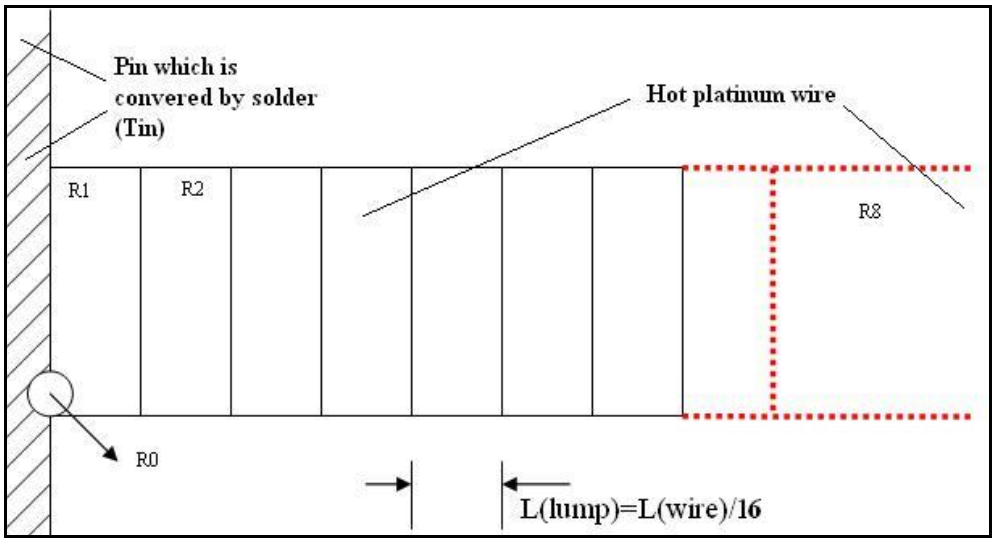

Figure 2.10 Thermal resistance to centre of hot wire

The first type of conductive thermal resistance $R_{thermal1}$ is expressed in Equation (2.59) [44]:

$$R_{thermal1} = \frac{L/16}{k_{c1} \times A} \times 16 = \frac{L}{k_{c1} \times A} \tag{2.59}$$

where k_{c1} is the thermal conductivity of platinum, and the average value 71.6 w/m.k is picked used [48] and A is the cross area of wire.

The second type of contact thermal resistance $R_{thermal2}$ exists between the first lump and the pin surface, as the cross sectional area of wire is smaller than the soldered tin surface. Bonding platinum wire and pins by soldering can be modelled as a disk (the first lump) with temperature T_1 on a semi-infinite medium of temperature T_0, shown in Figure 2.11. Then the conduction shape factor is applied to calculate the thermal resistance [45].

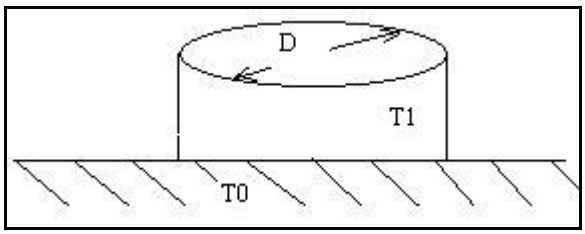

Figure 2.11 Contact thermal resistance

$$R_{thermal2} = \frac{1}{2Dk_{c2}} \tag{2.60}$$

where k_{c2} is the thermal conductivity of tin (the main constituent of solder), D is the diameter of wire. The heat power transferred in one half of wire, Q_{side}, can be obtained by knowing the temperatures and thermal resistances.

$$Q_{side} = \frac{T_8 - T_0}{R_{thermal1} + R_{thermal2}} \tag{2.61}$$

Equation (2.61) was multiplied by two to get the total heat loss power through conduction from hot wire, $Q_{conduct}$:

$$Q_{conduct} = \frac{16\Delta T}{R_{thermal1} + R_{thermal2}} \tag{2.62}$$

Equation (2.62) is the essential expression to develop the wire conductive heat loss model.

2.5 Radiant Heat Loss

To compute the radiant heat loss from the hot wire, according the assumption in section 2.1, the platinum wire is lumped into 8 equal parts from the middle point to the end, serially, temperature is distributed in Each lump as shown in Figure 2.11 2.12.

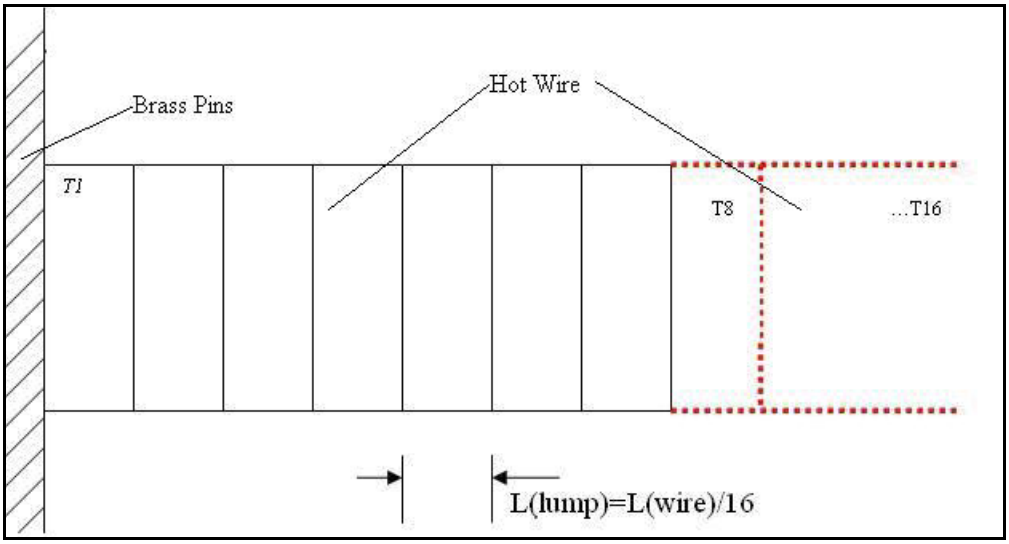

Figure 2.12 Temperature distribution of hot wire

The unit power of radiant heat loss $q_{radiate}$ is expressed as:

$$q_{radiate} = \varepsilon_{res}\sigma\sum_{i=1}^{8}(T_{wi}^4 - T_a^4) \tag{2.63}$$

where:

σ is the *Stefan-Boltzmann* constant which value is 5.67×10^{-8} W/m^2.K^4,

ε_{res} is the emissivity of the hot wire,

T_{w1}, T_{w2}, to T_{w8} are absolute temperatures of each lump of hot wire,

T_a is the ambient absolute temperature.

ε_{res} is found in the range of 0.1 to 0.4 [45], hence, it is assumed to have an average value of 0.3. Substituting the values into Equation (2.63) to get the heat loss power of radiation, $Q_{radiate}$:

$$Q_{radiate} = q_{radiate}\cdot\frac{A_w}{8} = \varepsilon_{res}\sigma.(L_w/8).W\cdot\sum_{i=1}^{8}(T_{wi}^4 - T_a^4) \tag{2.64}$$

where W is circumference of wire cross sectional area, L_w is length of wire. From Equation (2.64), it can be seen that the radiant heat loss is significantly affected by the wire temperature, thus, the hot wire is not allowed to operate in extreme high temperature so as to minimise the effect of radiant heat loss.

2.6 Natural Convective Heat Loss

Although the effect of natural convection is eliminated whilst forced convection occurs practically, for the purpose of the analysis, the natural convective heat loss was considered for situations of lower air velocity. The natural convective heat loss power over the surface in practice Q_{NC} can be represented by the follow Equation [44]:

$$Q_{NC} = \bar{h}\, A_s (\bar{T}_s - T_a) \tag{2.65}$$

where $\bar{T}_s$ is the mean value of wire surface temperature, $\bar{h}$ is the coefficient of natural convection, which is generally found from the mean value of Nusselt number, $\overline{Nu}_L$ [44]:

$$\overline{Nu}_L = \frac{\bar{h}\, L_c}{k} \tag{2.66}$$

where L_c is the characteristic length of geometry and k is the air thermal conductivity. There is another expression of $\overline{Nu}_L$, developed by Churchill [44], excludes the need to determine the convention film coefficient $\bar{h}$, rather a correlation that is applicable to a variety of natural convection flows for which the primary buoyant driving force is directly tangential to the surface is used.

$$\overline{Nu}_L = (\alpha + 0.331 b Ra_L^{1/6})^2 \tag{2.67}$$

where α and b are coefficients, Ra_L is the Reynolds number of characteristic length. Combining Equation (2.66) and (2.67) gives:

$$\frac{\overline{h}\,L}{k} = (\alpha + 0.331 b Ra_L^{1/6})^2 \tag{2.68}$$

Coefficient b is obtained from the follow Equation:

$$b = \frac{1.17}{[1+(0.5/\mathrm{Pr})^{9/16}]^{8/27}} \tag{2.69}$$

where P_r is calculated from Equation (2.7), and Ra_L is obtained from Equation (2.70):

$$Ra_L = \frac{g\beta(\overline{T}_s - T_a)L_c^3}{\nu\alpha} \tag{2.70}$$

where T_a is the reference fluid (air) temperature, g is gravity, β is the coefficient of thermal expansion for ideal gases , which is equal to $1/T$. For the surface of a horizontal cylinder, the characteristic length L_c is equal to the product of π and d [44], and the coefficient α is 1.06 . Applying both parameters to Equation (2.68) gives:

$$\overline{Nu}_L = (1.06 + \frac{0.331\times 1.17}{[1+(0.5/\mathrm{Pr})^{9/16}]^{8/27}} Ra_L^{1/6})^2 \tag{2.71}$$

Substituting Equation (2.66) into (2.65) gives:

$$Q_{NC} = \frac{\overline{Nu}_L \times k \times A_s(\overline{T}_s - T_a)}{L_c} \tag{2.72}$$

Assuming 8 lumps in each half side of wire, $\bar{T}_s$ is replaced by the individual temperature of each lump which relates to the maximum temperature of wire T_{Max}.

$$Q_{NC} = \frac{\overline{Nu}_L \times k \times (A_s/8) \times \frac{9(T_{\max} - T_a)}{2}}{L_c} = \frac{9\times \overline{Nu}_L \times k \times A_s \times (T_{\max} - T_a)}{16 L_c} \tag{2.73}$$

As all parameters in the right hand side of above Equation (2.73) can be obtained from previous equations.

2.7 Generated Heat Power

According to the fundamental operating of hot wire air flow sensors, the generated heat power on the wire $Q_{generate}$ is equal to the sum of all the heat losses mentioned previously.

$$Q_{generate} = Q_{convective} + Q_{conduct} + Q_{radiate} + Q_{NC} \tag{2.74}$$

From electrical laws, generated power is dependent on the wire current i_w and instant wire resistance, R_w.

$$Q_{generate} = i_w{}^2 R_w \tag{2.75}$$

Combining Equation (2.74) and (2.75), enable the wire current to be expressed as:

$$i_w = \sqrt{\frac{Q_{convective} + Q_{conduct} + Q_{radiate} + Q_{NC}}{R_w}} \tag{2.76}$$

The potential of hot wire e_0 can be computed as:

$$e_o = i_w \times R_w = \sqrt{R_w \times (Q_{convective} + Q_{conduct} + Q_{radiate} + Q_{NC})} \tag{2.77}$$

Since this measurement system is a first order system, the mean value of time constant can be obtained from Equation (2.77) and expressed as:

$$e_o(D) = \frac{1}{\tau D + 1} \times \sqrt{R_w \times (Q_{convective} + Q_{conduct} + Q_{radiate} + Q_{NC})} \tag{2.78}$$

where τ is the time constant which can be obtained from previous Equation (2.29).

2.8 Verify Strength of Platinum Wire

The sensor probe, which is the thin platinum wire, should be strong enough to withstand the cross-flow air stream. Otherwise it is not suitable for application within the CPAP system. The verification is arranged in following sequence with reference to Figure 2.13:

1. Calculate the air flow force apply on the wire surface.
2. Determine the stress of the platinum wire caused by the air flow.
3. Compare the stress to the maximum allowable stress permitted with the wire.

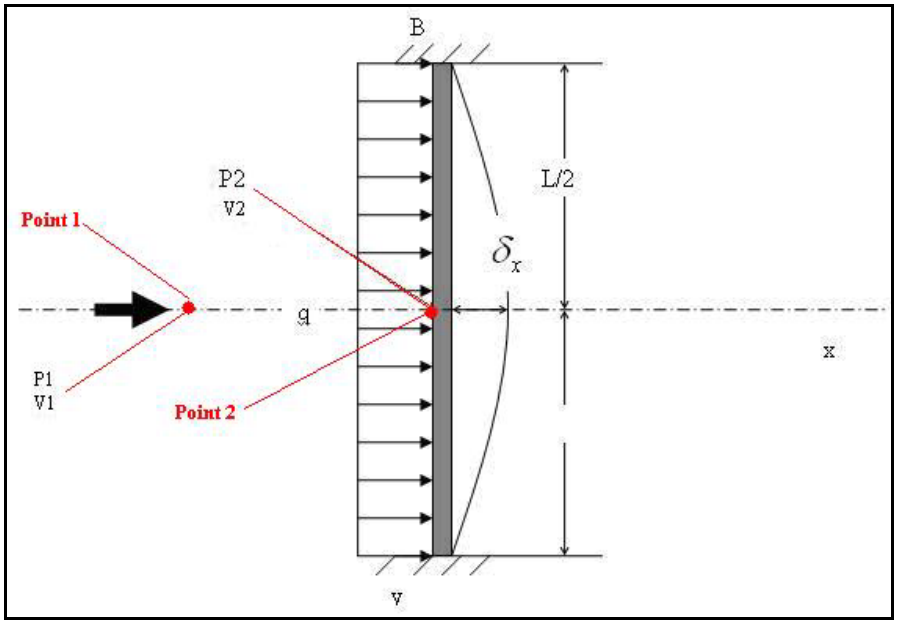

Figure 2.13 Air flow force on the hot wire

The bold arrow shown in Figure 2.13 indicates the direction of the air stream which is normal to the axis of wire. The wire is fixed at both ends with the length L. The air pressure on the wire causes unit force q along the wire. The pressure relationship between point 1 and point 2 in Figure 2.13 is expressed as following from Bernoulli's Equation [52, 53]:

$$P_1 + \frac{1}{2}\rho V_1^2 + \rho g h_1 = P_2 + \frac{1}{2}\rho V_2^2 + \rho g h_2 \tag{2.79}$$

where P_1 is the static pressure in the free stream, which value is zero, P_2 is the static pressure on the wire, V_1 is the air velocity of the stream and V_2 is the stagnation velocity on the wire surface, which is equal to zero. Assume the flow direction is

parallel to the ground. The height of two points, h_1 and h_2, are same, Equation (2.79) is simplified:

$$\frac{1}{2}\rho V_1^2 = P_2 \tag{2.80}$$

Assuming the diameter of platinum wire to be (ϕ) 0.02 mm and the length is 5.0 mm in this project, and applying the physical law of pressure, the force along x axis, F_x, is expressed as :

$$F_x = P_2 \times A = P_2 \times (d \times L) = P_2 \times 10^{-7} \tag{2.81}$$

Substituting Equation (2.80) into Equation (2.81) gives an expression of air flow force:

$$F_x = P_2 \times 10^{-7} = \frac{1}{2}\rho V_1^2 \times 10^{-7} \tag{2.82}$$

According to relevant Equations [54], the deflection δ_x along axis of x is caused by the air stream on the wire which can be expressed as:

$$\delta_x = \frac{5qL^4}{384EI} \tag{2.83}$$

where:

L is the length of wire, which value is measured 0.005 m,

q is the unit length load intensity on the wire,

E is Young's modulus of platinum, which value is 168×10^6 Pa [49],

I is the platinum area moment of inertia.

According to the definition of I and bases on the wire geometry, it can be expressed as:

$$I = M \cdot r^2 = \rho_p V (\frac{L}{2})^2 = 2104.78\times10^{-31} \tag{2.84}$$

where ρ_p is the density of platinum, given as 21.45×10^3 kg/m^3 [49], the uniformly distributed load on the wire can be expressed as:

$$q = F_x / L = \frac{1}{2}\rho V_1^2 \times 10^{-7} / 5 \times 10^{-3} = \rho V_1^2 \times 10^{-5} \tag{2.85}$$

Substituting Equation (2.84) and (2.85) into Equation (2.83) gives the deflection along x axis δ_x:

$$\delta_x = \frac{5qL^4}{384EI} = 4.8578 \times 10^{-18} \times V_1^2 \tag{2.86}$$

Assuming the air velocity to be a maximum of 10 m/s, means the air flow rate is about 3.14 l/s, which is higher than the maximum air flow rate experienced with typical CPAP system. Figure 2.14 shows the analysis of the wire deflections caused by the horizontal air stream. Point A is a fixed end of wire and point B is the middle point of wire in the static air. Point C is the middle point of wire deflected from point B in the flow air. Line AB is the original length of the half wire, line BC is the deflection δ_x and line AC is the deflection δ_y and length of the half wire in the air stream. Bases on the proposed wire geometry, the relationship of δ_x and δ_y are expressed in follow Equation:

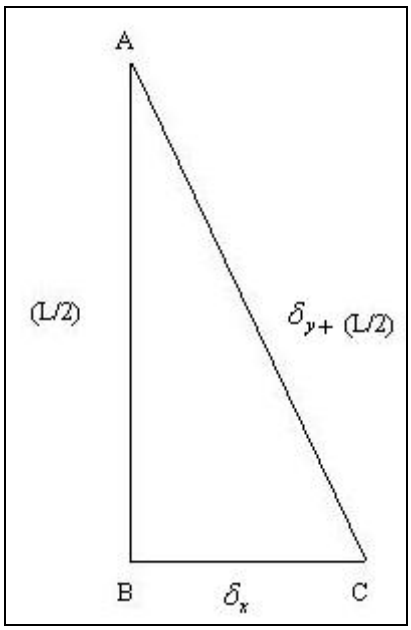

Figure 2.14 Wire deflection

$$\delta_y = \sqrt{(L/2)^2 + \delta_x^2} - (L/2) = 1.9 \times 10^{-12} \tag{2.87}$$

The strain along the wire axis ε_y is calculated as:

$$\varepsilon_y = \frac{\delta_y}{(L/2)} = \frac{1.9\times10^{-12}}{0.0025} = 7.6\times10^{-10} \tag{2.88}$$

From the definition of E, the stress of wire σ_y is:

$$\sigma_y = \varepsilon_y \times E = 7.6\times10^{-10}\times168\times10^{6} = 1276.8\times10^{-4} = 0.12768 \text{ Pa} \tag{2.89}$$

From the table of commercial grade platinum properties [55], The maximum strain is 90 KPSI (620500 kPa), which is absolutely larger than the calculated result in Equation (3.41), so the platinum wire will withstand the air flow velocity of 10 m/s typically experienced in the CPAP system.

2.9 Conclusions

Mathematical Equations of energy conversions have been developed. In order to deeply analyze the influence of wire properties and environmental condition during the measurement process, a model which is capable of variation in individual parameters is to be developed. Models of individual energy conversions were created by using Simulink™ software within Matlab™ environment. The output is obtained to compare the behaviour of the hot wire air flow sensor. The Simulation model of constant hot wire air flow sensor is presented in chapter 3.

Chapter 3 Model Simulation of Hot Wire Sensor

3.1 Introduction

The equations obtained to model the hot wire thermodynamic behaviour, in chapter 2, are now used to build a computer simulation model of hotwire sensor in the Matlab^{TM} environment. The general model flowchart is shown in Figure 3.1. The eight input parameters are utilised by five subsystems to determine the different kinds of heat loss from the hot wire and the response time of sensor. All four types of heat loss are investigated in the corresponding subsystems, and are summed together within a subsystem named generated power to compute generated power required to maintain a constant wire temperature. With the result of generated power and response time, wire current is obtained in a subsystem called Wire Current. Finally, the wire current is converted to the desired voltage within the Output Voltage subsystem. The general model is validated for accuracy and performance in Chapter 4.

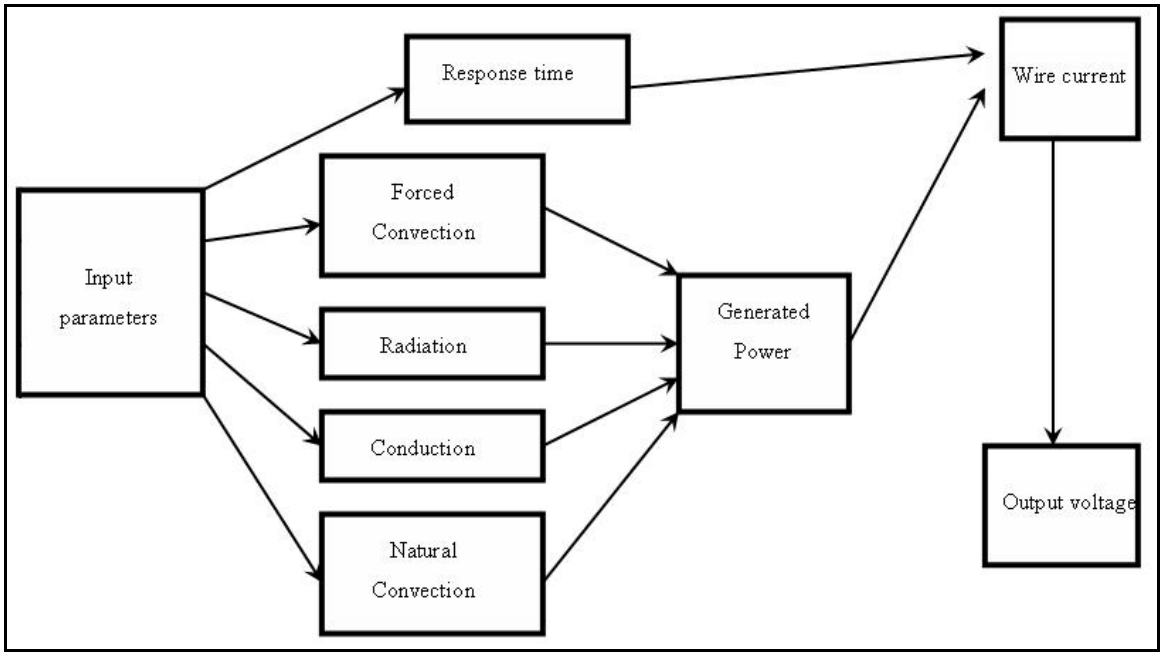

Figure 3.1 Flowchart of General Model

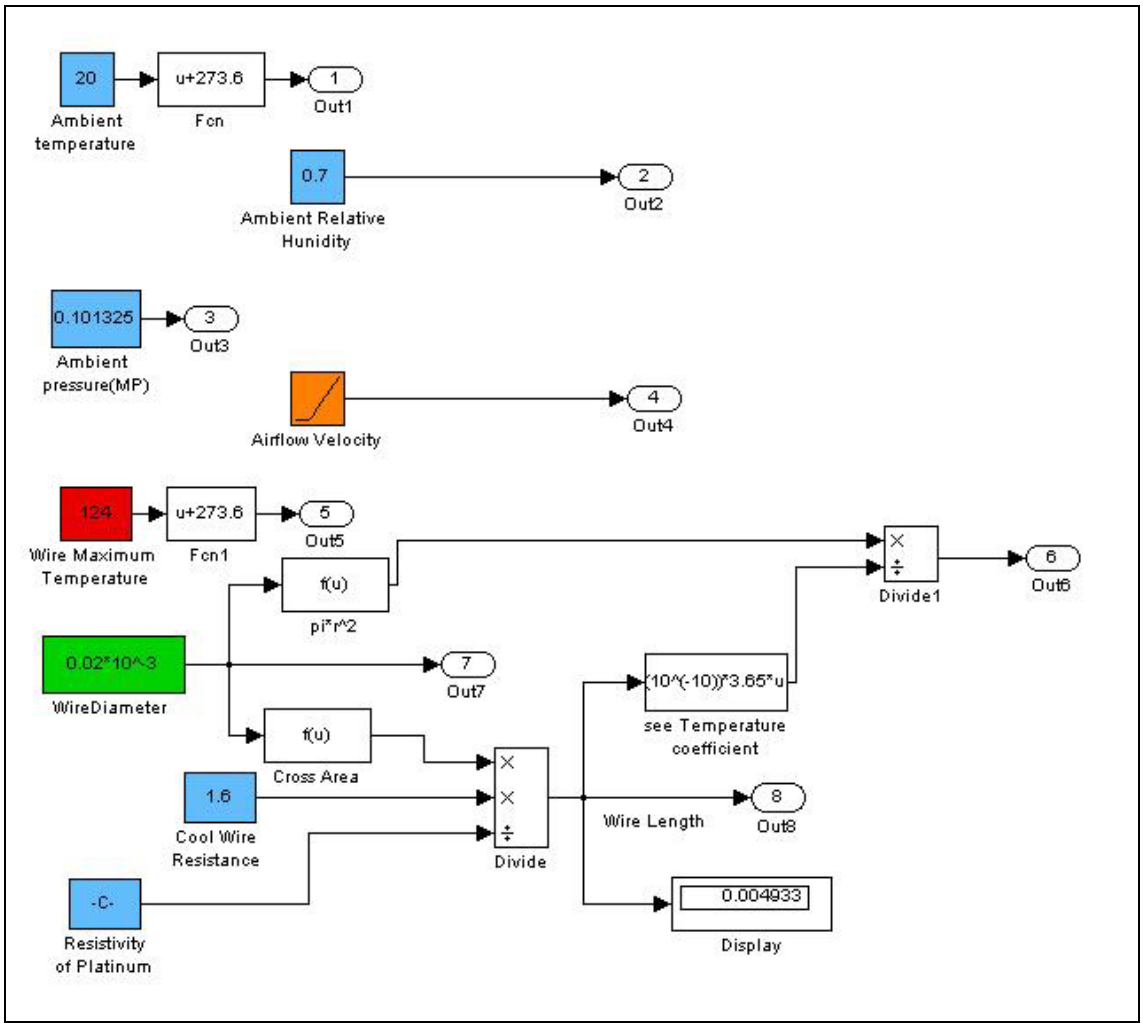

Figure 3.2 Details of Input Parameters Subsystem

Input parameters of the general model are listed in Table 3.1. The ambient conditions and wire properties are determined according to physical measurement. As the wire length is not easily measured after soldering, this parameter is obtained by measured wire resistance and the known wire resistivity. The maximum temperature is treated as one of the known input conditions, this value can be obtained by comparing the simulated hot wire resistance and the resistance value set up by the electronic circuit in relevant subsystem. Individual subsystems are expanded and presented in the following sections.

Table 3.1 Inputs of Input Parameters Subsystem

Input No.	Input name	Input source
1	air temperature	Reading ambient absolute temperature
2	RH	Reading relevant humidity
3	P	Reading ambient air pressure
4	air velocity	Setting value of air velocity
5	Wire Maximum Temperature	Setting maximum hot wire temperature
6	wire diameter	Reading wire diameter
7	Cool wire resistance	Measured value of wire resistance
8	Resistivity of platinum	Platinum resistivity at $20^0C = 10.19 \times 10^{-6} \Omega.cm$ [48]

3.2 Response Time

Physically the hot wire air flow sensor behaviours as a first order instrument of time constant corresponding to the response time. The subsystem model of sensor time constant is developed in Figure 3.3.

This subsystem model, called Response Time, is constructed by 5 smaller subsystem models. As the calculation of response time is quite complicated, parameters such as some air properties, wire mass, effective air flow velocity and forced convective coefficient are calculated in corresponding subsystem models. The output results of these subsystems are applied into the calculation subsystem model to obtain the response time. The response time value is then substituted into a subsystem called Wire Current (see section 3.8). All inputs of the Response Time subsystem are listed in Table 3.2. Ambient parameters such as temperature, relative humidity and pressure are obtained from actual measurement taken. Dimensions of wire such as diameter and length are measured. Specific heat capacity of wire (C) is obtained from literature [48-50]. Absolute temperature coefficient of wire is computed from relevant known conditions. Square of wire current (I2) is calculated from subsystem model of Wire

Current given in Section 3.9. Air velocity is the detected variable which directly affects model output. Inputs in

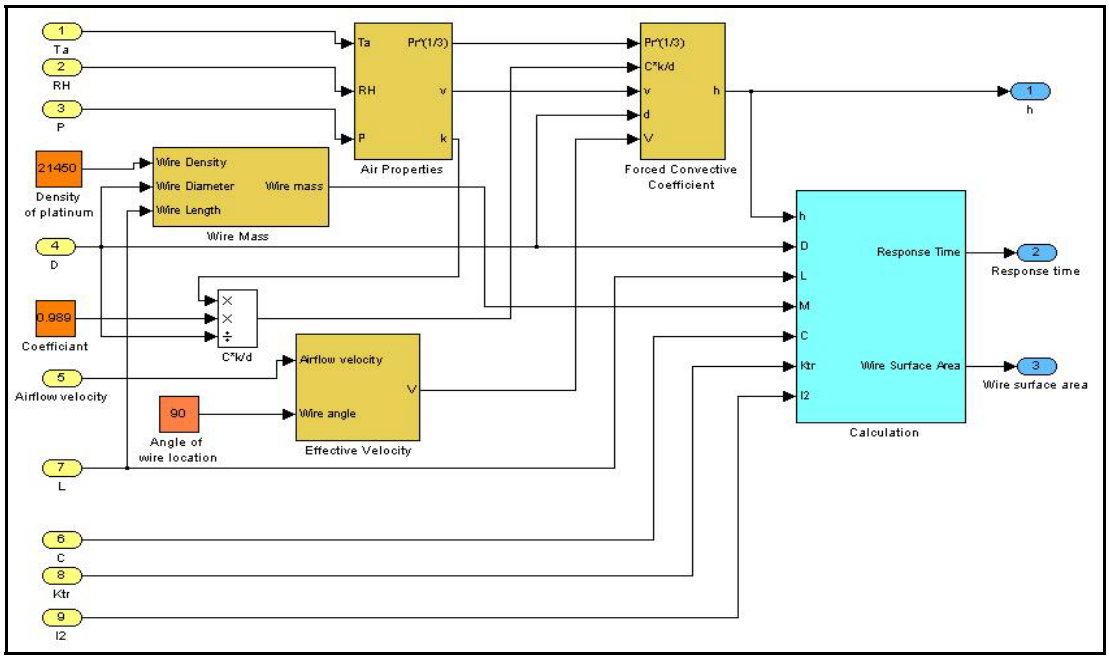

Figure 3.3 Details of Response Time Subsystem

Table 3.2 are applied to the 5 smaller subsystem models within the Response Time subsystem model. Details of the smaller subsystems are described from Section 3.2.1 to Section 3.2.5, respectively.

Table 3.2 Inputs of Response Time Subsystem

Input No.	Input name	Input source
1	Ta	Reading ambient absolute temperature
2	RH	Reading relevant humidity
3	P	Reading ambient air pressure
4	wire diameter	Reading wire diameter
5	Air velocity	Setting value of air velocity
6	C	Specific heat capacity of wire
7	L	Reading wire length
8	Ktr	Absolute temperature coefficient of wire
9	I2	Square of wire current

3.2.1 Air Properties

Several important air properties such as moisture content air density, specific heat capacity, viscosity, thermal conductive are determined from section 2.3. The simulation subsystem model is shown in Figure 3.4.

This subsystem has three inputs: ambient temperature, relative humidity and pressure. The outputs are Prandtl number, viscosity and thermal conductivity.

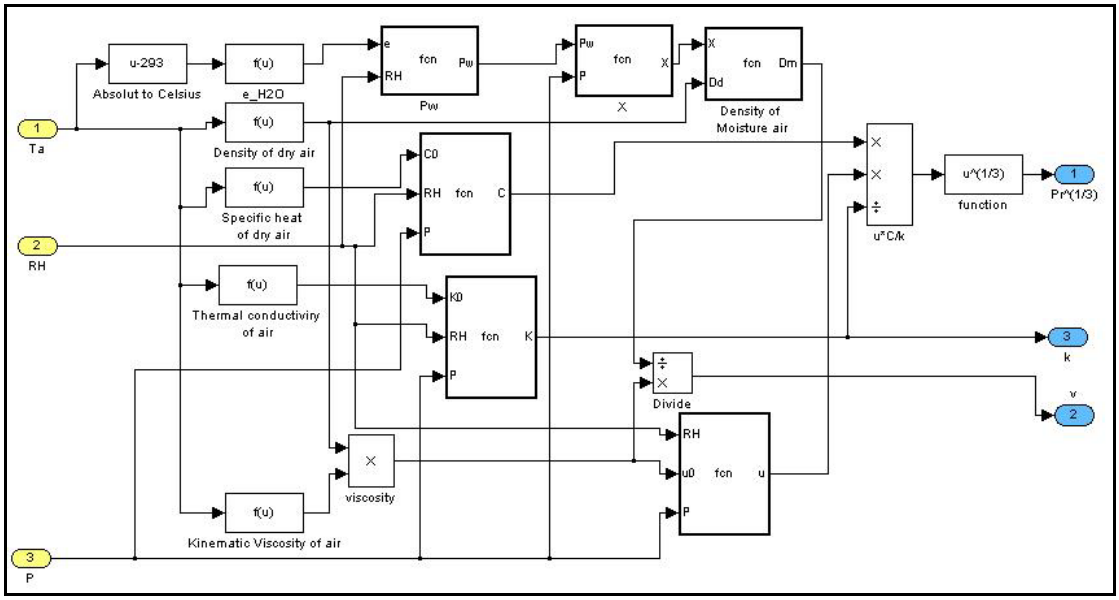

Figure 3.4 Details of Air Properties Subsystem

3.2.2 Wire Mass

One of the parameters that affect response time is wire mass which is determined from Equation:

$$M = \rho \times \pi (\frac{d}{2})^2 \times L \qquad (3.1)$$

There are three inputs in the subsystem, the wire (platinum) density, the wire diameter and the wire length and the output is platinum wire mass. The subsystem model is shown in Figure 3.5.

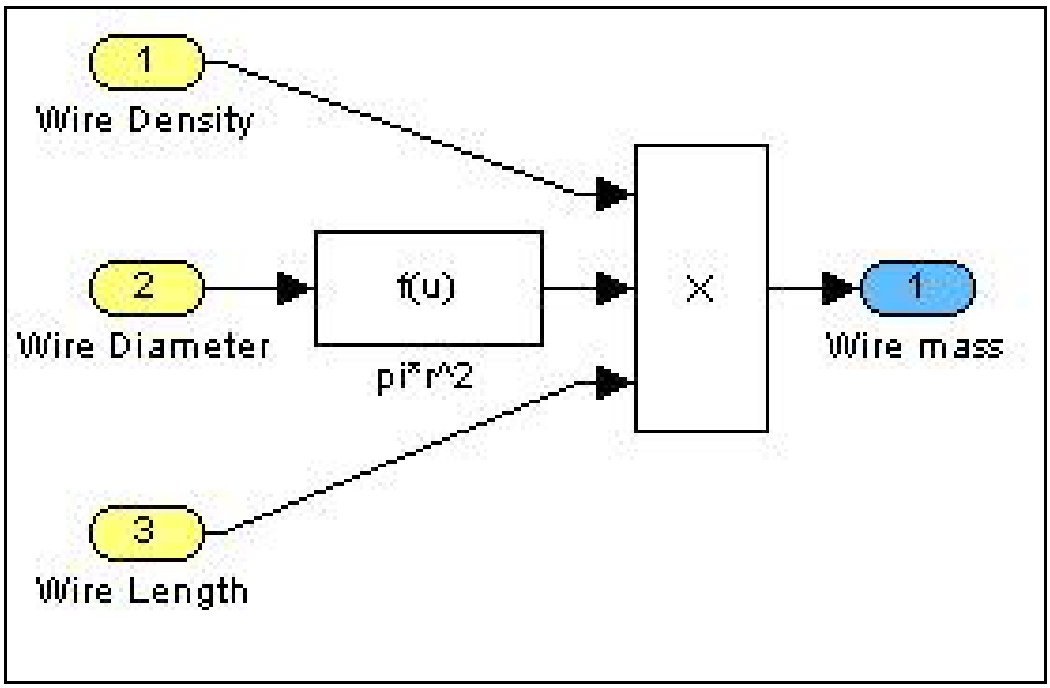

Figure 3.5 Details of Wire Mass Subsystem

3.2.3 Air Velocity

The effective air velocity subsystem model is developed in Section 2.2 and requires only two inputs into the model: the air flow velocity along the tube axis and the angle between wire axis and tube axis. Subsystem output is the effective air flow velocity. The subsystem model is shown in Figure 3.6 below:

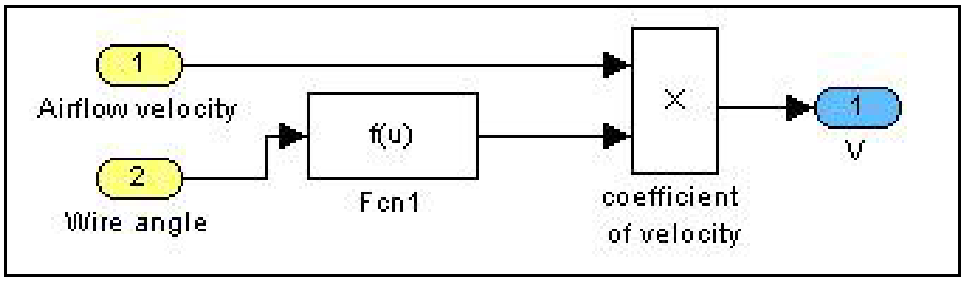

Figure 3.6 Details of Effective Velocity Subsystem

3.2.4 Forced Convective Coefficient

The forced convective coefficient subsystem model is developed in Figure 3.7. Inputs of the subsystem are listed in Table 3.3. As the result of Equation (2.7), the Prandtl number is determined from the subsystem called Air Properties, and the two parameters are input to simulate forced convective coefficient.

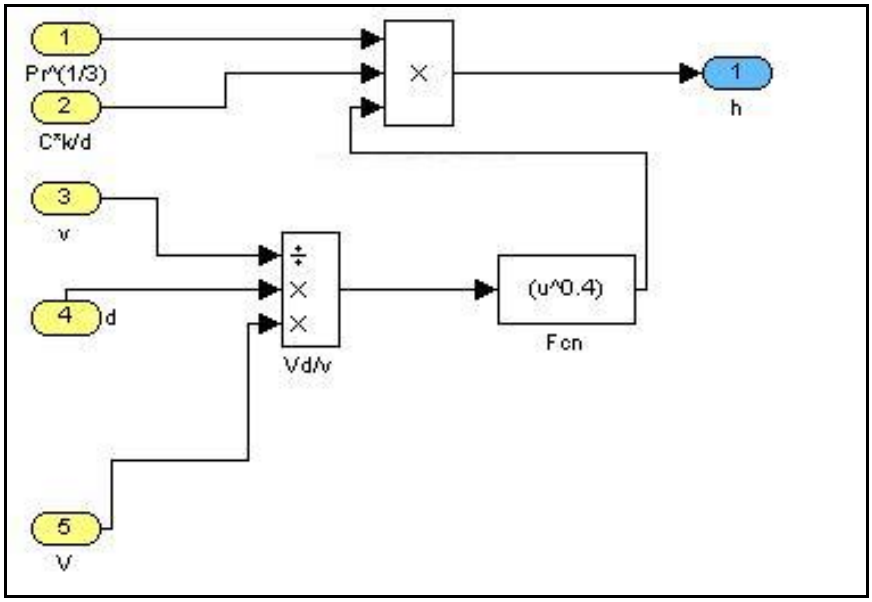

Figure 3.7 Details of Forced Convective Coefficient Subsystem

Table 3.3 Inputs of Convection Coefficient Subsystem

Input No.	Input name	Input source
1	Pr(1/3)	Prandtl number power of 0.33
2	C*k/d	0.9898*conductivity of air / wire diameter
3	v	The derivative kinematical viscosity of air
4	d	Reading wire diameter
5	V	Setting value of effective air velocity

3.2.5 Calculation

The calculation of the subsystem processes represents the final stage of the response time calculation, shown in Figure 3.8, and all inputs are listed in Table 3.4. Forced convective coefficient h is obtained from the Forced Convective Coefficient subsystem mentioned in Section 3.2.4, wire mass M is computed from the Wire Mass subsystem, given in Section 3.2.2. From the subsystem output, the wire time constant value is a function of air velocity. In order to obtain a properly mean value of time constant, the minimum air velocity in the CPAP operation range is considered. The corresponding time constant is applied into Wire Current subsystem presented in Section 3.9.

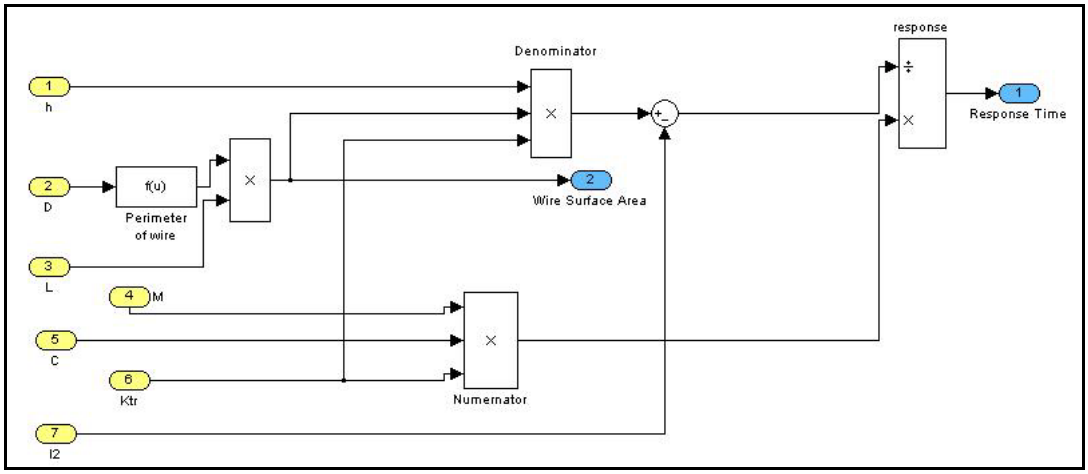

Figure 3.8 Details of Calculation Subsystem

Table 3.4 Inputs of Calculation Subsystem

Input No.	Input name	Input source
1	h	Forced convective coefficient
2	D	Reading wire diameter
3	L	Reading wire length
4	M	Wire mass
5	C	Specific heat capacity of wire
6	Ktr	Absolute temperature coefficient of wire
7	I2	Square of wire current

3.3 Forced Convection

The model of force convection heat loss is shown in Figure 3.9, which is developed in Section 2.3. Three inputs of forced convection subsystem are presented in Table 3.5, where current (A), forced convective coefficient comes from and Response Time subsystem, and wire temperature step comes from the calculation of ambient temperature and wire maximum temperature. The force convective heat loss of half of the 16 lumps along the wire results in 8 different temperatures being summed within this subsystem.

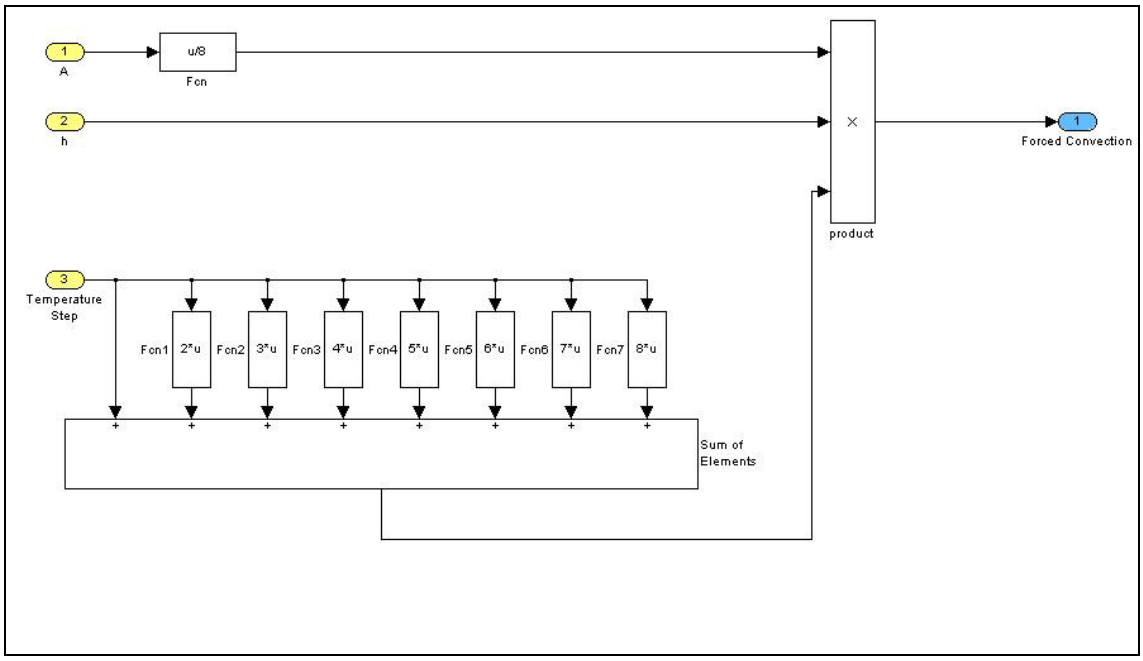

Figure 3.9 Details of Forced Convection Subsystem

Table 3.5 Inputs of Forced Convection Subsystem

Input No.	Input name	Input source
1	A	Wire surface area
2	h	Forced convective coefficient
3	Temperature Step	Temperature difference between neighbour lump of wire

3.4 Radiation

In the subsystem called Radiation (Figure 3.10), the resistance of the hot wire and the heat loss due to the radiation are obtained. Radiations of 16 lumps in 8 different temperatures were summed in this subsystem. Inputs of radiation subsystem are listed in Table 3.6.

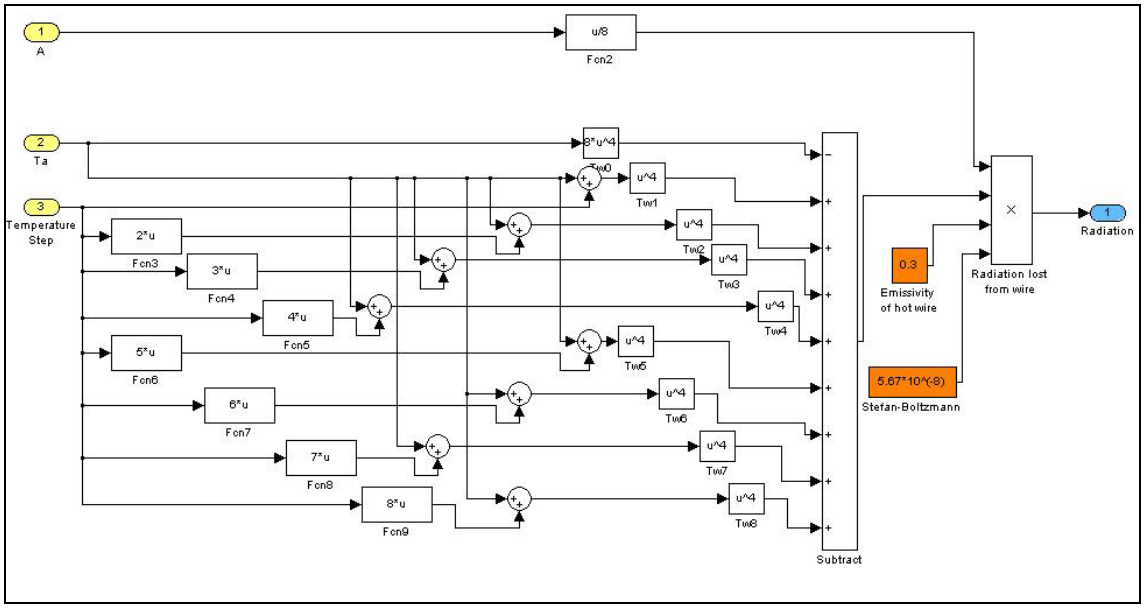

Figure 3.10 Details of Radiation Subsystem

Table 3.6 Inputs of Radiation Subsystem

Input No.	Input name	Input source
1	A	Wire surface area
2	Ta	Ambient temperature (pipe wall)
3	Temperature Step	Temperature difference between neighbour lump of wire

Inputs 1 and 2 come from the Input Parameters subsystem, Input 3 comes from the calculation of ambient temperature and wire maximum temperature.

3.5 Conduction

As the platinum wire is supported by two brass pins, thermal conduction loss from the hot wire to the cooler brass pins is unavoidable. Assuming the pins to have the same temperature as ambient air, the wire conductive heat loss is developed from section 2.4. The simulated model in Section 2.4 is presented in Figure 3.11. Relevant inputs are listed in

Table 3.7. Input 2, 3 come directly from the Input Parameters subsystem, and Input 1 is computed from wire temperature used in the Input Parameters subsystem. The conduction heat loss depends on the dimensions of wire and the maximum temperature different between hot wire and ambient air.

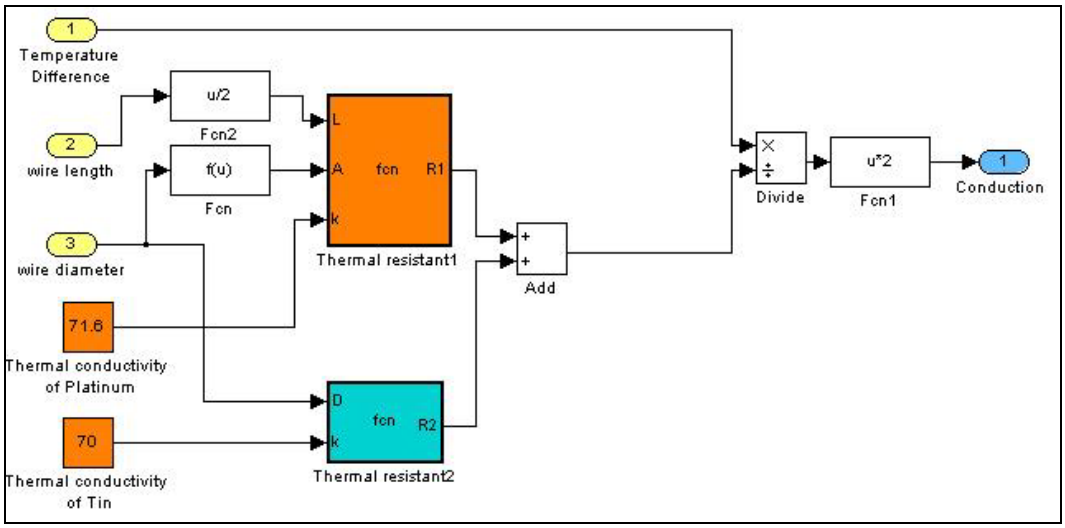

Figure 3.11 Details of Conduction Subsystem

Table 3.7 Inputs of Conduction Subsystem

Input No.	Input name	Input source
1	Temperature difference	Maximum temperature difference between wire and ambient
2	wire length	Calculated length of platinum wire
3	wire diameter	Reading diameter of platinum wire

3.6 Natural Convection

During period of low air flow, the air velocity is very small and can be considered as by natural convection only. The natural convection subsystem model is developed from section 2.5 shown in Figure 3.12. Temperatures and dimensions of wire are listed in

Table 3.8.

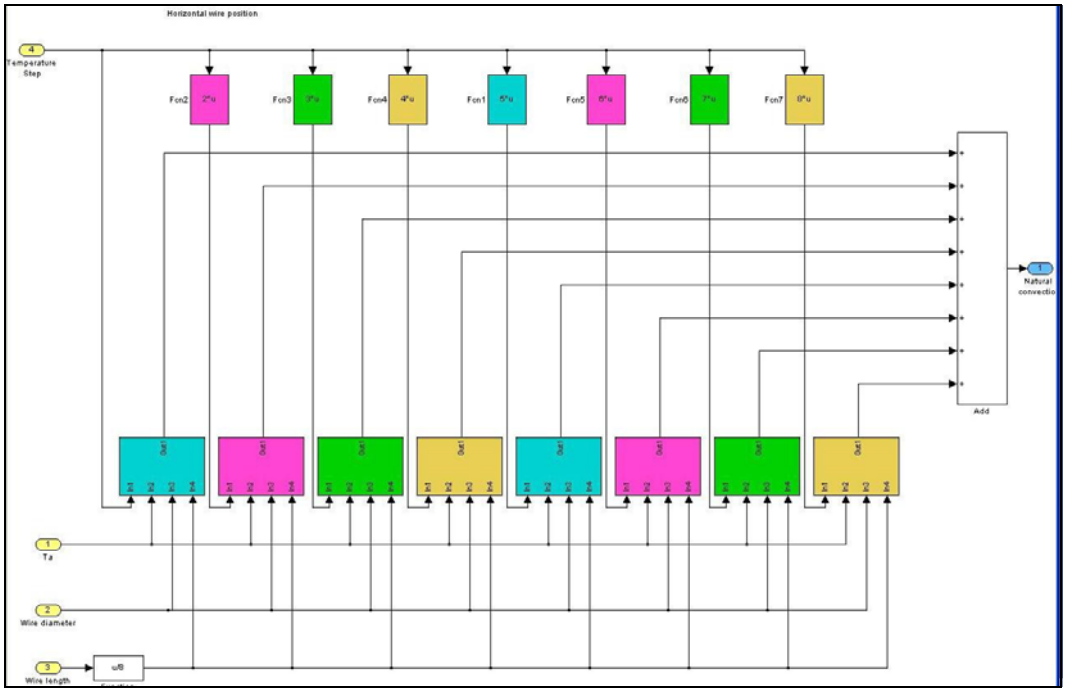

Figure 3.12 Details of Natural Convection Subsystem

Table 3.8 Inputs of Natural Convection Subsystem

Input No.	Input name	Input source
1	Ambient temperature	Reading temperature of air
2	Wire diameter	Reading diameter of platinum wire
3	Wire length	Calculated length of platinum wire
4	Temperature Step	Temperature difference between neighbour lump of wire

Input 1, 2 and 3 directly come from Input Parameters subsystem, and input 4 is computed from maximum wire temperature in parent subsystem.

3.7 Hot Wire Resistance

As states in Section 3.1, the maximum wire temperature is treated as one of the known conditions to be input, this value can be obtained by comparing the simulated hot wire resistance, which subsystem is shown in follow Figure 3.13:

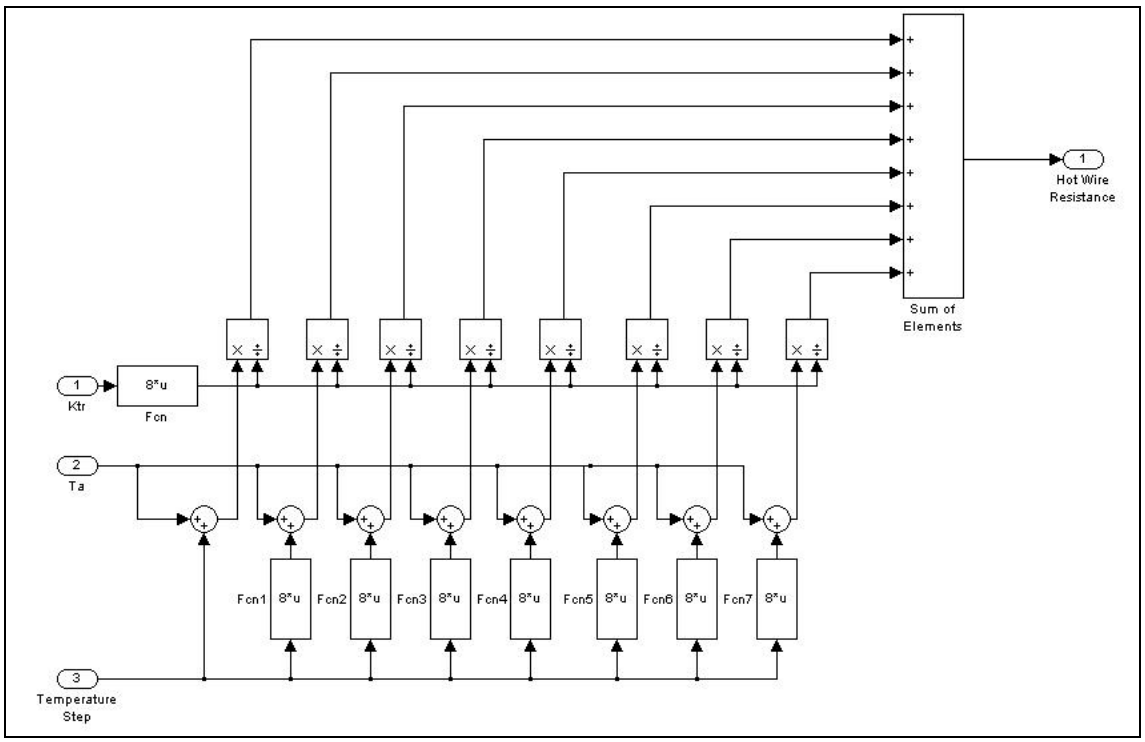

Figure 3.13 Hot Wire Resistance Subsystem

Assuming a linear temperature distribution along the wire, the temperature of each lump is related to the ambient temperature and maximum wire temperature.

$$T_i = T_a + \frac{(T_{\max} - T_a)}{8} \times i \tag{3.1}$$

Where i=1 to 8, is the lump order number from the end to the middle point of wire. According to the absolute temperature coefficient of wire K_{tr} , the lump resistance ($R_i = T_i / 8K_{tr}$), sums all lumps resistance which permits determination of the hot wire resistance. All inputs in the subsystem is listed in Table 3.9:

Table 3.9 Inputs of Hot Wire Resistance Subsystem

Input No.	Input name	Input source
1	Ktr	The absolute temperature coefficient of wire
2	Ambient temperature	Reading temperature of air
3	Temperature Step	Temperature difference between neighbour lump of wire

3.8 Generated Power

All of the heat losses described in Sections 3.3 to 3.6 are summed to get the generated power of the hot wire. The generated power subsystem is shown in Figure 3.14.

The output powers for each kind of heat loss obtained from the corresponding subsystems of, forced convection, natural convection, conduction and radiation are linked to the generated power subsystem as inputs, given in (Table 3.10). The single output of this subsystem is the generated power which accounts for all heat lost from the hot wire. As the hot wire is running at a constant temperature, the electrical resistance of hot wire is relatively stable. The input power to the wire is varied by adjusting the output current passing through the hot wire.

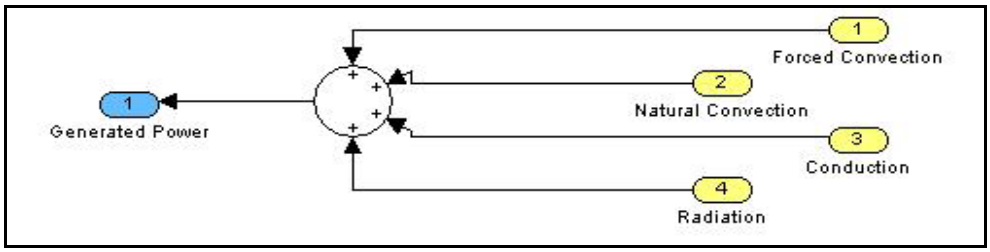

Figure 3.14 Details of Generated Power Subsystem

Table 3.10 Inputs of Generated Power Subsystem

Input No.	Input name	Input source
1	Forced convection	Forced convection subsystem model
2	Natural convection	Natural convection subsystem model
3	Conduction	Conduction subsystem model
4	Radiation	Radiation subsystem model

3.9 Wire Current

The wire current subsystem is shown below Figure 3.15. Input 1, the resistance of hot wire, and input 2, the generated heat power, are the main parameters used to determine hot wire current. The value of average response time is substituted into the first order function to simulate the practical current output. In order to conveniently observe the output, the output current is converted to output voltage by an electronic circuit.

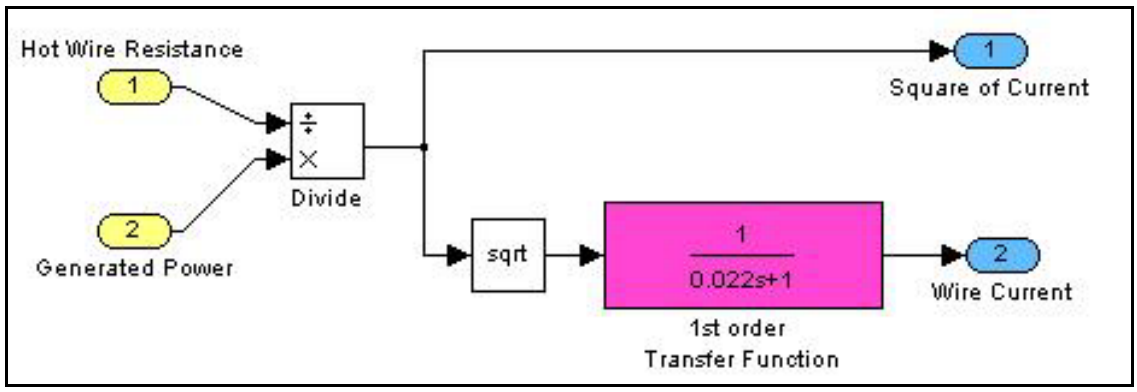

Figure 3.15 Details of Wire Current Subsystem

3.10 Conclusions

Physical properties of the hot wire sensor were considered to ensure the accuracy of hot wire air flow sensor simulation model. A computer simulation of the hot wire sensor has been produced to predict the behaviours of the sensor over a range of air flow conditions. As the essential factor related to the air flow velocity is the wire current of air flow sensor, whilst maintaining a constant temperature, the wire current is the focus object of this research and is verified in Chapter 4.

Chapter 4 Model Validation

4.1 Introduction

In Chapter 3 the simulation model of hot wire air flow sensor was developed. The purpose of this chapter is to find out whether the model can predict the dynamic behaviour or the sensor, a series of experiments were preformed to validate the model.

The operating principle of a hot wire air flow sensor prototype is described in Section 4.2. The effect of various environmental conditions and the sensor measurement is investigated in Section 4.3. Normally, the effect of the air temperature and press are considered the major factors that caused measurement error.

In order to understand the influence of ambient conditions on the sensor accuracy, a suitable location for the sensor was chosen and tested by experimentation in Section 4.4. Several experiments were performed to characterise the current curve of the hot wire, in Sections 4.6 to 4.9. Finally, the improved experimental result verified the model over the full range of CPAP air flow. The experimental current curve was applied to validate the corresponding simulation model obtained in Chapter 2, presented in Section 4.10.

4.2 Electronic Circuit and Prototype

The Wheatstone bridge is an essential element of the hot wire air flow sensor and is shown on the right hand side of the circuit (Figure 4.1). Elements of the circuit are listed in Table 4.1. Constant resistors R_1, R_2, R_3 and the hot wire resistor R_w form the Wheatstone bridge. The resistance rate between R_2 and R_3, is set to be equal to the rate between R_1 and hot wire resistance R_w. One amplifier in the dual low power operational amplifier LM258D is used in the role of comparator to compare the potential difference of R_4 and R_6 that is directly affected by voltage V_t (point between R_1 and R_w) and voltage V_r (point between R_2 and R_3).

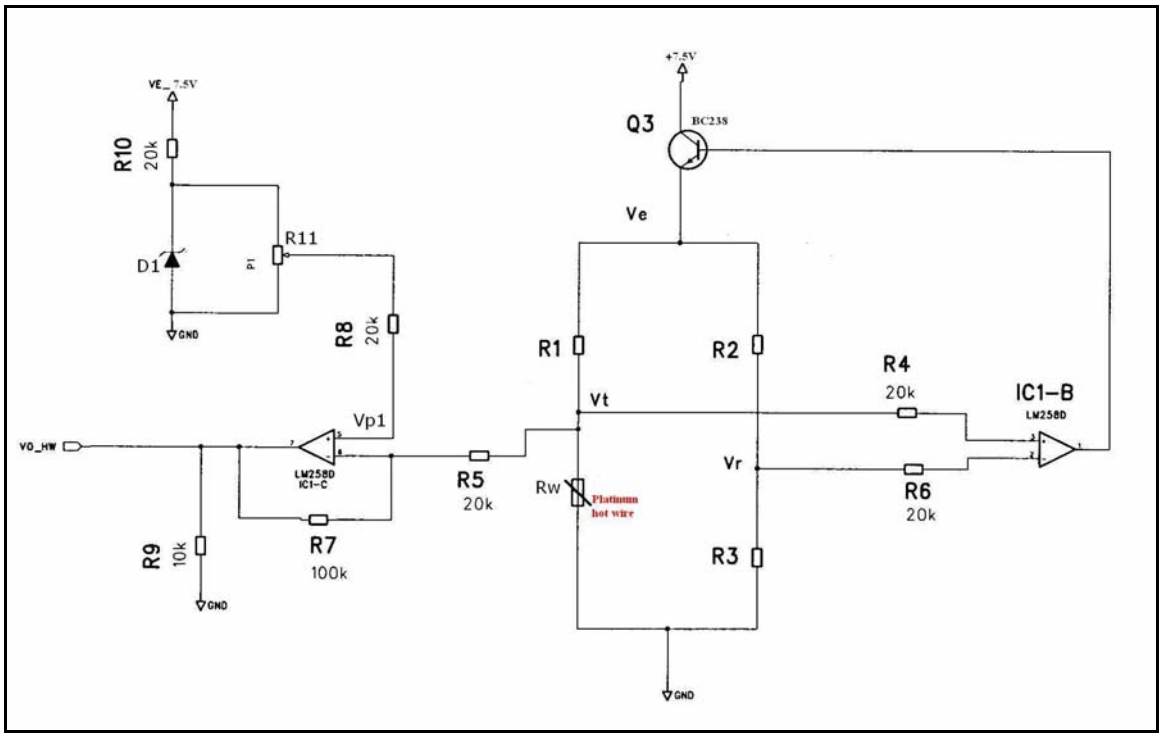

Figure 4.1 Electronic circuit of prototype

When air flow passes the hot wire, the temperature drops below the setting value, thus decreasing the hot wire resistance. This causes V_t to be smaller than V_r, which cause the comparator to output a logical positive voltage output V_b. As V_b is linked to the base of an amplifier transistor (BC238), the amplifier then increases the current of the emitter (hot wire current i_w) according to the serial electrical law, V_e divided by the sum of R_1 and R_w will give hot wire current i_w. The variation of emitter current can be detected by measuring the emitter voltage V_e.

The increase in hot wire current, i_w, causes wire temperature, T_w, to rise above the set value, which causes the wire resistance to increase, leading to the potential V_t being higher than the reference setting value V_r. Under this condition, the output voltage of the comparator immediately drops, causing the amplifier (BC238) to turn off and the wire current, i_w, decrease. Hence the wire temperature T_w goes back to the set value. Using this method, the wire temperature, T_w. can be reliably kept a constant value.

The left side of the circuit, Figure 4.1, has dual low power operational amplifier LM258D to raise the output voltage. In this part of the circuit, V_t presents the response

to the input signal which directly affects the generated power. The reference output voltage V_{p1} can be adjusted through variable resistor, R_1. The finished prototype is shown as Figure 4.2

Table 4.1 Elements of prototype circuit

Symbol	Elements	Function
R_1	Constant resistor	Construct Wheatstone bridge
R_w	Hot wire in the maintain temperature	Air flow probe
R_2	Constant resistor	Construct Wheatstone bridge
R_3	Constant resistor	Construct Wheatstone bridge
R_4	Constant resistor	Pass potential V_t to comparator
R_5	Constant resistor	Construct output amplifier
R_6	Constant resistor	Pass potential V_r to comparator
R_7	Constant resistor	Construct output amplifier
R_8	Constant resistor	Drop down output reference voltage
R_9	Constant resistor	Ground resistor of output voltage
R_{10}	Constant resistor	Resistor for zene diode
R_{11}	Variable resistor	Adjust output reference voltage
D1	Zene diode	Keep reference voltage stable
Q3	Amplifier transistor(BC238)	Offer maintain current to hot wire
IC1-B	Dual operational amplifier(LM258D)	Comparator and output amplifier

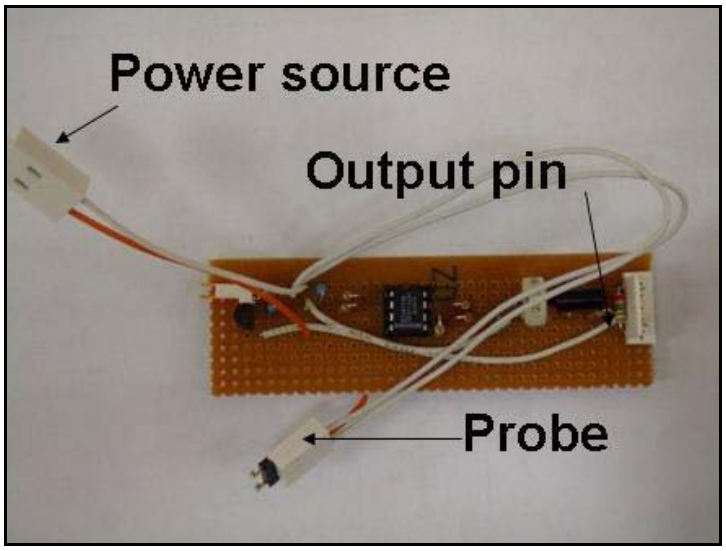

Figure 4.2 Prototype hot wire sensor control circuit

4.3 Influence of Variation in Ambient Conditions

Before setting up the experimental rig, sensor location within the CPAP system needs to be determined to ensure the accuracy of measurement. Excluding the properties of the hot wire, ambient conditions such as temperature, relative humidity and air pressure, will affect the accuracy of measurement as given in Chapter 2. In order to determine the effect of these factors, it was assumed that each ambient condition would vary as a sinusoidal wave within 2 second time period. The fluctuating conditions were set to the input of the model simulation and was called unstable model. Another simulation model with a constant input condition was called stable model. The input air flow rate was set to 2.0 m/s as a constant parameter for both models. The output difference between the unstable model and the stable model was divided by the stable model output to get the percentage error and expressed as a percentage for the level of accuracy.

Effect of Ambient Air Temperature

A fluctuated sinusoidal wave representing ambient air temperature in the range of 10 ^{o}C (283 K) to 30 ^{o}C (303 K) was input to the unstable model, as shown in Figure 4.3. The stable model had a constant ambient temperature input of 20 ^{o}C (293 K) applied. The output difference of these two models was divided by the output of stable model to get the percentage error shown in Figure 4.4. The percentage error varied from + 0.12 % to ─ 0.12 % corresponding to the fluctuating temperature input. Therefore the error is so small that it can be neglected without significant effect with measurment.

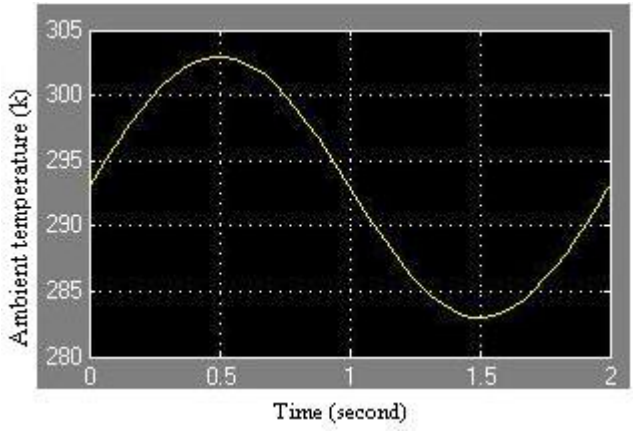

Figure 4.3 Ambient temperature fluctuation

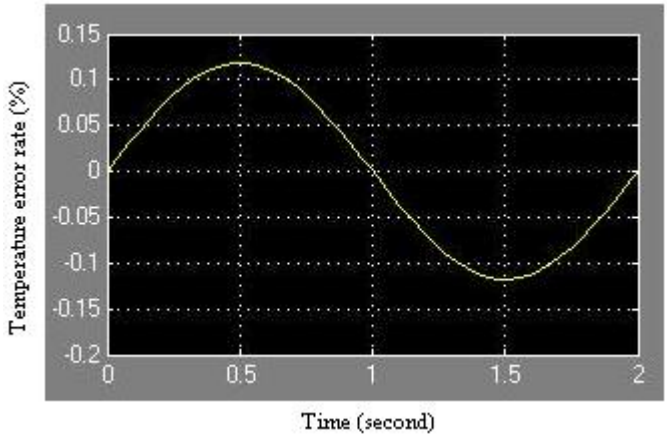

Figure 4.4 Percentage error of ambient temperature

Effect of Relative Humidity

A fluctuated sinusoidal input wave of relative humidity in the range of 60 % to 80 % was input to the unstable model, shown as Figure 4.5, while the stable model had a constant ambient relative humidity 70 % applied. The output difference of these two models was divided by the output of stable model to get the percentage error as shown in Figure 4.6. The percentage error varied from + 0.048 % to − 0.048 % corresponding to the fluctuating humidity input. The percentage error of relative humidity was so small it can be neglected without any significant effect on the measurement.

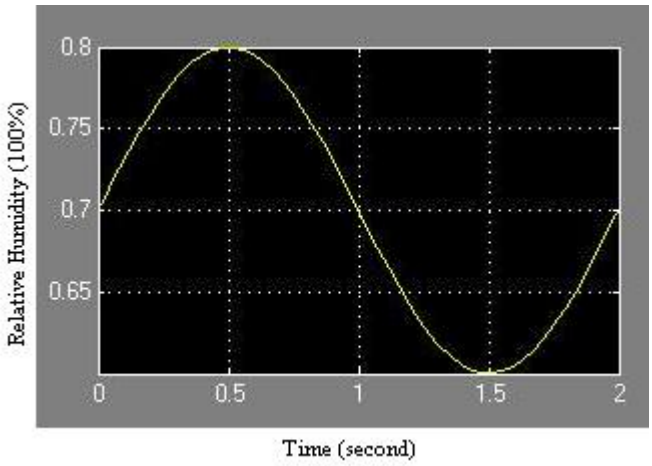

Figure 4.5 Ambient relative humidity fluctuation

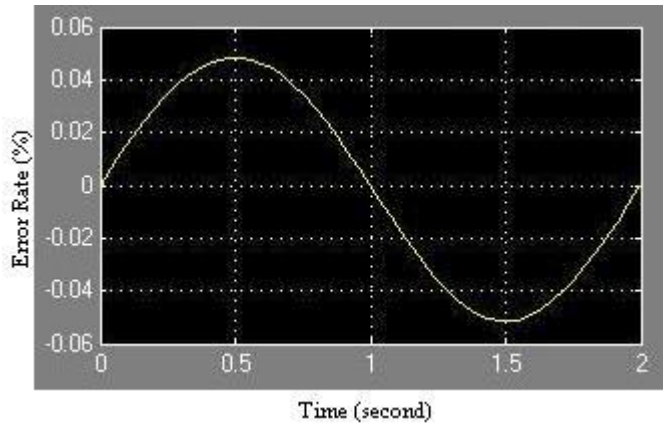

Figure 4.6 Percentage error of relative humidity

Effect of Air Pressure

Finally a fluctuating air pressure, represented by a sinusoidal wave in the range of 100.3 to 102.3 kPa was input into the unstable model, as shown in Figure 4.7, while the stable model had a constant ambient air pressure of 101.3 kPa applied. The output difference of these two models was divided by the output of stable model to get the percentage error as shown in Figure 4.8. The percentage error varied from − 0.00006 % to + 0.00006 %. The percentage error of air pressure is also very small that it can be neglected without affecting the measurement.

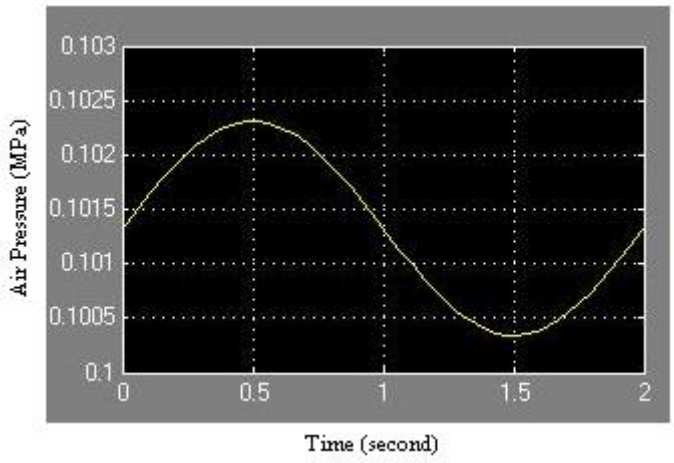

Figure 4.7 Ambient air pressure fluctuation

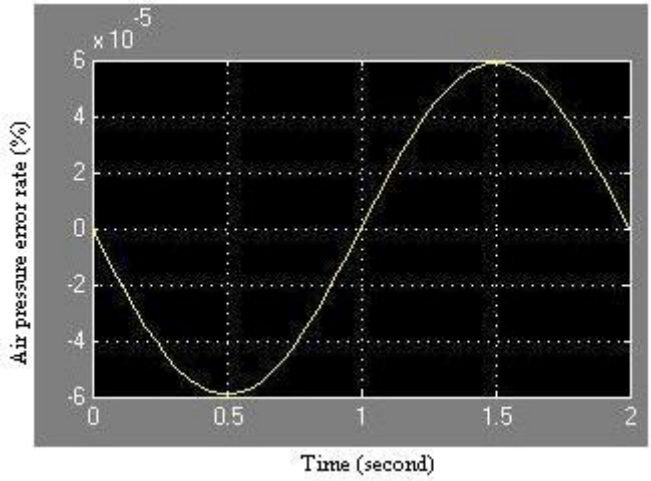

Figure 4.8 Percentage error of air pressure

Compared to the air pressure and the relative humidity error results, the ambient temperature will possibly have a very minor affect on the accuracy of the hot wire sensor. Experiment will be required to verify the influence of ambient temperature on the hot wire sensor, however, this work is beyond the scope of this project and the model is assumed to be suitable. Since there were several positions available to locate air flow sensor within the CPAP system, the position with less fluctuation of air temperature was considered the best location of the hot wire air flow sensor.

4.4 Best Location forHot Wire Sensor

There were several positions available for an air flow sensor within the CPAP system, such as the inlet of the blower, the outlet of the blower, the outlet of the humidifier, the tube port and the mask. As the tube and the mask were flexible, installing the sensor in

these positions could likely cause higher risk of broken tube or wires, thus these two positions were not considered. The remaining three positions were then compared.

The result of the comparison experiment was obtained using an ambient temperature of 22.0 ^{o}C. Blower air flow was set from 19.9 to 40.8 l/min which correlates approximately to a mask pressure of 4 to 20 cm H_2O. The hot wire multifunction anemometer TSI^{TM} 4000 was used to measure the air flow rate, temperature and pressure. The purpose of this test was to compare the temperature error in each position and select the minimum value that has the least temperature fluctuation to permit the accuracy of air flow measurement. The set up of different locations are shown in Figure 4.9, Figure 4.10 and Figure 4.11 respectively.

Figure 4.9 Temperature measurement of the outlet of the humidifier

Figure 4.10 Temperature measurement of outlet of blower

Figure 4.11 Temperature measurement of inlet of blower

In order to avoid transient temperature drift caused by changing heating effect of the blower in the CPAP system, the data was recorded 2 hours after the machine was switch on, at which time the machine had definitely reached a stable state. When changes were made to either air flow rate or pressure setting then the system was left to stabilise for 3 minutes period to as further readings being taken. The experimental data was recorded and plotted in Figure 4.12, Figure 4.13 and Figure 4.14 respectively. Temperature deviation of all three positions were computed and compared in Table 4.2.

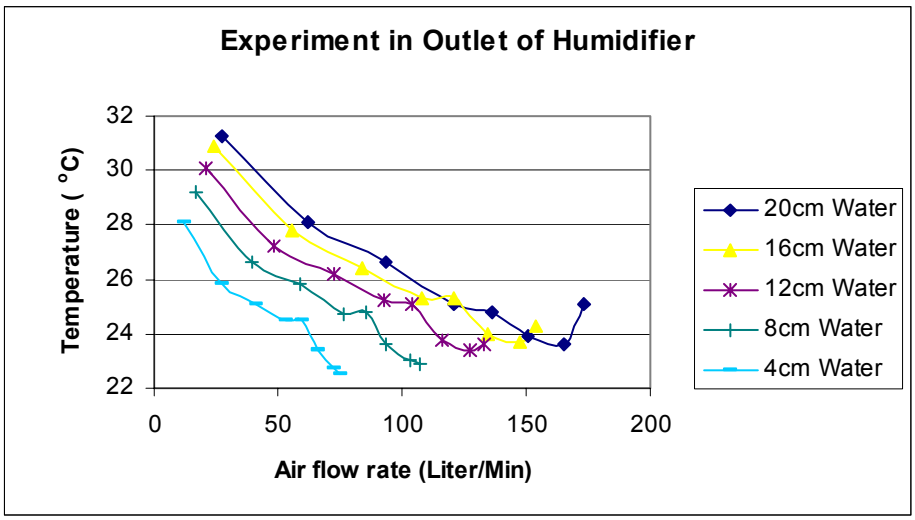

Figure 4.12 Temperature at outlet of humidifier

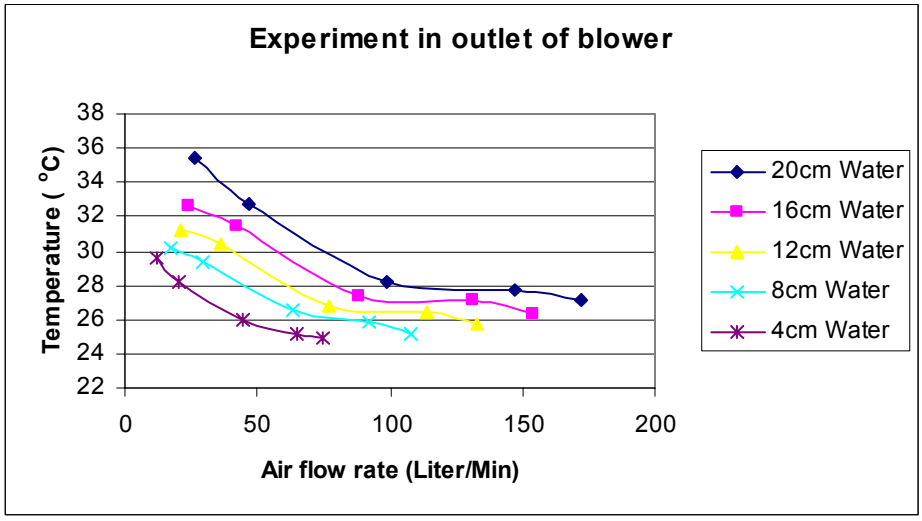

Figure 4.13 Temperature at outlet of blower

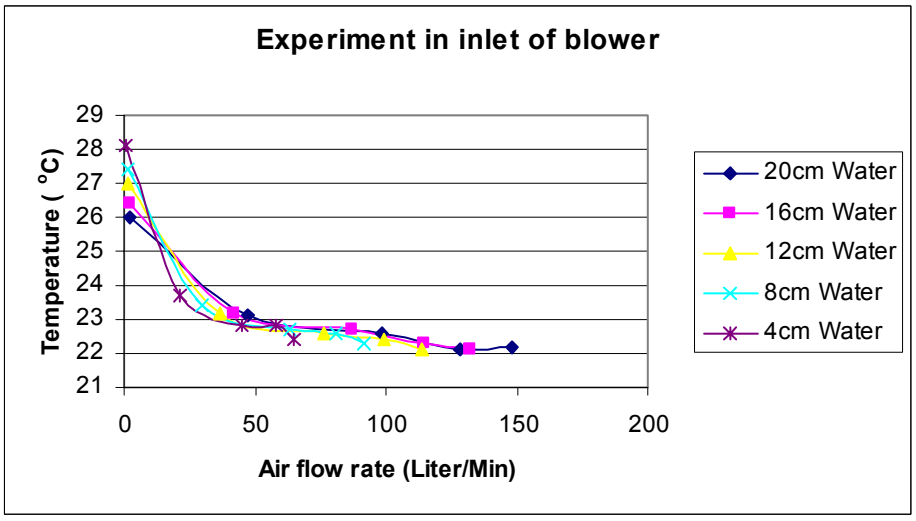

Figure 4.14 Temperature at inlet of blower

Table 4.2 Temperature comparison of different positions

Position	*Maximum*	*Minimum*	*Average Deviation*	*Standard Deviation*
Out let of humidifier	23.4	31.3	1.697685185	2.18896078
Outlet of blower	24.9	35.4	2.25888	2.767893302
Inlet of blower	22.1	28.1	1.39456	1.802336262

From table 4.2, the minimum temperature deviation occurs at the blower inlet, where the temperature influence would be minimized by locating the hot wire air flow sensor at this position. Then the best location of hot wire probe was determined, the experiment was set up, Section 4.5.

4.5 Experimental Set up

A Fisher & Paykel CPAP machine 600 was utilised as the air flow supplier in the following experiments. The experimental set up was simplified to a block scheme shown in Figure 4.15. The power source supplied direct current power (7.5 V) to the prototype electrical circuit. All sensed points on the circuit were connected to Labview^{TM} connection board by a group of wires. The outlet of CPAP system was connected to a metal ball valve via a flexible plastic tube. The hot wire probe of the prototype was fixed normal to the pipe axis in a short white plastic pipe, where one end of the pipe was linked to the inlet of blower through a sealed funnel, the other end of the pipe was assembled with a reference flow meter TSI^{TM} 4000, set up shown in Figure 4.16.

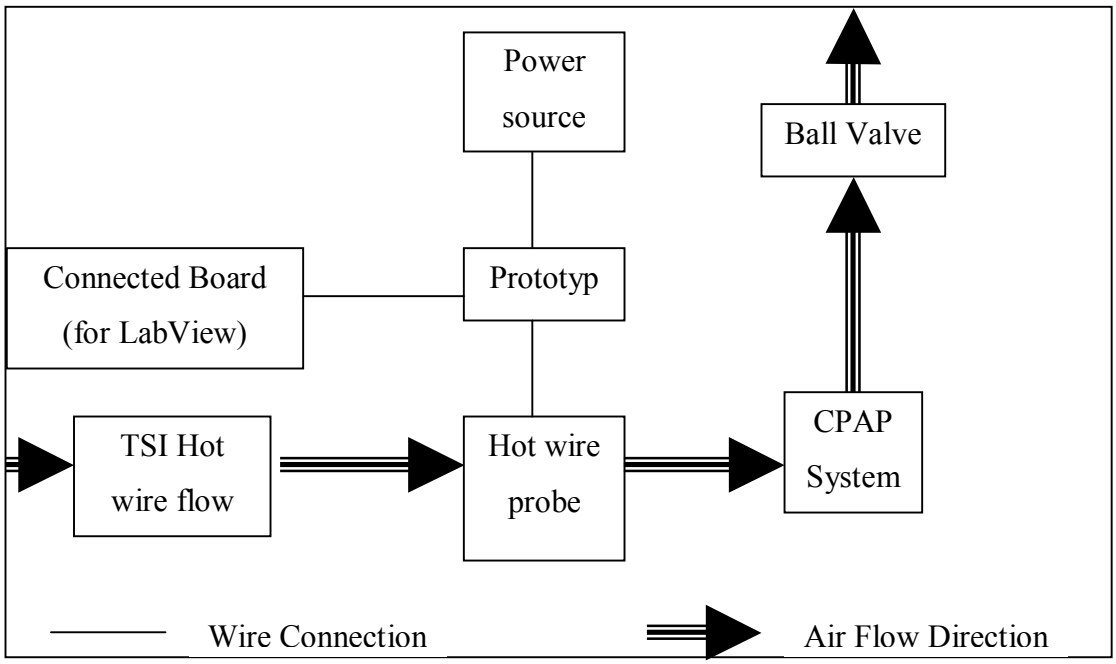

Figure 4.15 Experimental block scheme

The air flow rate was varied by adjusting the valve. Equipments used in this experiment are listed in Table 4.3.

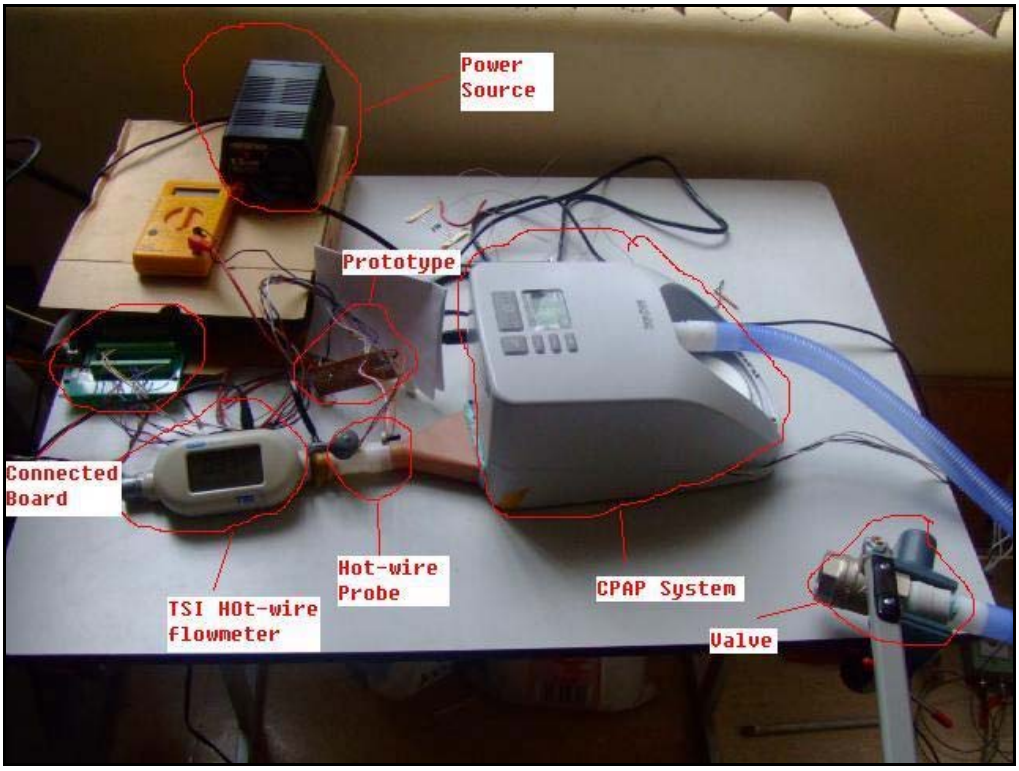

Figure 4.16 Experimental set up

Table 4.3 Equipment list of experiment rig

Equipment	Function
Power source	Supply DC power to prototype
Prototype	Supply and detect current to the platinum wire probe
Connected board	Collect relevant reading data for Labview^{TM} from circuit
TSI hot wire flow meter	To be the reference air flow rate sensor
Hot wire probe	Detect the various air stream
CPAP system	Supply stable air stream source
Valve	Change the air flow rate

4.6 Initial Air Flow Experiment

In order to conveniently adjust the static current of the sensor wValiire, the electronic circuit was amended, as shown in Figure 4.17 below.

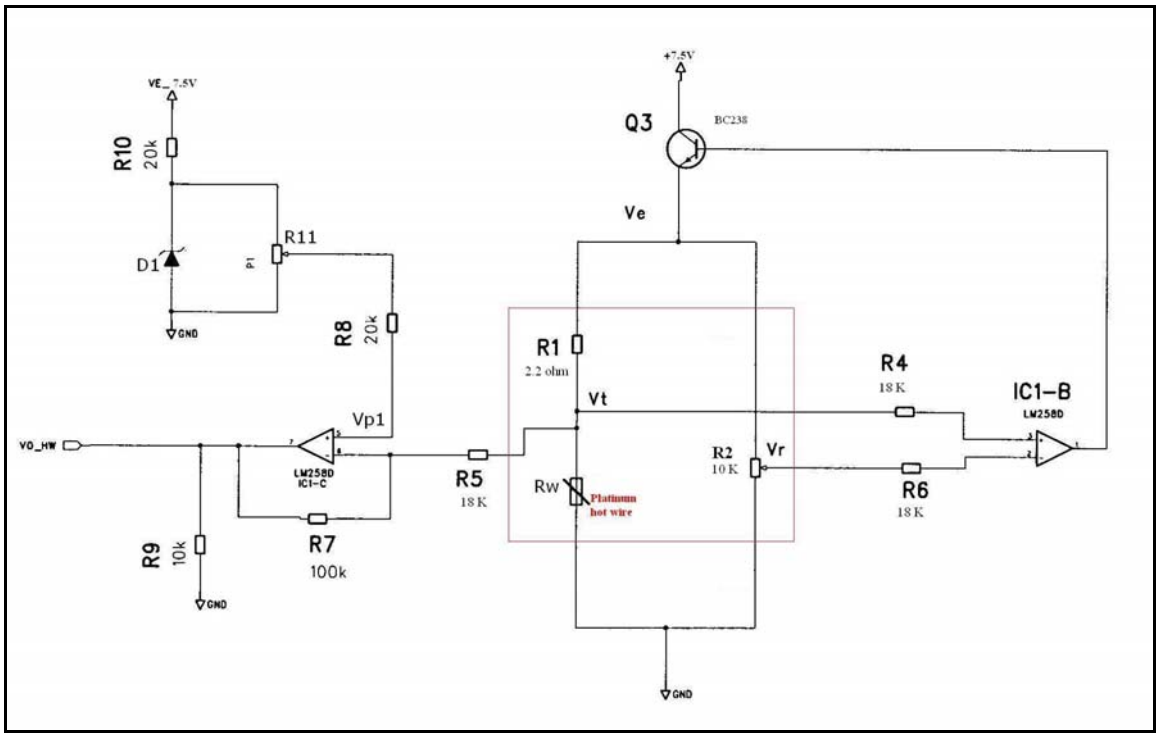

Figure 4.17 Modified circuit of prototype

Resistor R_1 was increased to 2.2 Ω as the calculated hot wire resistance was close to this value. The platinum wire was soldered on two copper pins 5 mm apart. The cold (room temperature 22 ^{o}C) resistance of platinum wire was measured to be 1.27 Ω. The variable resistor R_2 (10 K Ω) with an adjustable leg between two ends replaced Constant resistors R_2 and R_3. The reference voltage V_r was detected from the adjustable leg of R_2. The rate of upside R_2 resistance and downside R_2 resistance varied depend on the position of the adjustable leg.

Several points of electronic circuit were connected to the Labview^{TM} connected board for data sampling. These points were emitter voltage V_e, wire voltage V_t, reference voltage V_r and output voltage V_{o_HW}. In order to obtain the outputs thought the whole air flow range from 0 to 10 m/s, the ball valve was slowly turned from the fully closed position to fully open position, and then slowly turned to the fully closed position again. The same process was repeated several times. A total of four groups of output data were obtained for the full range of air flow velocities within the CPAP device. From the law of serial circuit, the current of platinum hot wire i_w was calculated from Equation (4.1):

$$i_w = \frac{V_e - V_t}{R_1} \tag{4.1}$$

Discussion of Initial Testing:

Four groups of data were calculated to get the output wire current value i_w, which were plotted as four curves in Figure 4.18. Considering the maximum allowable current of the amplifier BC238, the static wire current was adjusted to be around 50mA. When the air valve was closed, the air was not totally static. So it was assumed that the wire current in air velocity of 0.1 m/s was static wire current.

By analysing these results from Figure 4.18, it was determined that the minimum static current (which was detected while the air flow rate was 0.1m/s, or less) in this experiment was 51.5 mA. The dynamic current varied from 51.5 to 73.5 mA during air flow velocity of 5.1 m/s, leading to a variable range of 22 mA. Secondly it was found that there were offsets between different curves while they had various static current values from 51.5 to 57.5 mA.

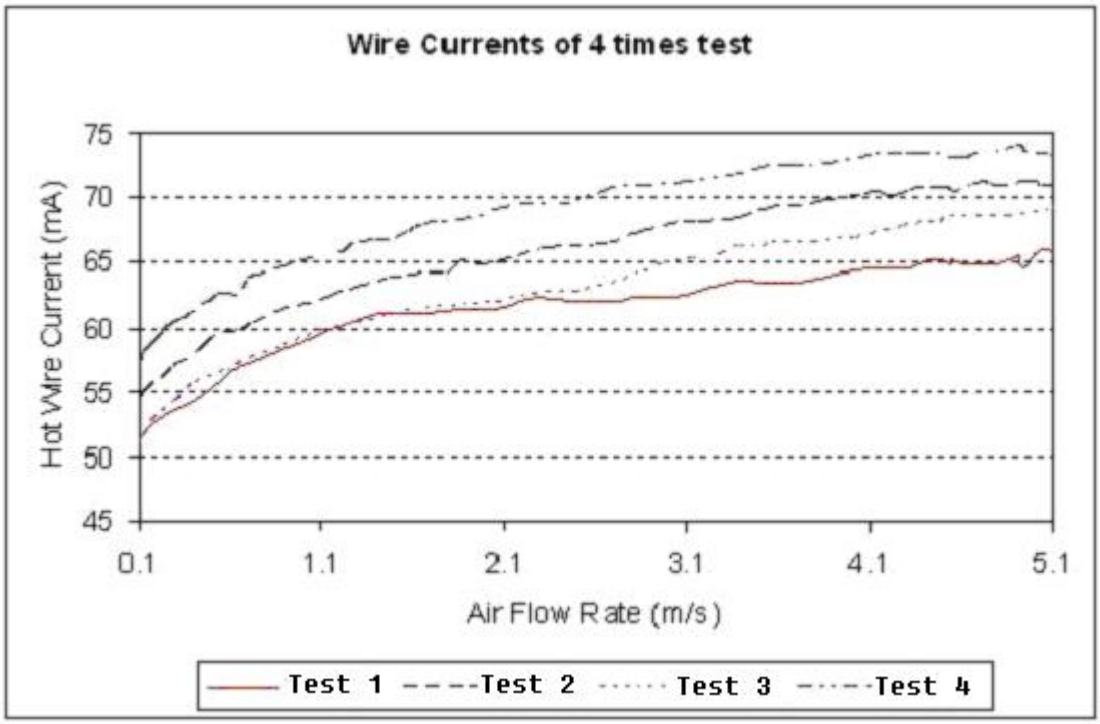

Figure 4.18 Comparison of various hot wire currents

There were individual ground terminators for each virtual signal channel in Labview™ connected board. As these ground terminators were virtual grounds, the curves offsets could be eliminated by connecting the real ground terminators to the virtual grounds by high resistance resistors. This point was verified in experiment detailed in Section 4.7.

In order to obtain the current diagram of the simulated model, the platinum wire cold resistance (1.27 Ω in 22 ^{o}C) was set by adjusting dimensions of wire in the simulation model. Hot resistance was set by adjusting the average wire temperature difference with the ambient temperature in the simulation model. The resistance of hot wire R_w can be calculated as follows:

$$\frac{V_e - V_t}{V_t} = \frac{R_1}{R_w} \Rightarrow R_w = \frac{R_1 \times V_t}{V_e - V_t} \tag{4.2}$$

From the experimental recorded data, the hot wire resistance was 1.299 Ω, which when converted to wire temperature indicates that it was 6.5 ^{o}C higher than the ambient temperature (22 ^{o}C).

The output wire current of simulation model is shown in Figure 4.19. Comparing test simulation results shows that although the curves appear to be similar, there were some unsatisfactory aspects between experiment curves and simulated curve.

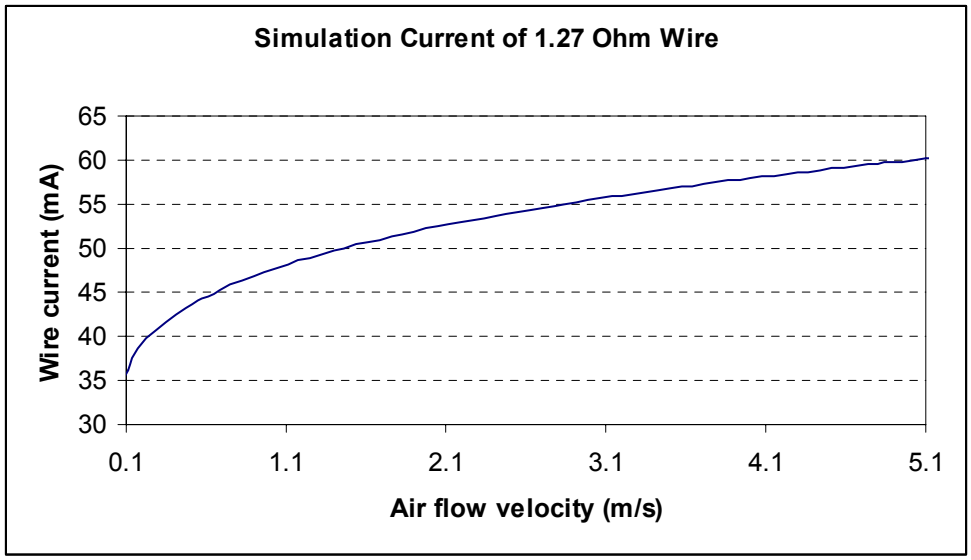

Figure 4.19 Simulation current of first experiment

There are 3 conclusions that can be drawn from these initial results:

1. Generally the experimental current curves were higher than the simulation current curve. This maybe caused by an offset problem, it will be investigated after eliminating the output offset, described in Section 4.8.

2. The range of current (25mA) was too small to obtain a sufficiently sensitive output and the sensitivity of the prototype being too small to practically apply. As mentioned earlyer, the hot wire was 6.5 ^{o}C higher than the ambient temperature, which was obviously too low to have good sensitivity. The range of current flow within the hot wire depends on the air flow velocity and wire temperature, in stationary air, the higher hot wire temperature would cause more heat loss than lower hot wire temperature. As the maximum transistor (BC238) current was 100 mA [70], if the accumulated heat in the transistor could not be cooled down in time, the transistor would be burned out (Four transistors were burned during these experiments).

3. The experimental current curves were not as smooth as the simulation current curve. This can be attributed to the fact that the air flow rate value in horizontal axis of Figure 4.18 was read from a reference linear mass flow meter (TSI^{TM} 4000). According to its specifications, there was ±2% error of reading accuracy in low flow rate. So the output curve of experiment can't be expected very smooth.

4.7 Experiment In Static Air

The experiment scheme was modified to account for the effect of ground offsets and to enable the measurement of hot wire current during static air condition (Figure 4.20).

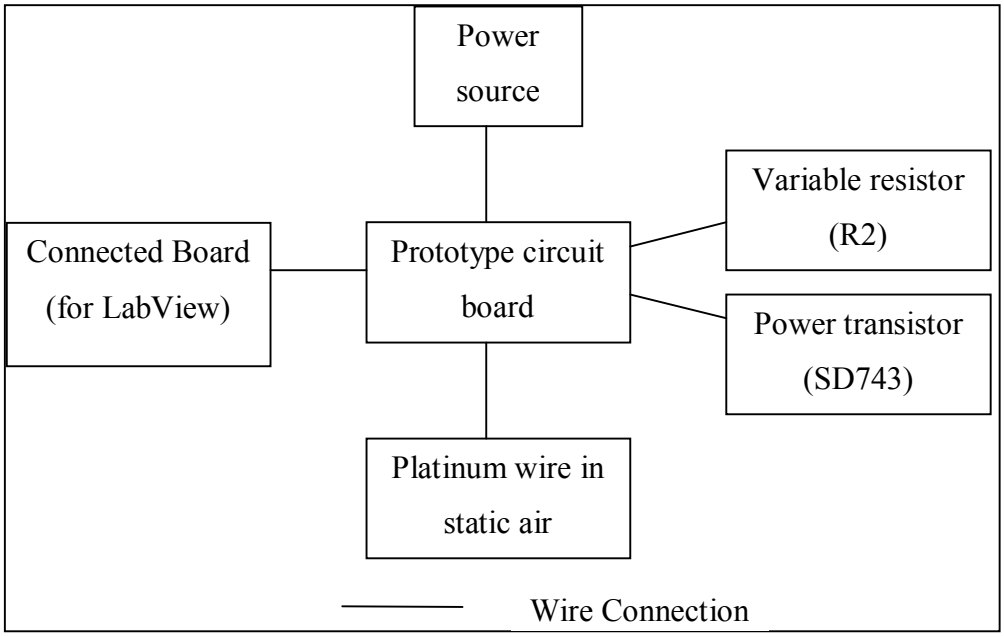

Figure 4.20 Scheme of experiment in static air

The variable resistor was installed into the circuit board to enable convenient adjustment to the mode during operation. The power resistor was taken out from the circuit board and attached to a heat sink. From Figure 4.21, Resistor R_1 in the circuit board was replaced with a 3.3 Ω, 5W resistor to reduce the temperature drift that occurred to test this modified circuit's ability to detect low air flow velocities, the probe of platinum wire was covered by a transparent glass pipe which avoided the air motion fluctuation around the wire.

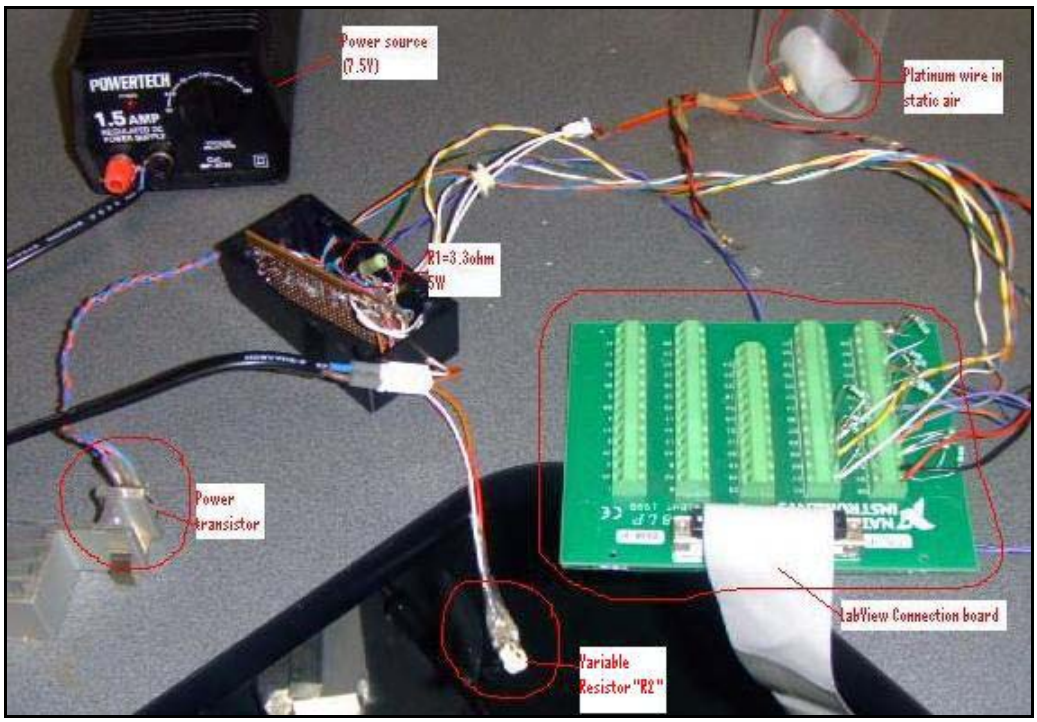

Figure 4.21 Experiment in static air

The power transistor SD743 was attached to an aluminium heat sink to avoid heat accumulation subsequent burning out. Variable resistor R_2 was used to obtain a static current. 7.5 V DC power source was connected to the sensor circuit and all terminals of the Labview^{TM} connected board were grounded to avoid ground offsets. The emitter voltage V_e, the computed emitter current I_e (same as wire current), the reference potential V_r and wire potential V_t were plotted in Figure 4.22.

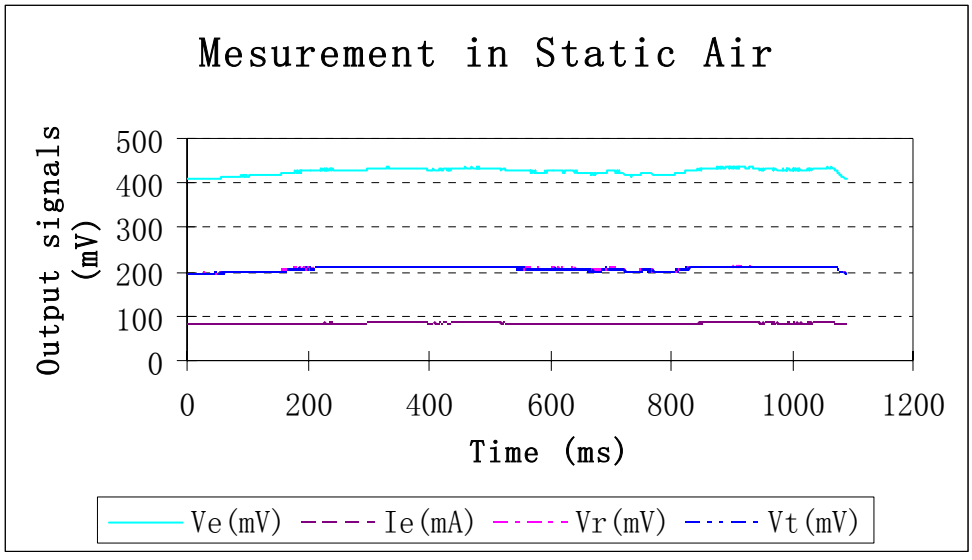

Figure 4.22 Output signals in static air

From Figure 4.22, it can be seen that all potential are stable, the small fluctuation is difficult to avoid since the air of the experiment was not absolutely static enough. Theoretically the resistance rate between downside and upside (R_3 / R_2) was changing from zero to positive infinite. Using the principle of a Wheatstone bridge circuit, the theoretical resistance value of hot wire can be calculated as:

$$R_w = R_1 \times (R_3 / R_2) \tag{4.3}$$

Until this value R_1 was adjusted to greater than the measured platinum wire resistance at room temperature, there should be no current flows in the platinum wire. The voltage across the wire V_t should be zero and this period is called the breakdown period. From Figure 4.23, it can be seen that voltage of emitter V_e and voltage of wire V_t was not zero, rather, it was found to be 65 mV for V_e and 55 mV for V_t during the breakdown period (Figure 4.23). Considering the resistance of R_1 ($3.3\,\Omega$) and room temperature resistance of wire ($2.1\,\Omega$), this potential value would affect the final calculated wire current by more than 10 mA. This is considered the effect of conduction, natural convection and radiation heat lost, or the error caused by high power transistor SD743. By comparison, it seems that transistor BC238 can be used to obtain a more precise output data. But in order to improve the measurement ability in higher air flow range, the prototype was amended again to prepare for the next experiment.

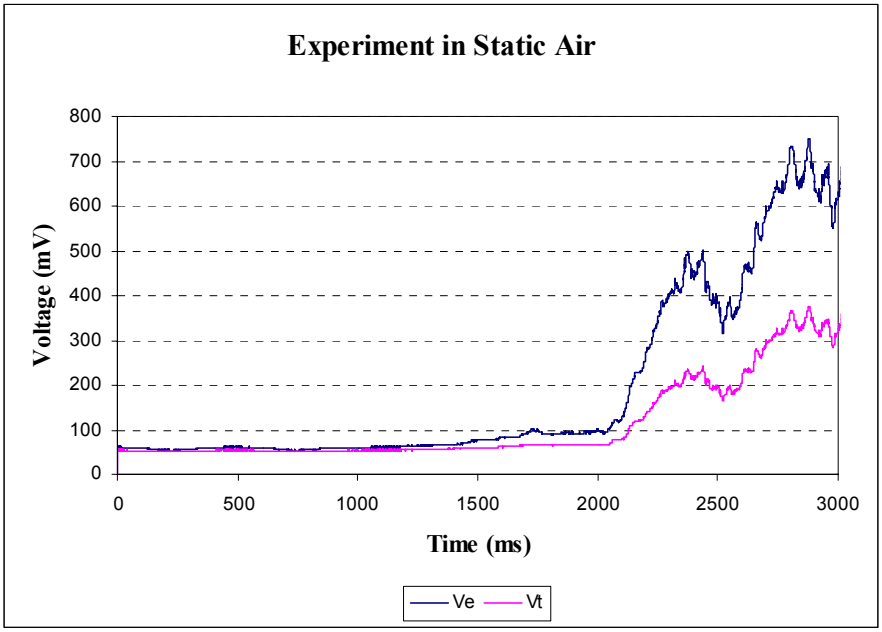

Figure 4.23 Wire & emitter voltage in static air

4.8 Modification to Prototype Circuit

The replacement BC 238 transistor was attached to an aluminium heat sink, as shown in Figure 4.24, to avoid burning out under high current situations.

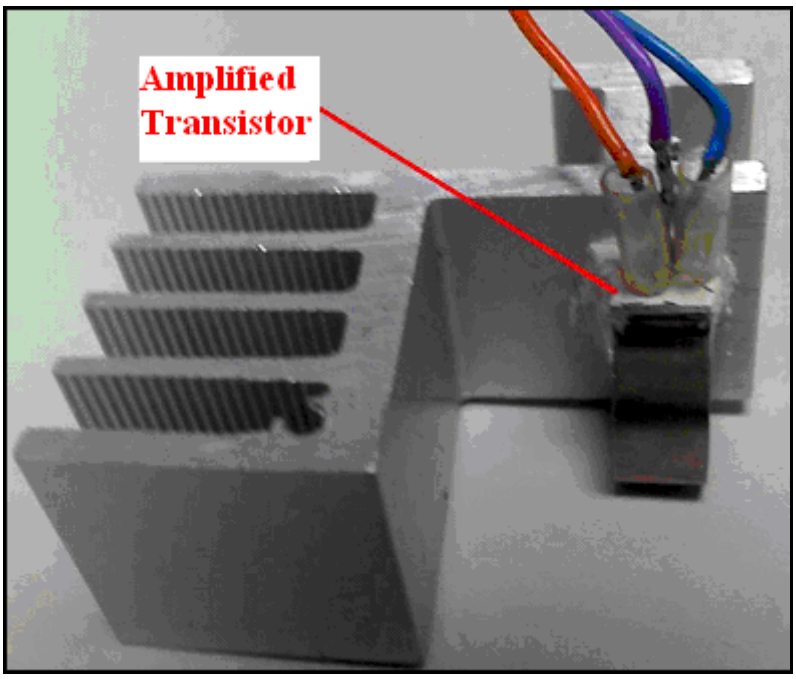

Figure 4.24 Amplified transistor with heat sink

In order to create a higher sensitivity than the first experiment, the hot wire temperature was set higher than before. The hot wire temperature can be preset by three constant resistors R_1, R_2 and R_3 according to Equation (4.3). The constant resistor R_2 (Figure 4.1) was replaced by a constant 269 Ω resistor. The other constant resistor R_3 was replaced by a 4 channel switch which was soldered with 4 individual 2 W resistors shown in Figure 4.25. These resistance values were $120\,\Omega$, $130\,\Omega$, $150\,\Omega$ and $180\,\Omega$ respectively. Thus the rate of R_3 / R_2 could be regulated to 4 different values by the switch.

Figure 4.25 Four constant resistors soldered on four channel switch

The constant resistor R_1 was replaced to a 5 watt, 4.9 Ω resistor (shown in Figure 4.26). Since the higher power capacity of this resistor avoids the resistance drift during high current flow conditions.

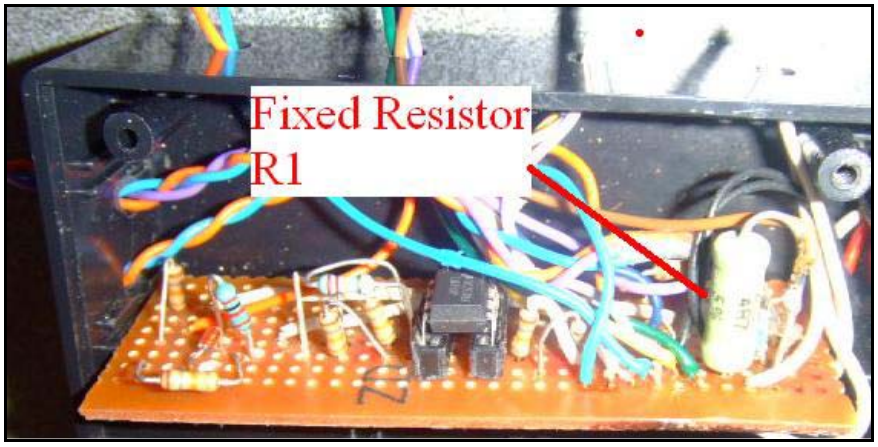

Figure 4.26 Constant resister R1

4.9 Final Testing

The pipe containing the platinum wire was placed between the reference TSI air flow meter and the inlet port of CPAP blower, all gaps of the inlet were sealed by blue plasticine and the platinum wire was positioned horizontally. The reference value of air flow rate was read from the LCD screen shown in Figure 4.27. The source of air supply

(CPAP) was not absolutely stable and the reference air flow meter has maximum of 2% accuracy error.

The CPAP machine was adjusted to get arrange of constant air flow rates for each test. The sampling rate was set at 25 Hz and data was collected over 16 second period, more than 400 data points were collected for each flow rate test.

The median value of the different parameters such as wire potential, wire current, air flow velocity was calculated to determine the hot wire current curve over the whole range of air velocity within CPAP systems.

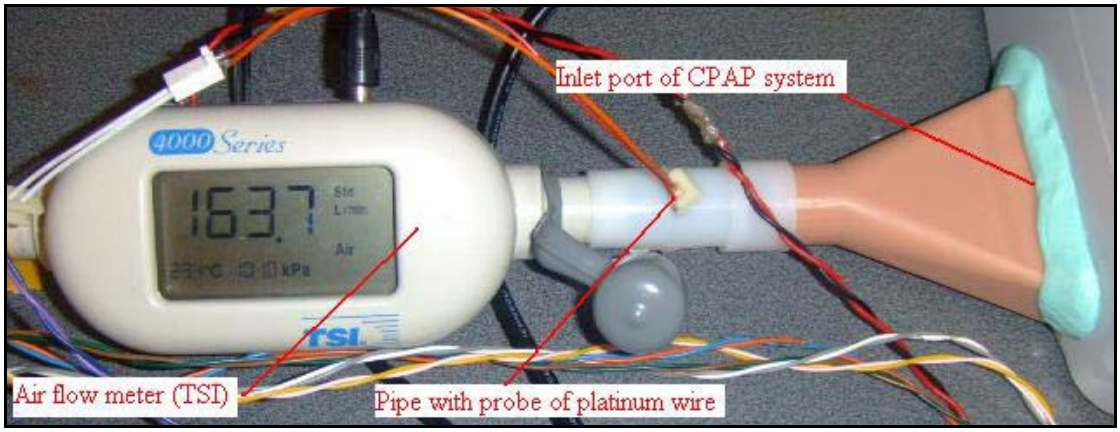

Figure 4.27 Experimental set up of hot wire sensor

The CPAP machine was set to the maximum air pressure value (20 cm H_2O) to obtain the maximum air flow rate. The outlet of CPAP was connected to a metal ball valve as shown in Figure 4.28. The air flow rate was varied by turning the ball valve.

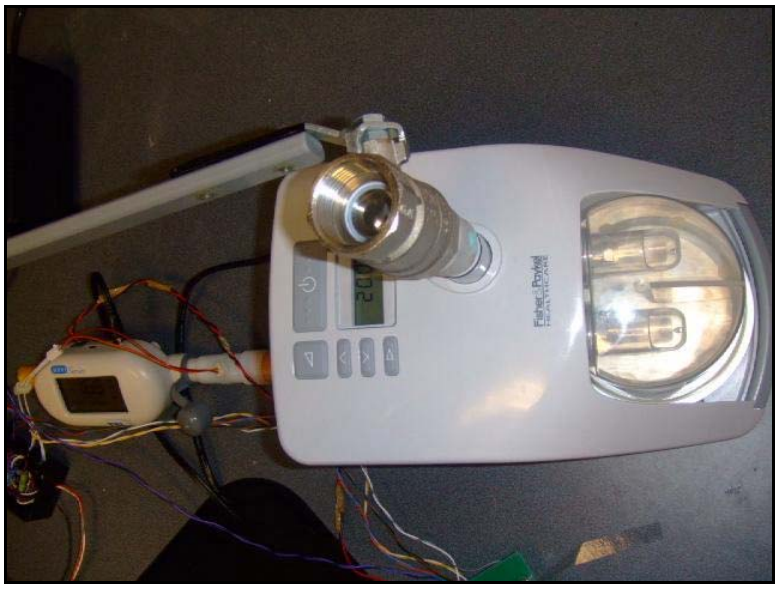

Figure 4.28 Experimental setup of metal ball valve

Firstly the resistor switch was set to connect the 130 Ω resistor which replaced the constant resistor R_3. The hot wire voltage was detected in different air flow rate.

Experiment result:

When the air velocity was higher than 4 m/s, the output voltage V_e and V_t became unstable and fluctuated seriously as shown by Figure 4.29. But if the air velocity was less than 4 m/s, the wave of signal was normal as shown in Figure 4.30. The reason that caused such phenomenon was due to the transistor nit being able to tolerate a current above 165 mA which occurred during the air velocity exceeding than 4 m/s.

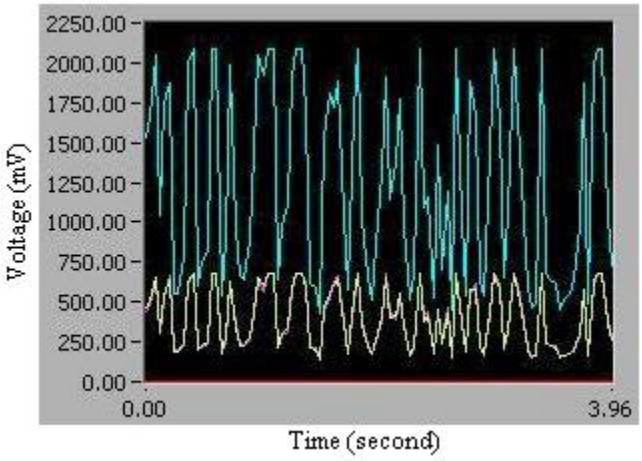

Figure 4.29 Fluctuated output voltages

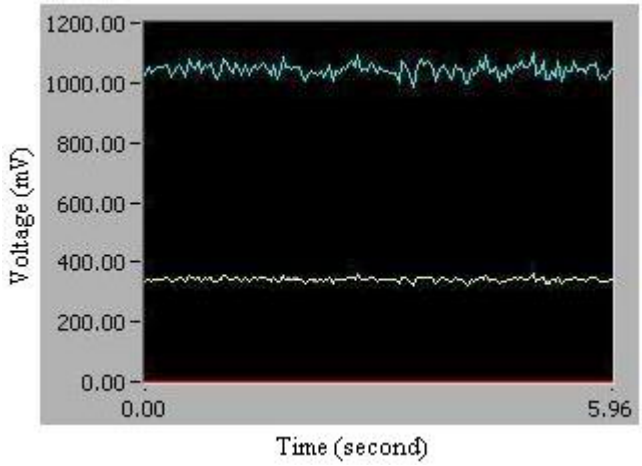

Figure 4.30 Stable output voltages

The corresponding current value was obtained by dividing the voltage by the hot wire resistance which was calculated from the known resistor values R_1, R_2, and R_3. The calculated resistance of hot wire was 2.38 Ω. The curve of wire current was shown in Figure 4.31.

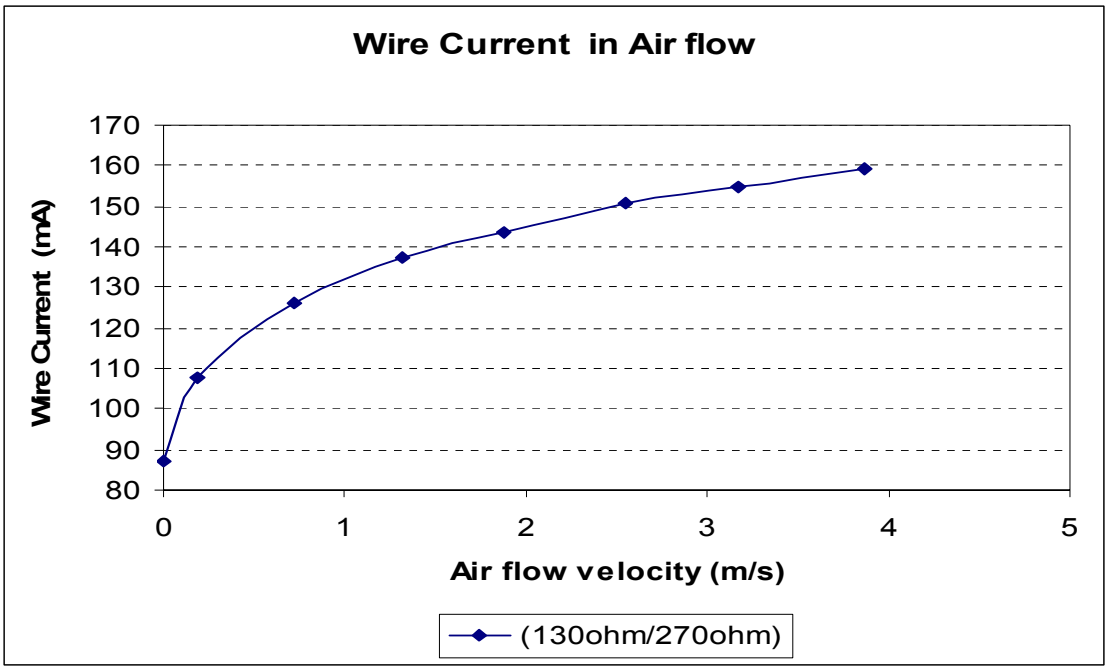

Figure 4.31 Hot wire current (R_3 was set to be 130 Ω)

From Figure 4.31, it was found that the measurable range of air flow velocity was limited to 4 m/s. In order to extend the measurable range to 10 m/s while allowing for the maximum current of the transistor, the working temperature of wire needs to be set lower by reducing the rate of R_3 / R_2. This requirement was achieved by switching resister R_3 from 130 Ω to 120 Ω. Then the calculated resistance of hot wire would be 2.21 Ω which was smaller than the previous setting. This corresponded to a working temperature of platinum wire on average being 52 ^{o}C higher than the ambient temperature which was 20 ^{o}C in this experiment. Nineteen different tests were implemented over different air flow velocities.

By the same method of treatment, the experimental current curve was plotted in Figure 4.32. Substituting the resistance and dimensions of hot wire, ambient temperature and relative humidity, and properties of platinum into the modified simulation model to plot the current curve of hot wire gave Figure 4.32. The experimental current curve and simulated current curve match very well with the error between the two curves being

very small. The rate of error in Figure 4.33, which was the value of current difference divided by the value of experimental current, was smaller than 1.5 % when the air flow velocity was bigger than 1.0 m/s. This kind of error can be improved by using a more accurate reference air flow instrument than the TSI^{TM} 4000.

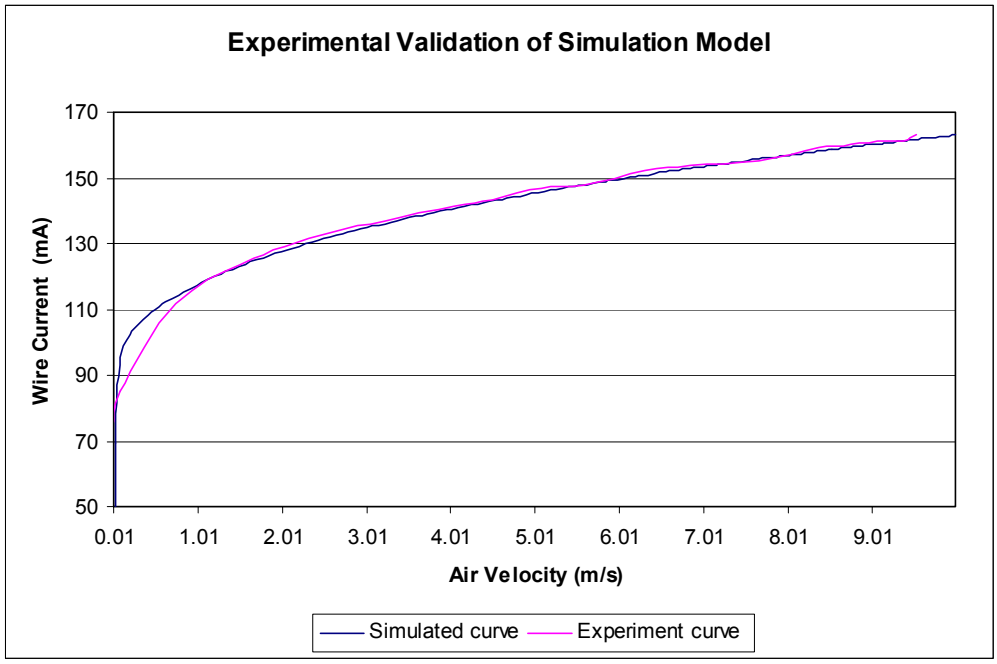

Figure 4.32 Comparison of current curve

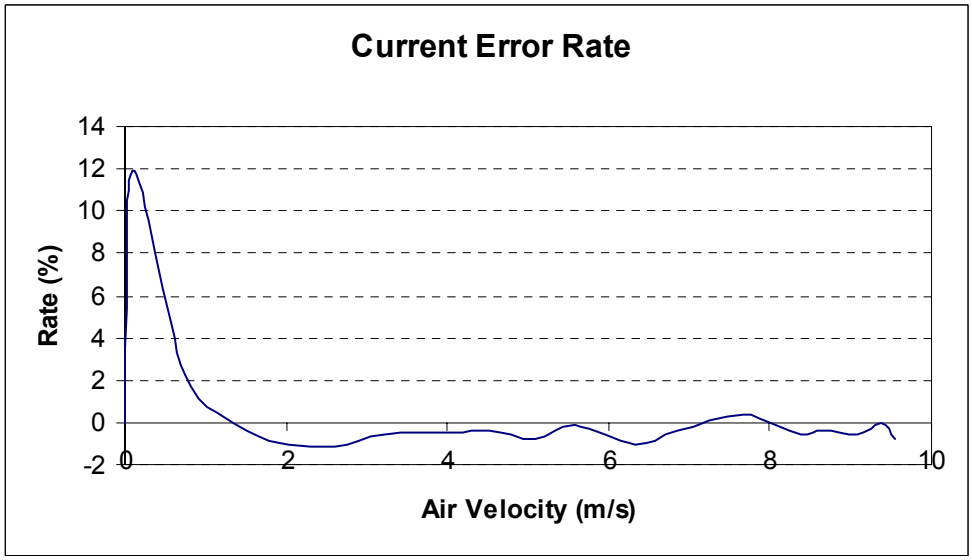

Figure 4.33 Rate of Current Error

4.10 Conclusions

The simulation model of hot wire air flow sensor was successfully validated by experiment. The accuracy percentage error was 1.5% which was smaller than the reference flow meter TSI^{TM} 4000 (2%). The simulation model can accurately predict the behaviour of the actual prototype. During the measurable range, dynamic and static output predictions of the simulation model have perfect correlation with the practical sensor.

Chapter 5 Discussion and Conclusion

5.1 Introduction

Validating the theoretical model using several sensors would improve accuracy and consistency; Within this project, however, determining the suitability of hot wire flow sensor with CPAP system application, the experiments were limited to similar wire length (approximate 5 mm) and constant lab room conditions (22 ^{o}C and 70% RH) to prove the simulation model. By comparing simulation & experiment results, the improved simulation model has good accuracy and ability of prediction to be used for further analysis.

The simulation model was developed to replace difficulties encountered and the sort involved in running many experiments. Effects of different hot wire settings and various ambient conditions on the constant temperature air flow sensor are discussed. The sensor measurement process changes in dynamic responses under varying air flow input are also simulated and investigated in Section 5.2 and 5.3 by considering the CPAP machine application. An optimized scheme of wire design is presented in Section 5.4. The advantage of this simulation model and possible applications in other fields are mentioned in Section 5.5. This mathematical simulation model is developed mainly as a design tool to predict the wire current output performance of the air flow sensor under different operating conditions and wire probe designs.

5.2 Effect of Hot Wire Setting

In this project, there are three main setting parameters for the hot wire probe. They are the wire diameter, the wire length and the wire operating temperature. The wire diameter and the length can be measured directly. But the hot wire resistance is indirectly set by varying the relevant resistor rate in the Wheatstone bridge of electronic circuit given in Section 4.6. As the resistance of cold wire is measurable, the difference between cool wire resistance and hot wire resistance determine the wire operating

temperature. In order to simplify the simulation model, the wire operating temperature is treated as a directly adjustable parameter. The effects of each parameter setting on the sensor output wire currents and measurement response time is discussed in this section.

5.2.1 Wire Diameter

The wire diameter is one important parameter to consider when designing the air flow sensor for the CPAP system. However once the product is made this parameter can't be varied so it must be selected according to different application requirements. The wire electrical resistance and wire mass are inversely proportional to the diameter, thus not only the output wire current but also the response time is affected. In order to critically compare the effects of wire diameter in the simulation model, the ambient conditions are set as 22 ^{o}C, 70% RH, and the wire length is constant at 5 mm, the wire operating temperature is 52 ^{o}C over ambient (22 ^{o}C). For high accuracy, all these conditions are the same as that used to validate the model by experimentation, given in Chapter 4. Three diameter values, 0.02 mm, 0.03 mm and 0.05 mm are substituted into the simulation model and processed respectively. The result in Figure 5.1 shows a noticeable rising of output current as the wire diameter increased.

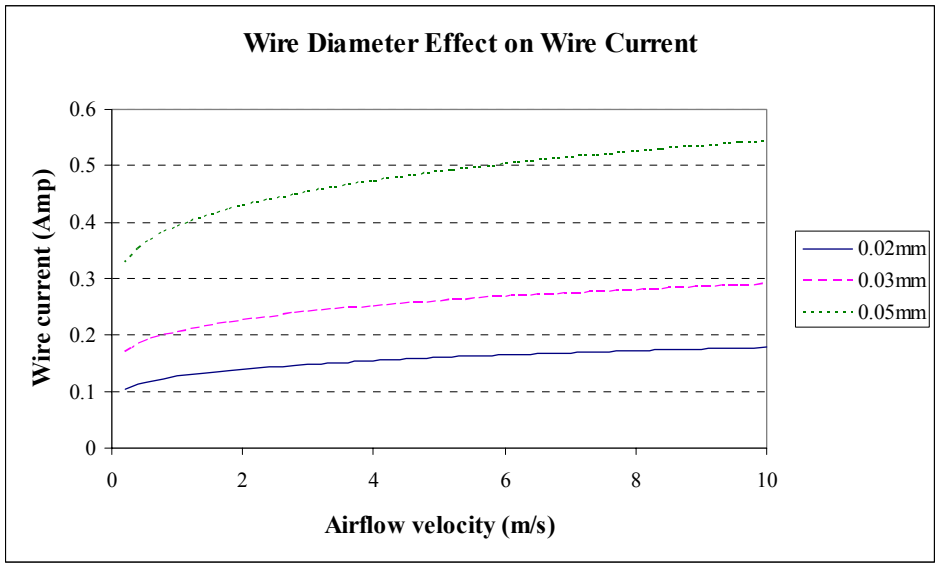

Figure 5.1 Wire diameter effect on output wire current

An increase of air flow velocity past the hot wire increases the heat lost rate at the wire surface. In order to maintain the heat balance from the wire (constant temperature), the increasing generated compensation power causes the wire current to increase. Three

current (Figure 5.1) show the same trend of the wire current increment as air flow velocity increases.

From this simulation result, it is noticed that under 0.05 mm wire diameter, the wire current increases to approximately 225 mA as the air flow velocity rises from 0.2 m/s to 10 m/s. But for the similar curve for the 0.02 mm wire diameter, the wire current increases to approximately 80 mA. This means that bigger diameter wire can achieve a higher sensitivity.

The main reason for the wire current rising as wire diameter increased is due to the fact that the bigger diameter wire has a corresponding larger wire surface area enabling more heat loss. Another reason is due to the fact that bigger diameter wire has a smaller electrical resistance, even for the same quantity of heat loss, so requires a higher current to compensate for this effect. The rate of forced convective heat loss during the low air flow velocity range is not as high as that during the high air flow velocity range which explain the difference in gradient as the air flow velocity is increased.

The effect of wire diameter on the dynamic response time of the air flow sensor is simulated and shown in Figure 5.2. Notice that all curves have the same trend with the response time decreases as the air flow rate increases. The response time decreases very rapidly in the low air flow velocity range (< 2 m/s) and very slowly in the high air flow velocity range (> 2 m/s). The main reason of this is the wire has greater rate of heat loss during a higher air flow rates stream. The other noticeable factor is thicker wires have longer response times at the same air flow velocity, while smaller wire obtain faster response speed. The response time difference becomes larger as the air flow velocity dropped from 10 to 0.2 m/s and this can be explained in Section 2.2.

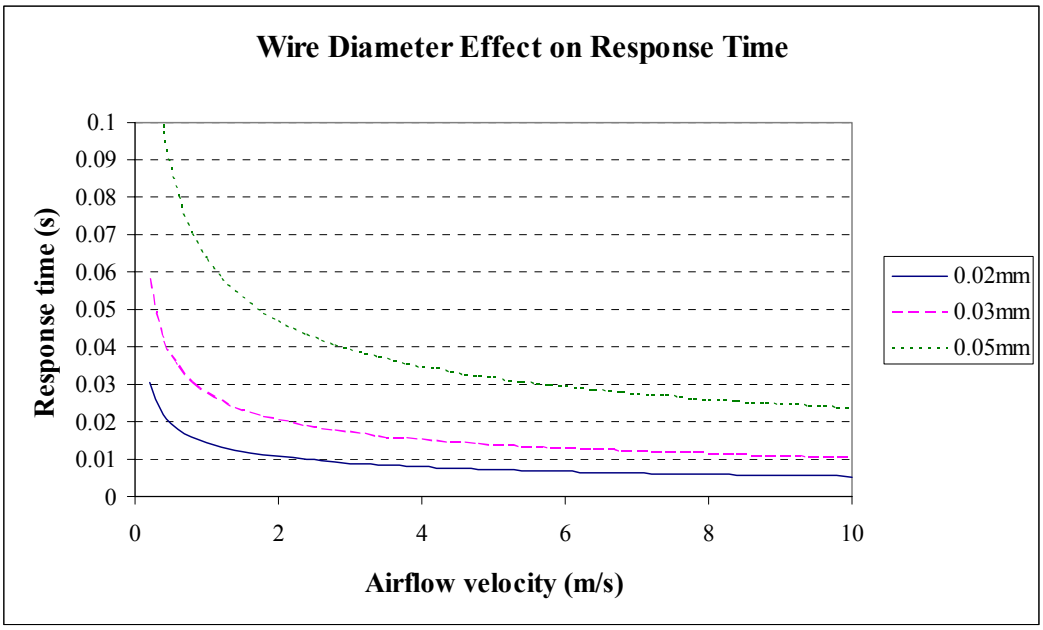

Figure 5.2 Wire diameter effect on response time

Another contributing factor is thinner wire means lower mass and hence lower heat capacity, thus the stored heat power is less. The other physical reason is that thinner wire has smaller surface area which reduces the heat loss. All of these factors contribute to the thinner wire at a new heat balance more rapidly than a thicker wire given the same input power.

5.2.2 Wire Length

According to different application requirements, wire length is critical since the wire electrical resistance and wire mass are proportional to the wire length. Not only the output wire current but also the response time is affected by changing these parameters. The effect of wire length of the sensor is tested using the simulation model. The wire current simulation results of different air flow velocities from 0.2 to 10 m/s under various wire lengths are shown in Figure 5.3. In the simulation model the ambient conditions are set as 22 ^{o}C and 70% RH, the wire diameter is 0.02 mm, the wire operating temperature is 52 ^{o}C over ambient (74 ^{o}C). Three wire lengths 5.0, 8.0 and 10.0 mm are substituted into the simulation model, respectively.

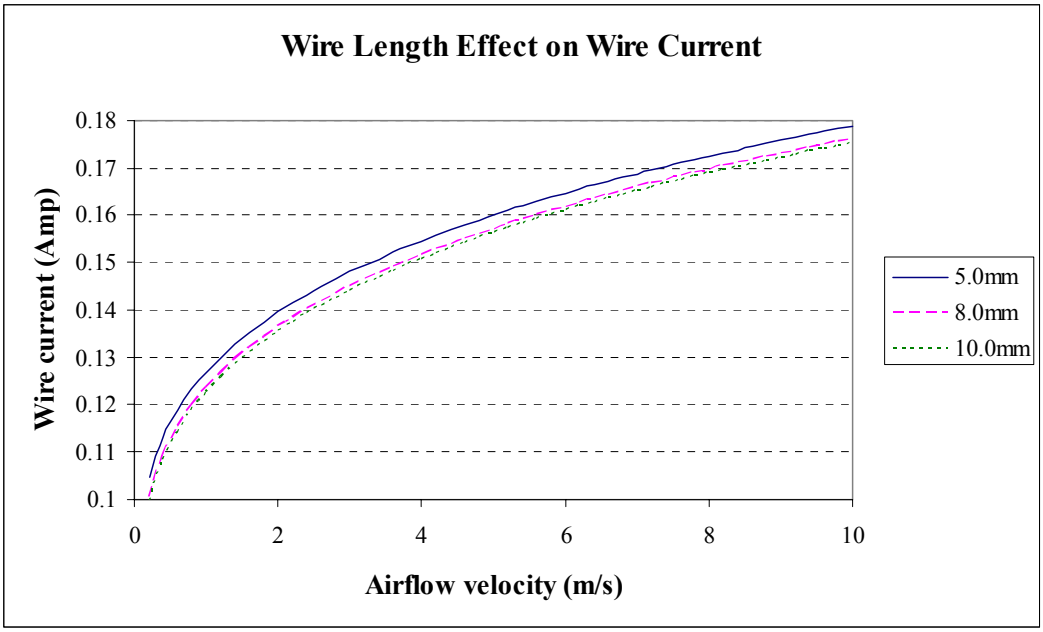

Figure 5.3 Wire length effect on output wire current

By comparing the output wire current for different length wires, it is shown that the longer wire has slightly smaller output current than the short wire thoughout the whole air flow velocity range. Theoretically, when the temperatures of wire are set to be same and the diameters are also the same for all three wires, the longer wire has proportionally larger surface area which causes a proportionally larger forced convective heat loss. But as the longer wire has a proportional larger electrical resistance too, according to the relationship that the heat loss power is the product of current squared and electrical resistance, the wire current caused by the forced convective heat loss of various length wire are same. Current difference is not caused by the difference in forced convective heat lost. It is known that the longer wire has higher thermal resistance. Under the same temperature difference, the bigger thermal resistance causes less conductive heat loss from the long wire, thus influencing the amount of general heat loss. As the conductive heat loss is not the main part of the general heat loss, it therefore causes a slight reduction in the input heat power compensation, however, the wire current drops significantly.

The effect of varying wire length on response time is shown in Figure 5.4. Since the difference is very small, to observe clearly, the range of air velocity from 4 to 6 m/s is zoomed in. From Figure 5.4, it can be seen that the longer wire given faster response. The response time is slightly decreased (less than 0.1 ms) when using the longer wire which can be explained by the same reason as that given for variation in current. The

longer wire has less conductive heat loss per unit length, thus the unit length general heat loss is slightly less than the shorter wire. After the initial heat balance is peaked, the longer wire need less time to compensate for heat lost given the same initial current.

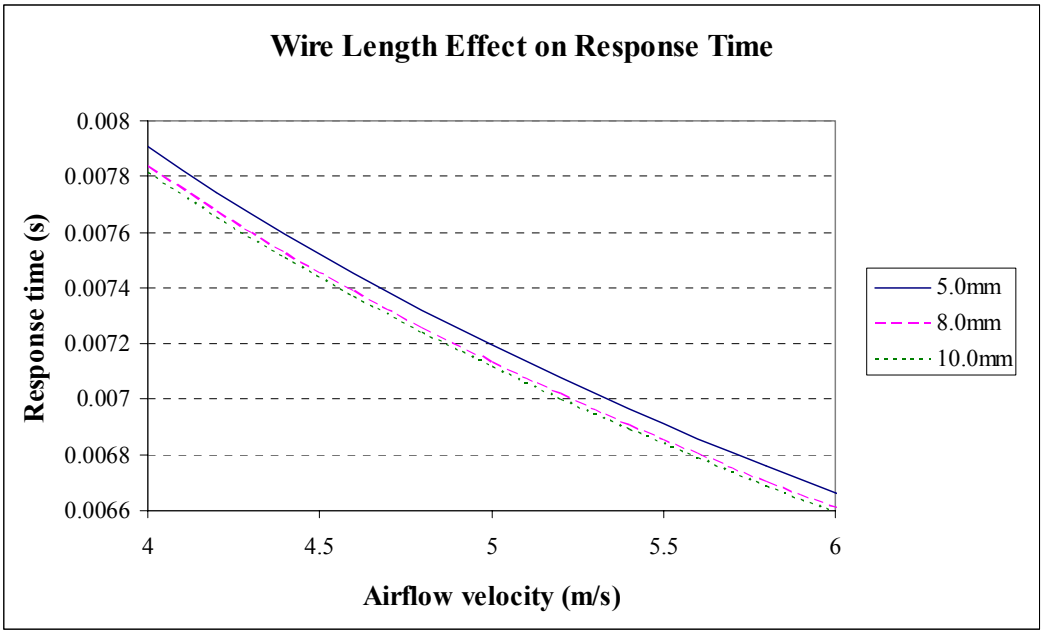

Figure 5.4 Wire Length Effect on Response Time

5.2.3 Wire Temperature

The wire temperature can be adjusted if the corresponding electrical resistor R_3 in the Wheatstone bridge circuit is used as a variable resistor. The conditions of this simulation process are similar to previous simulations: ambient temperature is 22 ^{o}C, 70% relative humidity, 0.02 mm wire diameter, 5 mm wire length. The wire temperature is set to be 50 ^{o}C, 100 ^{o}C, 150 ^{o}C and 200 ^{o}C higher than the ambient air temperature respectively. The simulation model is processed in the range of air flow velocity from 0 to 10 m/s.

Figure 5.5 shows the simulation results of the output wire current levels at various air flow velocities and wire operating temperature settings. Notice that the wire current significantly rises as the wire temperature increases.

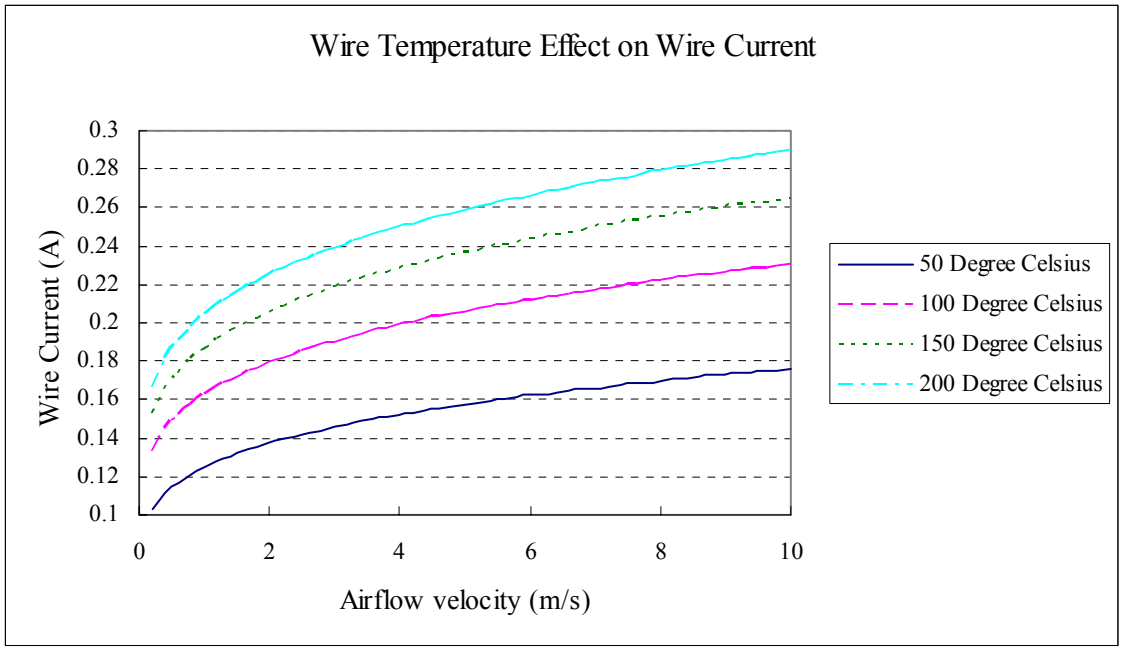

Figure 5.5 Wire temperature effect on output wire current

Obviously the curve of 200 ^{o}C has the highest wire current output at the same air flow velocity, the current difference between various curves increases as the air flow velocity raise.

The platinum wire has higher sensitivity when operating at a higher temperature due to the increased temperature difference between the platinum wire and ambient air temperature, causing a larger heat loss along the hot wire. Even for the same condition that all heat loss coefficients are the same, there is more heat loss compensation when operation at a higher wire temperature.

Figure 5.6 shows the simulation results of the response time over various air flow velocities and wire operating temperature setting. At the lower wire temperature setting (50 ^{o}C), the figure shows steeper reduction response time level. At lower wire temperature setting, the heat loss on the wire is less than that at higher wire temperature setting if the air flow velocity is the same. Therefore, as the heat balance on the hot wire is disturbed, the hot wire need less response time to compensate for the new heat loss to achieve a new heat balance. In higher air flow velocity range, the difference response time of various wire temperature setting will obviously get smaller.

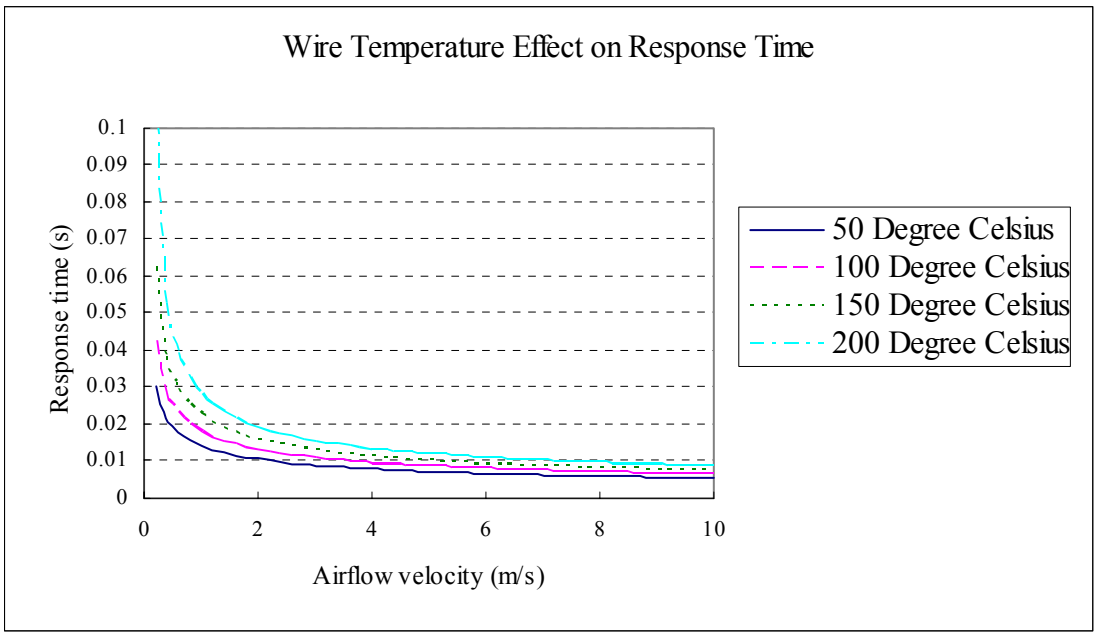

Figure 5.6 Wire temperature effect on response time

This effect is due to the fact that the forced convective heat power loss increases the rate of general heat loss power as the air flow velocity increases. Tin summary, to achieve a faster response speed a lower wire operating temperature is required.

5.3 Effect of Ambient Conditions

Changes in ambient conditions affect the accuracy of the hot wire air flow measurement as mentioned in Section 4.3. However, it was proved that the air pressure does not affect the measurement therefore only ambient temperature and relative humidity (RH) are discussed in this section. The effects of each parameter setting on the sensor output wire currents and measurement response time are discussed.

5.3.1 Ambient Air Temperature

The ambient temperature is directly related to the rate of heat lost from the hot wire surface in the air flow sensor. Figure 5.7 shows the output wire current under different ambient temperature from 0 to 40 ^{o}C and various air flow velocities. This simulation model is run at a constant ambient relative humidity of 70%, constant wire temperature 72 ^{o}C and platinum wire which size is ϕ 0.02 $\times$5 mm. It can be seen that all curves have the same trend: as the ambient temperature is raised, the wire current level decreases (approximately 0.65% per ^{o}C).

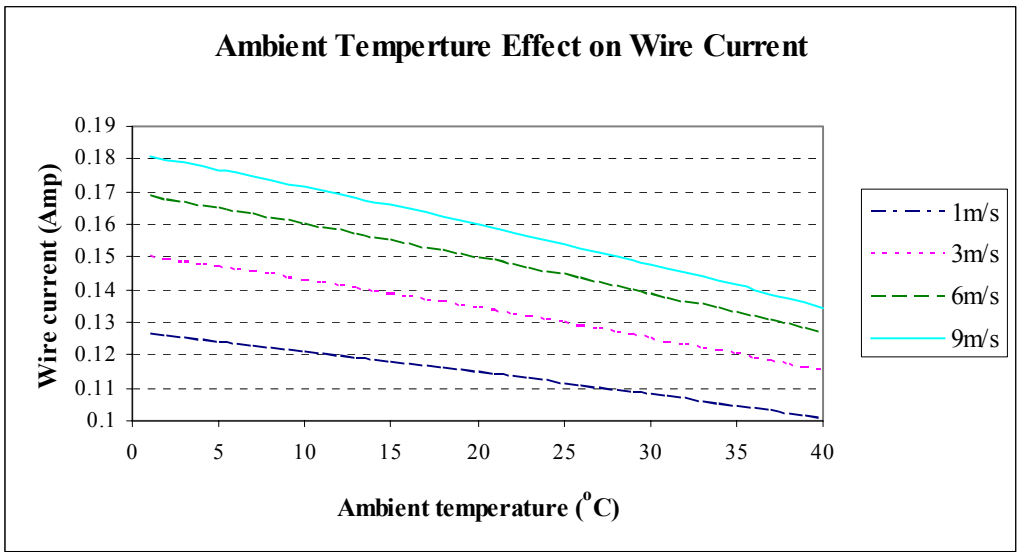

Figure 5.7 Ambient temperature effect on output wire current

This is attributed to the fact that as the ambient temperature increases the temperature difference between hot wire and ambient air is reduced. Decrease in the temperature difference between these two results in a decrease in the heat power lost which directly drops the compensation heat requirement, reducing the generated power and causes the wire current to drop.

All wire currents dropped in a linear fashion as the ambient temperature increased. For higher air flow velocities, the current has a steeper gradient which means in a higher air velocity range, the wire current is more influenced by the ambient temperature. This effect is due to the increase in the forced convective coefficient occurring in fast air flow streams. Higher air velocity leads to a steeper gradient of the wire current in terms of ambient temperature. During the same condition of reduced temperature, the higher forced convective coefficient gives a greater reduction in heat lost which leads to more current drop.

Figure 5.8 shows the dynamic response time of the hot wire to a step input of ambient temperature from 0 to 40 ^{o}C under various air flow velocities. From this figure, it can be observed that all curves have the same dynamic behaviour. The response time slightly decreases as the ambient temperature increases. A decrease in the output wire current i_w results in a decrease in the response time τ.

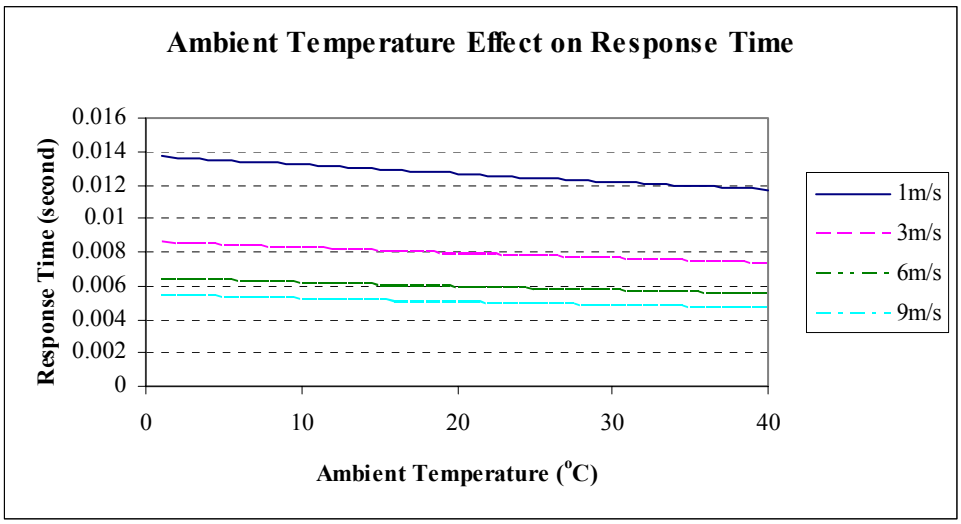

Figure 5.8 Ambient temperature effect on response time

The response time during rising ambient temperatures has the same trend as the wire current. Notice that higher air velocities produce a steeper gradient for the change in response time in terms of ambient temperature variation. Obviously this can be explained by the same behaviour of output wire current and the relationship between wire current and response time.

5.3.2 Ambient Relative Humidity

The simulation predictions of wire current of the sensor, under different ambient relative humidity and air flow velocities are shown in Figure 5.9.

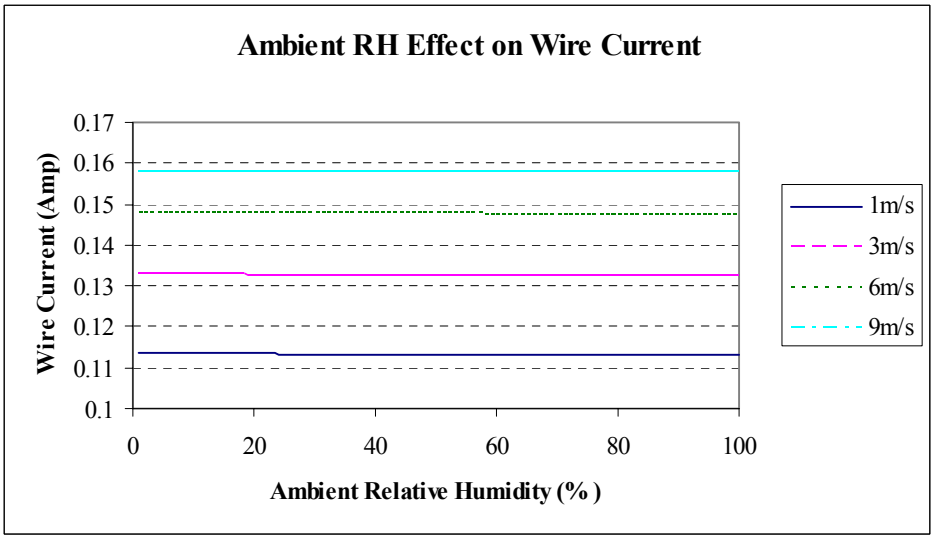

Figure 5.9 Ambient RH effect on wire current

It reveals the relationship between wire current and ambient relative humidity from 0 to 100%. This simulation model is run at a constant ambient temperature of 22 ^{o}C, constant wire temperature of 72 ^{o}C for a platinum wire size of ϕ 0.02 $\times$5 mm. It can be seen that no significant change occurs between the predictions under various air flow velocities. Obviously fluctuation in ambient relative humidity does not have observable influence to the wire current due to the fact that the relative humidity has very small effect on air properties. Parameters of air properties affect the value of forced convective coefficient which influence the general heat lost from the wire and change the wire current. According to relative equations, all coefficients are very small. Thus the effect to the air properties is very minimal. Further more, several parameters relatives to variation of air properties are partly eliminated. Therefore the influence of ambient relative humidity in the wire current is too small to be considered.

Figure 5.10 shows the response time of the hot wire sensor to inputs of ambient relative humidity under different air flow velocities. It can be observed that no significant change occurs between the predictions under various air flow velocities.

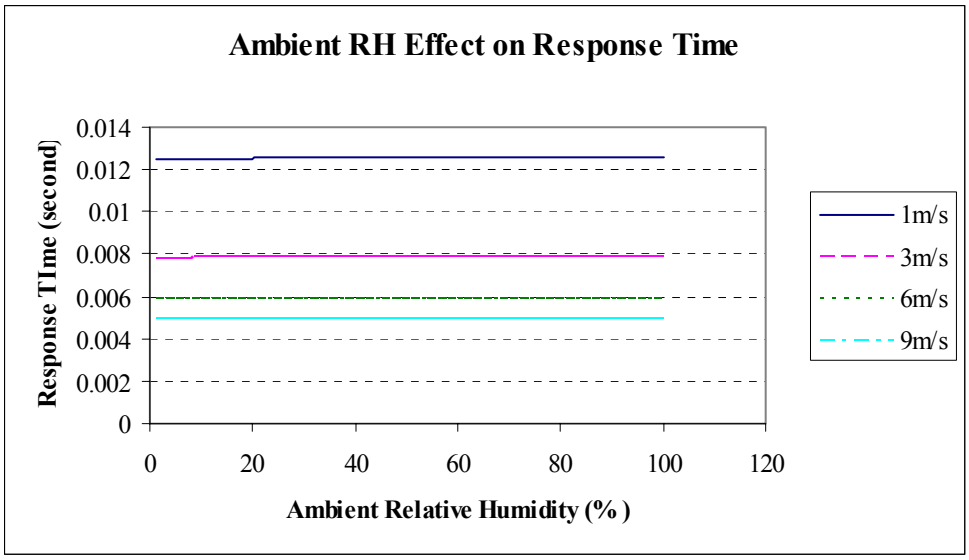

Figure 5.10 Ambient RH effect on response time

Obviously variation in ambient relative humidity does not produce observable influence on the response time. The ambient relative humidity indirectly affects the response time through the forced convective coefficient h. Based on the same reason mentioned in Section 5.3.1, the influence of ambient relative humidity in the wire response time can be neglected.

5.4 Incorporation of Sensor within CPAP System

From the discussions in Section 5.3, the thinner platinum wire will produce lower sensitivity and lower response times. One of the main goals of the project is to ensure that different harmonics in the patients' breathing cycle can be detected to diagnose relevant diseases (Section 2.2) thus lower response time is a design priority. The 0.02 mm diameter platinum wire has the desired response time even during period of very slow air velocity (0.1 m/s). Also its sensitivity is high enough so that it can be successfully implemented in the air flow sensor of CPAP device.

The length of the platinum wire did not show significant effect on both response time and electrical charge flow rate. Thus for the physical dimension of the inlet channel in the CPAP machine, a 5.0 mm length platinum wire is sufficient.

Theoretically, higher settings of wire temperature produce higher sensitivity and longer response time. Very high temperature settings are not advisable as it increases the risk of wire breakage. The range of 50 to 100 ^{o}C above the ambient temperature offers the best balance between sensitivity and breakage risk of wire in a CPAP device.

The temperature effect on the performance of the hot wire air flow sensor can't be neglected, there are two ways to minimize it: one is by maintaining the ambient temperature by using HVAC, the other way is by adding temperature compensation circuit in the air flow sensor. The humidity compensation is not necessary as its effect is negligible.

5.5 Model Operation

The literature indicates that in most of available work the calculations of the relationship between the air flow sensor output (wire current) and air flow velocity were only considered during steady state conditions. Many articles have involved different methods of ambient temperature compensation, but these articles rarely quantify the ambient temperature effect. The mathematical function for the relationship between hot wire output and air velocity is determined empirically under different hot wire or hot film conditions and this function is only validated under average ambient conditions and

the setting of hot wire or film. The simulation model developed in this project predicts the sensor behaviour in both transient and steady state situation under different probe (wire) settings and ambient conditions.

The experiment in Chapter 4 validated that the mathematical model as being capable of predicting the output of the hot wire air flow sensor. Using this prediction an appropriate control system can be produced for the CPAP blower or air flow rate controller to achieve the eventual air stream output level at the nasal mask under a broad range of different conditions. The fast response speed makes the diagnostics of patient OSA possible.

In the model calculations, the physical properties of probe and ambient air were taken into account. For any new design of probe, it just requires changes made to the modelling parameters for the particular element to enable the static and dynamic changes of sensor output to be predicted even before the sensor prototype is made. The sensor design engineers can use the model to optimize the design by changing modelling parameters and monitor the difference to the sensor output. The general simulation model has an efficient interface for users by requiring only the input values in the subsystem called Input Parameters and then running of the program to generalize the output results (see user instruction in Appendix I).

5.6 Conclusions

The objective of this project was to improve the understanding of the air stream flow measurement using a hot wire sensor within a CPAP device and to investigate the dynamic characteristics of this flow sensor by simulating a validated mathematical model. During the project, the energy balance of a sensor was undertaken and the relationship between the sensor probe setting, ambient conditions and supply air flow velocity were investigated. Through the project, the following conclusions are made:

- The sensor output current rises significantly as the probe wire diameter increases. The sensor response time grows up notably as the probe wire diameter increases.

◆ An increase in the probe wire length can slightly decrease the sensor output current. The wire length design alters the sensor response time very slightly by varying the unit length heat loss power.

◆ The sensor wire current is mainly dependent on power input which is considerably affected by the constant wire temperature setting. Higher wire temperature setting causes higher output wire current at the same air flow velocity range. The lower wire temperature setting can achieve a faster response speed due to the lower wire temperature change and current.

◆ Ambient temperature is directly related to the heat power losses from the hot wire in the air flow sensor. An increase in ambient temperature can reduce the output wire current. Ambient temperature can alter the wire current thus it can vary the sensor response time. An increase in ambient temperature does not drop the response time much especially in a high air flow velocity stream.

The effect of ambient relative humidity can be neglected in the hot wire air flow sensor. The mathematical model has been successfully developed and validated using empirical data within the normal operating range of a CPAP device. It can predict the static and dynamic activities of the measurement process for the improvement and modification of hot wire air flow sensor.

5.7 Future Work

Throughout the study of this thesis, future investigation is required in specific fields to optimise sensor behaviour. Some points include:

- The experiments of different dimensions wire, wire temperature setting and ambient conditions should be validated in a more stable air flow stream source in the future.

- The reference air flow meter TSI4000 is not accurate enough and better reference instrument or equipment should be applied in future experiments.

- If this model is considered to be applied in the field that require slower response and higher sensitivity, the amplifier transistor should be replaced with a better transistor which has bigger power capable and less current leakage.

- An alternative binding method to secure the platinum wire to the brass pins should be found to replace manual soldering used in this prototype, especially for large scale production. All individual wire probes should have almost same resistance at ambient room temperature.

- Develop an improved air stream control system which would be able to control the blower speed and valve to maintain the constant positive air flow rate at desired level.

REFERENCES

1. sleep well clinic, " Sleep Apnoea" WWW document: http://www.sleepwellclinic.co.nz/sleepapnoea.html, Accessed 18/01/2007

2. Gail Demko, B (2005 - 2007), "Obstructive Sleep Apnea ", WWW document: http://www.sleepapneadentist.com/obstructivesleepapnea/, Accessed 18/01/2007

3. Piccirillo, J, Duntley, S, Schotland, H, (2000) "Obstructive Sleep Apnea", JAMA September 27 (284), Issue (12), Page 1492-4,

4. Lyled, D, Victor, M D, (1999), "Obstructive Sleep Apnea", WWW document: http://www.aafp.org/afp/991115ap/2279.html, Accessed 18/01/2007

5. Department of Otolaryngology / Head and Neck Surgery, "Uvulopalatopharyngoplasty (UPPP) for Obstructive Sleep Apnea ", WWW document: http://www.entcolumbia.org/uppp.htm, Accessed 18/01/2007

6. The Free Encyclopedia Wikipedia, "Uvulopalatopharyngoplasty", WWW document: http://en.wikipedia.org/wiki/Uvulopalatopharyngoplasty, Accessed 18/01/2007

7. University Virginia Health System, "Nasal Surgery", WWW document: http://www.healthsystem.virginia.edu/uvahealth/adult_plassurg/nasal.cfm, Accessed 18/01/2007

8. Mayo Clinic, "Jaw Surgery for Obstructive Sleep Apnea", WWW document: http://www.mayoclinic.org/sleep-apnea/osa-jaw-surgery.html, Accessed 18/01/2007

9. United States Patent, (2005), "Mandibular-repositioning Devices", WWW document: http://www.freepatentsonline.com/20050175954.html, Accessed 18/01/2007

10. 21st Century Dental, "Sleep Apnea and Snoring ", WWW document: http://www.21stcenturydental.com/smith/sleepapena_tapappliance.htm, Accessed 18/01/2007

11. The American Academy of Otolaryngology—Head and Neck Surgery (AAO-HNS), " Continuous Positive Airway Pressure (CPAP)" WWW document: http://www.entnet.org/healthinfo/snoring/cpap.cfm, Accessed 18/01/2007

12. EzineArticles.com, " What Is Bipap/Cpap Therapy? " WWW document: http://ezinearticles.com/?What-Is-Bipap/Cpap-Therapy?&id=664425, Accessed 18/01/2007

13. Fisher & Paykel Healthcare , "Sleep Style 600 CPAP Series", WWW document: http://www.fphcare.com/osa/cpaps.asp, Accessed 18/01/2007

14. Fisher & Paykel Hearthcare, "FlexiFit 405 Nasal Mask", WWW document: http://www.fphcare.com/osa/flexifit405.asp, Accessed 18/01/2007

15. Stanford Univeristy, (1999), "Sleep Apnea Information and Resource", WWW document: http://www.stanford.edu/~dement/apnea.html, Accessed 18/01/2007

16. Behbahani, K, Yen, F-C, Burk, J R, (1995) "Automatic Control of Airway Pressure for Treatment of Obstructive Sleep Apnea", IEEE transactions on Biomedical Engineering (42) October,Page 1007,

17. Varady, P, Micsik, T, Benehek, S ,(2002) "A Novel Method for the Detection of Apnea and Hypopnea Events in Respiration Signals", IEEE transactions on Biomedical Engineering (49) September, No 9,Page 936-42,

18. Ozaki, Y, Ohyama, T , Yasuda, T, Shimoyama, I ,(2000), "An Air Flow Sensor Modeled on Wind Receptor Hairs of Insects", Page 531-6,

19. Saad, N H, Janin, Z, Sahab, A R M, (2003) "Instrumentation of Digital-Propeller-Anemometer", AsiaSense 2003 Asian Conference on Sensors, Page 341-5,

20. Bennion, D, (1992) "Electromagnetic Flowmeters for Difficult Media", Chemical Engineer, Issue (516), Page 33,

21. Zbinden, M, (1987) "Electromagnetic Flowmeters", Electricite de France, Bulletin de la Direction des Etudes et Recherches, Serie A: Nucleaire, Hydr, Issue (4), Page 51,

22. Doebelin, Ernest O, (2004), "Measurement Systems: Application and Design", Mc Graw Hill; 5th Edited, ISBN (0-07-243886-X), Page 103-214,578-672,

23. Tang, S, Federspiel, C C, Auslander, D M, (2003), "Pulsed Type Ultrasonic Anemometer Based on a Double FFT Procedure", Proceedings of IEEE Sensors, Institute of Electrical and Electronics Engineers Inc., Vol (2), Page 326-31, Toronto, Ont., Canada

24. Stephan, C H, Zanini, M, (1991) "A Micromachined, Silicon Mass-air-flow Sensor for Automotive Applications", International Conference on Solid-State Sensors and Actuators, Digest of Technical Papers, TRANSDUCERS '91, Page 30-3,

25. Aleksic, O S, Nikolic, P M, Lukovic, D, Savic, S, Pejovic, V Z, Radojcic, B M, (2004), "A Thick Film NTC Thermistor Air Flow Sensor", 24th International Conference on Microelectronics, Vol (1), Page 185-8,

26. Takahashi, S, Sekozawa, T, (1995) "Air-fuel Ratio Control in Gasoline Engines Based on State Estimation and Prediction Using Dynamic Models",

Proceedings of the 1995 IEEE IECON 21st International Conference on Industrial Electronics, Control, and Instrumentation, Vol (1), Page 217-27,

27. Takahashi, S, Arita, H, Uchiyama, K, (1996) "Adjustment Technique for Air Flow Sensor of Vehicle-Development of Auto Adjustment Technique for Hybrid IC",

28. Horn, M, Ruser, H, Umar, L, (2002) "Self-calibrated PTC Air Flow Sensor", Proceedings of IEEE Sensors,, Vol (2), Page 1771-4

29. Pei-Chung, C, (2005) "Neuro-fuzzy-based Fault Detection of The Airflow Sensor of An Idling Gasonline Engine", Proceeding of the I MECH E Part D Journal of Automobile Engineering,Professional Engineering Publishing, Issue (4), Page 511-24, April

30. Changchuan, J, Guangjun, L, Jin, J,(2005), "A Self-validating Algorithm for HotThermistor Constant Differential Temperature Air Flow Sensor", CCA 2005 Proceedings of 2005 IEEE Conference onControl Applications, Page 669-74,

31. Ohyama, Y, Ohsuga, M, Nogi, T , Minowa, T, (1991), "A Totally Integrated Electronic Control System for The Engine and Transmission", Eighth International Conference on Automotive Electronics, Page 39-42,

32. Teerawatanachai, S, Komiya, K, Sasamoto, H, (1991), "Estimating the Velocity Profile of Air Flow by Means of The Ultrasonic TranslationTime Computed Tomography Method", Vol (3), Page 2379-84

33. Aprilesi, G C, De Cicco, G, Taroni, A, (1983) "A Microprocessor-Based, Three Axes, Ultrasonic Anemometer", Ultrasonics Symposium, Page 295-8,

34. Siebert, H, Teichmann, U, (2000) "Behaviour of An Ultrasonic Anemometer Under Cloudy Conditions", Boundary-Layer Meteorology,Vol (94), 1, Page 165, http://dx.doi.org/10.1023/A:1002446723575

35. Stock, C, (2002) "WindSonic-A New Ultrasonic Anemometer", Sensor Review,Vol (22), Issue (3), Page 218-22, http://dx.doi.org/10.1108/02602280210433052

36. Kudo, K, Mizutani, K, Itoga, K, (2005) "A Simple Technique for Realizing An Ultrasonic Anemometer Using A Loudspeaker", Japanese Journal of Applied Physics, Part 1 (Regular Papers, Short Notes & Review Papers), ISSN (0021-4922), Vol (44), Page 4407-10, http://dx.doi.org/10.1143/JJAP.44.4407

37. Ishida, H, Yoshikawa, K, Moriizumi, T, (2004), "Three-dimensional Gas-plume Tracking Using Gas Sensors and Ultrasonic Anemometer", Proceedings of the IEEE Sensors 2004 (IEEE Cat. No.04CH37603), IEEE, Vol (3), Page 1175-8, Vienna, Austria

38. Van Wagenberg, A V, Leeuw, D, Mark, T J, (2003), "Measurement of Air Velocity in Animal Occupied Zones Using An Ultrasonic Anemometer", Applied Engineering in Agriculture, American Society of Agricultural Engineers, Vol (19), Page 499-508,

39. "Speed of Sound - Temperature Matters, Not Air Pressure", WWW document: http://www.sengpielaudio.com/SpeedOfSoundPressure.pdf, Accessed 18/01/2007

40. Tontechnik-Rechner-sengpielaudio, "Calculation: Speed of Sound in Humid Air", WWW document: http://www.sengpielaudio.com/calculator-airpressure.htm, Accessed 18/01/2007

41. Koninklijke Philips Electronic N V, (2006), "LPC214x User Manual", WWW document: http://www.standardics.nxp.com/support/documents/microcontrollers/pdf/-user.manual.lpc2141.lpc2142.lpc2144.lpc2146.lpc2148.pdf, Accessed 18/01/2007

42. TSI Incorported, (2004), "Mass Flowmeters for Gases", WWW document: http://www.tsi.com/documents/PN2980137RevE.pdf, Accessed 18/01/2007

43. Yunus, A C, (2003), "Heat Transfer A Practical Approach", ISBN (0-07-245893-3), Page 373. Equation7-19; Page 86 table 7-1 . Equation7-19; Page 86 table 7-1,

44. Thomas, L C (1999), "Hear Transfer-Professional Version", Capstone Publishing Corporation; ISBN (1-893317-00-5), Page 99-119,576-8, www.capstonepc.com

45. Bejan, A, Kraus, A D, (2003), "Heat Transfer Handbook", JOHN WILEY & SONS,INC; ISBN (0-471-39015-1), Page 161-260,

46. King, D J, "Resistance Elements and RTD's", WWW document: http://-www.omega.com/temperature/Z/ResistanceElements.html, Accessed 18/01/2007

47. Tempco' electric heater corporation, "Resistance Temperature Detectors", WWW document: http://www.tempco.com/Sensors/accu_ohm_rtds.htm, Accessed 18/01/2007

48. Miscellaneous Data, "Platinum (Pt) ", WWW document: http://www.platinummetalsreview.com/jmpgm/data/datasheet.do?record=1219&database=cesdatabase#Poisson's%20Ratio, Accessed 18/01/2007

49. Platinum metals review, " Notes For Young's Modulus @ RT Attribute Of Platinum", WWW document: http://www.platinummetalsreview.com/jmpgm/-data/notes.do;jsessionid=E491D478EB4A4B581A11BE292BAFDFC4?record=1219&type=0&attribute=35&database=cesdatabase, Accessed 18/01/2007

50. Microwave101.com, (2004), "Platinum ", WWW document: http://-www.microwaves101.com/encyclopedia/platinum.cfm, Accessed 18/01/2007

51. Temperatures.com, "Resistance Temperature Detectors (RTDs)", WWW document: http://www.temperatures.com/rtds.html, Accessed 18/01/2007

52. Bernoulli, Bernoulli's Law, WWW document: http://scienceworld.wolfram.com/-physics/BernoullisLaw.html, Accessed 18/01/2007

53. Bernoulli, Bernoulli's Equation, WWW document: http://www.princeton.edu/-~asmits/Bicycle_web/Bernoulli.html, Accessed 18/01/2007

54. Gere, T (1991), "Mechanics of Materials Third SI Edition", Chapman & Hall; ISBN (0-412-36880-3), Page 466,

55. Sigmund Cohn Corp, "Properties of Metals and Alloys", WWW document: http://-www.sigmundcohn.com/chinese/art/SCC%20literature.pdf, Accessed 18/01/2007

56. The Engineering ToolBox, (2005), "Density of Dry Air, Water Vapor and Moist Humid Air", WWW document: http://www.engineeringtoolbox.com/density-air-d_680.html, Accessed 18/01/2007

57. Answer.com, "Density of air", WWW document: http://www.answers.com/-topic/density-of-air, Accessed 18/01/2007

58. The Engineering ToolBox, (2005), "Specific Humidity or Humidity Ratio of Air", WWW document: http://www.engineeringtoolbox.com/humidity-ratio-air-d_686.html, Accessed 18/01/2007

59. WW2010, "Relative Humidity ", WWW document: http://-ww2010.atmos.uiuc.edu/(Gh)/guides/mtr/cld/dvlp/rh.rxml, Accessed 18/01/2007

60. Cactus2000, "Air Humidity Calculation", WWW document: http://www.cactus2000.de/js/calchum.pdf, Accessed 18/01/2007

61. P R Lowe, J M Ficke, (1974), "The Computation of Saturation Vapour Pressure", Page 4 to74,

62. WPI, "Density of Air VS Temperature", WWW document: http://users.wpiedu/-~ierardi/PDF/air_density_plot.PDF, Accessed 18/01/2007

63. PiRhoMania, (2000), "Air Property Calculator", WWW document: http://users.wpi.edu/~ierardi/FireTools/air_prop.html, Accessed 18/01/2007

64. INC Techware Engineering Applications, "Thermodynamic properties and transport properties of moist air: @Air 3.1", WWW document: http://www.techwareeng.com/prodAA.htm, Accessed 18/01/2007

65. Air Property Calculator, "Specific Heat of Air VS Temperature", WWW document: http://users.wpi.edu/~ierardi/PDF/air_cp_plot.PDF, Accessed 18/01/2007

66. Air Property Calculator, "Kinematic Viscosity of Air VS Temperature", WWW document: http://users.wpi.edu/~ierardi/PDF/air_nu_plot.PDF, Accessed 18/01/2007

67. Air Property Calculator, "Thermal Conductivity of Air VS. Temperature", WWW document: http://users.wpi.edu/~ierardi/PDF/air_k_plot.PDF, Accessed 18/01/2007

68. Onsemi.com, (2003), "Dual Different Input Operational Amplifiers", WWW document: http://pdf1.alldatasheet.com/datasheet-pdf/view/11675/-ONSEMI/LM258D.html, Accessed 18/01/2007

69. Stmicroelectron, "Low Power Dual Operational Amplifiers ", WWW document: http://pdf1.alldatasheet.com/datasheet-pdf/view/22767/STMICROELECTRONICS/LM258D.html, Accessed 18/01/2007

70. Datasheetcataloge.com, (2007), "BC238", WWW document: http://www.datasheetcatalog.com/datasheets_pdf/B/C/2/3/BC238.shtml, Accessed 18/01/2007

71. MOSPEC, "Complementary Silicon Plastic Power Transistors (2SD743)", WWW document: http://pdf1.alldatasheet.com/datasheet-pdf/view/2529/MOSPEC/-2SB703.html, Accessed 18/01/2007

Appendix I. Model User Instruction

I.1. Introduction

This section gives instructions on how to use the Simulink™ mathematical model. It is in fact the "user manual" for the simulation model. The main purpose of this manual is to give a basic idea of how to use this software.

I.2. Getting Started

The basic requirement to run this software is to have a MATLAB™ 7.0 and a Pentium base computer that meets the requirements to run the package.

Starting procedure:
Start MATLAB 7.0
Type "simulink" in the command window then press ENTER
Open file from the tool bar at the top of the Simulink™ Library Browser window.

I.3. User Interface

The blocks are colour coded as an aid to usage (see Figure III.1):
Data inputs: Light blue
Simulation output: Orange
Simulation output: Green (Graph in time based)
Simulation calculation: Yellow

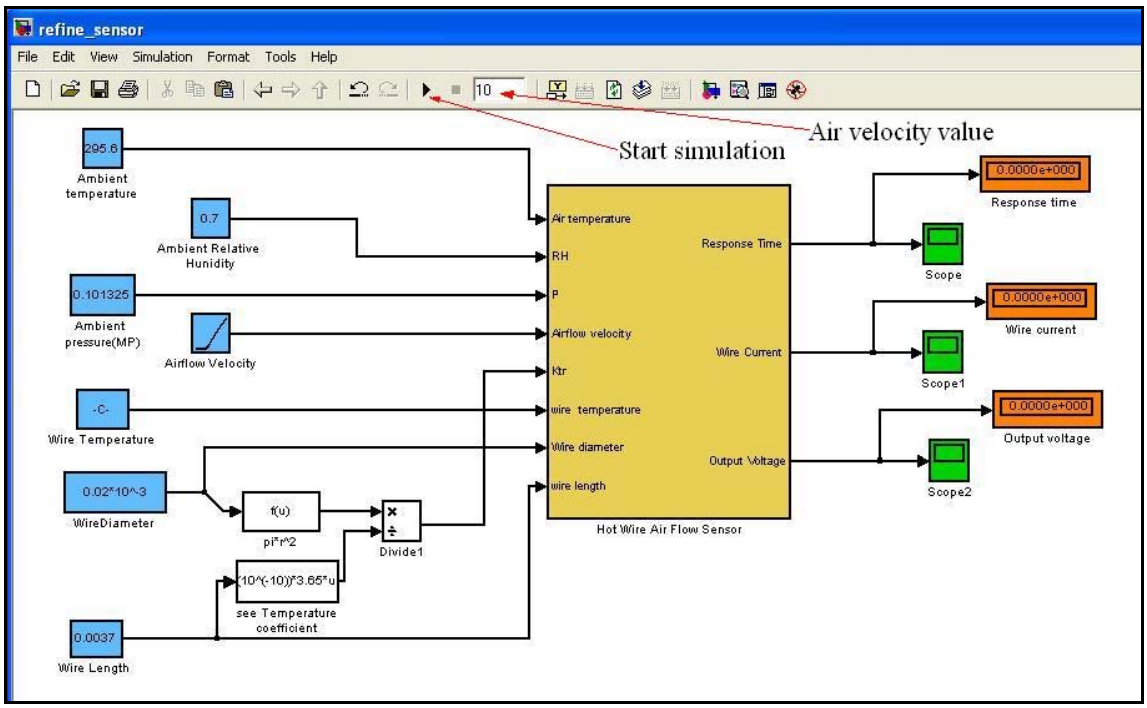

Figure I.1 Simulation model user interface

I.4. Calculation Procedure and Entering Input Data

The model blocks have been setup so that all the input data are entered. Air flow velocity is set as ramp inputs (the value can be changed by input different process time value). Others parameters are set as constant input. The calculation procedure is initiated manually by click on the "Start simulation" icon. The calculation procedure will take a few seconds to run and then gives simulation results will show in the output display blocks. Double click on the "Scope" display block to get the dynamic behaviour of the system outputs. The simulation air velocity range can be easily setup by go to the "simulation" icon on the top toolbar and then click on "Simulation parameters". A new window would shows up and type in the start and stop time to get the desired simulation air velocity range.